Location-aware and Cooperative Communication in an OFDM based Ultra-wideband Radio System

Von der Fakultät für Ingenieurwissenschaften

der Universität Duisburg-Essen

zur Erlangung des akademischen Grades eines

Doktors der Ingenieurwissenschaften (Dr.-Ing.)

genehmigte Dissertation

von

Dong Xu

aus

Shandong, China

Referent: Prof. Dr.-Ing. Peter Jung

Korreferent: Prof. Dr.-Ing. Klaus Solbach

Tag der mündlichen Prüfung: 06.08.2012

Danksagung

"*Lernen, ohne zu denken, ist eitel;*
denken, ohne zu lernen, ist gefährlich."

Konfuzius (551 v. Chr.-479 v.Chr.), Analekten des Konfuzius

Die vorliegende Arbeit entstand während meiner Tätigkeit als Stipendiat am Lehrstuhl für Kommunikationstechnik der Fakultät für Ingenieurswissenschaften der Universität Duisburg-Essen von September 2008 bis April 2012. Ich danke all jenen, die zur Entstehung dieser Arbeit beigetragen haben.

An erster Stelle bedanke ich mich herzlich bei Herrn Prof. Dr.-Ing. habil. Peter Jung, dem Leiter des Lehrstuhls für Kommunikationstechnik der Fakultät für Ingenieurwissenschaften der Universität Duisburg-Essen, für seine engagierte Betreuung und die Übernahme des Referats der vorliegenden Arbeit.

Des Weiteren danke ich allen meinen Kolleginnen und Kollegen des Lehrstuhls für Kommunikationstechnik: Zijian Bai, Dr. Guido Bruck, Bärbel Clausen, Sven Dudda, Barbara Frischemeier, Stanislaus Iwelski, Christian Kocks, Sebastian Rickers, Ernest Scheiber, Andrey Skrebtsov, Christoph Spiegel, Alexander Viessmann, Andreas Waadt, Ali Al-Humairi, Rani Al-Maharmah, Mohammed A. A. Al-Olofi, Wei Chen, Laith Khalil, Xue Liu und Duan Zhao. Insbesondere möchte ich mich bei den Herren Zijian Bai, Sebastian Rickers und Ernest Scheiber für die in diese Arbeit eingeflossenen fachlichen Diskussionen und Anregungen bedanken.

Ich bedanke mich bei meinen Eltern, die mir immer Kraft und Unterstützung geben, und meine Ehefrau Tiantian Yang, die mich durch ihr Verständnis und ihre Geduld unterstützte.

Zuletzt spreche ich einen herzlichen Dank an den China Scholarship Council für die finanzielle Unterstützung aus.

Übersicht

Die auf dem orthogonalen Frequenzmultiplex (OFDM, Orthogonal Frequency Division Multiplexing) basierende Ultra-Breitband-(UWB, Ultra-wideband) Technologie stellt eine verheißungsvolle Technologie dar, um hohe Datenübertragungsraten und Lokalisierungs- und deren Tracking-Anwendungen zu realisieren. Im Gegensatz zu anderen Systemen ist die Reichweite von OFDM UWB Systemen durch eine strenge Regulierung sehr stark begrenzt. Darüber hinaus ist die Lokalisierung nicht zufriedenstellend. Damit sind bereits die beiden größten Nachteile im Bezug auf bestehende OFDM UWB System benannt. Die Motivation und Hauptaufgabe dieser Arbeit ist damit die Lösung der eben genannten Nachteile.

Es wird ein OFDM UWB System vorgestellt, das Space Frequency Block Coding (SFBC) und FFH OFDM miteinander verbindet. Dieses vereinte System wertet die räumliche und frequentielle Diversität eines OFDM-Symbols aus und zeigt dabei eine hohe Güte in der Punkt-zu-Punkt Kommunikation. Beim Design von kooperativen UWB-Systemen wird ein AF-(Amplify-and-Forward) basiertes echtzeitfähriges SFBC-TFC (Time Frequency Code) Protokoll vorgestellt. In Kombination mit den oben genannten Strategien, kann eine Erhöhung in den Reichweite von OFDM UWB Systemen erreicht werden.

In den Ausführungen zur Ortung anhand von OFDM UWB Signalen wird ein Algorithmus entwickelt, der aufgrund einer Kanalschätzung eine Minimierung des Phasenversatzes zwischen geschätztem und realem Kanal im Frequenzbereich durchführt. Diese Minimierung erwirkt eine Unterdrückung der Energie am Ende der Kanalimpulsantwort (CIR, Channel Impulse Response) im Zeitbereich. Zum Zweck der einfachen Implementierbarkeit wird das RTT (Round-Trip-Time) Messprotokoll in WiMedia UWB Systemen dahingehend verändert, dass das mobile Gerät keine Minimierung vornimmt. Es leitet seine Informationen an das mit ihm Kommunizierende, stationäre Gerät weiter, das direkt den gesamten Zeitversatz innerhalb des RTT berechnet. Der vorgeschlagene Algorithmus und das vorgeschlagene Protokoll haben ein besseres Ortungsvermögen als bekannte UWB Lokalisierungsprozeduren und bedürfen nur etwas zusätzlicher Berechnungsleistung.

Diese Arbeit zeigt, dass Systeme mit hohen Datenraten wie OFDM UWB auch eine gute Lokalisierungsgenauigkeit erreichen können. Zusätzlich ist die Schwachstelle einer limitierten Reichweite ebenso kompensiert worden. Diese

Erweiterungen dienen der Entwicklung von nützlichen UWB-Applikationen und sichern den Anteil der OFDM UWB Technik im Markt der drahtlosen Kommunikationssysteme der Zukunft.

Abstract

The Orthogonal Frequency Division Multiplexing (OFDM) based Ultra-wideband (UWB) is one of the most promising technologies for high data rate transmission and localization and tracking applications. However, the restricted transmit power causes a shorter communication range compared to other indoor radio systems. In addition, the ranging functionality is still not well supported by the current OFDM based UWB technology. These two drawbacks are the main disadvantages existing in the current OFDM UWB systems. To get rid of the two drawbacks, is the motivation and main task of this thesis.

Within the scope of this thesis, a joint design of Space Frequency Block Coding (SFBC) with Fast Frequency Hopping (FFH) OFDM scheme is investigated in a multiple antenna OFDM UWB system. The joint scheme is able to exploit spatial and frequency domain diversity within one OFDM symbol, and can improve the data transmission quality in point-to-point communication. To the cooperative communication in UWB systems, an Amplify-and-Forward (AF) based distributed SFBC-TFC (Time Frequency Code) protocol is designed. In combination with the aforementioned strategies an increase in the communication range is achieved.

Within the scope of this thesis, accurate ranging schemes for the OFDM UWB systems are designed. Fine ToA detection method based on the estimated channel is developed. The fine ToA is estimated by minimizing the accumulated energy of the tail taps of the estimated Channel Impulse Response (CIR). For the purpose of a feasible implementation, the Round-Trip-Time (RTT) measurement protocol in [WiM09] is modified in a way that the complicated computational tasks are burden onto the powerful device. The proposed fine ToA detection method and modified RTT protocol provides an accurate ranging capability and ensures feasible implementation to the MB-OFDM UWB systems. In carrying out this scheme, only some computational tasks are needed, no extra hardware support is required.

It is shown in this thesis, OFDM UWB systems with very high data rate transmission and good ranging capability could be achieved, and the weakness of limited communication range is also compensated. These improvements will cause the rise of more valuable UWB applications for customers and ensures a bright future for the OFDM UWB technique.

Table of Contents

Chapter 1

Introduction

1.1 Overview of UWB

1.1.1 History and Development of UWB

Ultra-wideband (UWB) is defined as a radio modulation technique with a minimum bandwidth of 500 MHz or a bandwidth of at least 20% of the central frequency [FCC02]. As shown in Figure 1.1, compared to the radio signals with conventional wireless communication systems, UWB radio signal covers very broad frequency spectrum in the range of 3.1 to 10.6 GHz. However, these frequency resources might be already occupied by other licensed systems, like satellites, military radar, or civil wireless communication systems, such as IEEE 802.11a Wireless Local Area Network (WLAN). Therefore UWB devices are only allowed to operate at extremely low transmit power to avoid interfering the licensed systems. It is specified in [FCC02] that the maximum mean Equivalent Isotropically Radiated Power (EIRP) of unlicensed UWB radio is not larger than -41.3 dBm/MHz from 3.1 to 10.6 GHz.

By virtue of the enormous bandwidth inherent to UWB radio, huge channel capacity and high data rate transmission could be achieved without invoking high order modulation techniques. Low power consumption and very high speed transmission makes UWB radio an attractive solution to the short range communication systems. Until now data rates up to 1024 Mbits/s in an MB-

OFDM UWB system are specified in [WiM09]. Therefore UWB technology is suitable to be integrated onto mobile network terminals, consumer electronics, and applied in wireless sensor networks (WSNs). In addition, UWB radio has high time resolution, and is able to provide high precision ranging and localization applications.

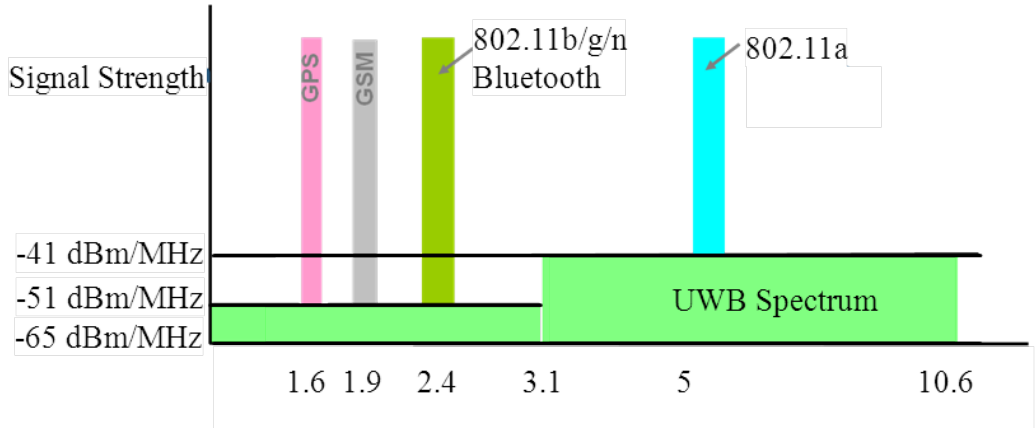

Figure 1.1 Emitted signal strength comparison between UWB and other radio systems

When talking about wireless communication, most people are not unfamiliar with it. However when being asked about UWB, most of us might have no idea what exactly it is. Actually the wireless communication technique was discovered and developed from UWB radio. The original UWB system can be traced back to the spark-gap transmission design of Marconi and Hertz in late 1890s, and the first Morse code sequences transmission from Isle of Wight to Cornwall on the British mainland using spark-gap transmitters [Nik09]. Nevertheless people may probably argue that radio was unintentionally UWB. In the 1950s, impulse based radio transmission gained momentum in military used radar and communication systems. Through the late 1980s, UWB was referred only to baseband, carrier-less, or impulse technology [Sir06]. The term Ultra-wideband was coined in 1989 by U.S. Department of Defense [Sir06]. Until the 1990s, UWB technologies were still restricted to military applications. Nowadays UWB technologies are no longer limited to short impulse and carrier-less. One of the most popular UWB technologies is based on OFDM modulation. In 1998 the U.S. Federal Communication Commissions (FCC) recognized the significance of UWB technology and initiated the regulatory review process. In February 2002, the FCC approved the first report about UWB regulation, and the emission power of the unlicensed users in the range from 3.1 to 10.6 GHz was regulated [FCC02].

After the release of FCC UWB regulation, UWB technologies have made quick developments in the first decade of the 21 century. Countries and regions except for USA also drafted their own spectrum regulations for UWB. For instance, the European Union (EU) has by now released several specifications for UWB radio spectrum management and applications. International organizations are also quite active in UWB specifications and standardizations, some of the representative organizations include, IEEE 802.15 work group for wireless personal networks (WPAN), and the WiMedia Alliance [WiM11]. In Section 1.1.3, status of UWB regulations and specifications are overviewed.

Generally there are mainly two popular UWB techniques, short impulse based UWB and OFDM based UWB. The short impulse based UWB technique is mostly used in localization and tracking systems, and also suitable for low data rate (LDR) transmission. The IEEE 802.15.4a work group specified an impulse based UWB PHY layer in [IEE07]. The OFDM based UWB is more suitable for high data rate (HDR) transmission. Standardization of OFDM base UWB could be found in WiMedia Alliance [WiM09]. Researches on UWB were also intensively carried out in the EU financed Sixth Framework Programme (FP6) project, Pervasive Ultra-wideband Low Spectral Energy Radio Systems (PULSERS II) and the FP7 project, Co-Existing Short Range Radio by Advanced Ultra-wideband Radio Technology (EUWB). In these two projects the leading techniques, the fascinating future applications, and the actual regulation and standardization process of UWB technology in Europe were investigated. PULSERS II project aimed at exploration of the enormous potential of the innovative and disruptive radio technology embodied in UWB and at enabling the introduction of new services, applications and devices based on this technology [Bra06]. The EUWB project was focusing more on the co-existence problems of UWB with other radio systems [EUW08].

UWB technology is still in its infancy and under developed. In the next generation UWB systems, advanced technologies and concepts shall be integrated. For instance, the Software-Defined-Radio (SDR) and Cognitive Radio (CR) technologies could provide flexible frequency allocation. The Detection and Avoidance (DAA) mitigation technique can improve the spectrum efficiency and avoid interfering to other radio systems. Low Duty Cycle (LDC) mitigation techniques are able to lower power consumption and interference. Accurate localization and tracking methods and location aware services in UWB systems shall be exploited. The development of UWB technologies is in a multi-disciplinary ascending progress. With rapidly developed semiconductor and other related electronic techniques, UWB technologies will be greatly promoted.

1.1.2 UWB Applications and Market

1.1.2.1 UWB Applications

One of competitive edges of the UWB technology is its low power consumption and high data rate transmission. There are a lot of applications of UWB radio in the communication area, such as Wireless Universal Serial Bus (WUSB), wireless loudspeaker, WSNs, wireless High Fidelity (Hi-Fi) headphones, high-speed Wireless Personal Area Networks (WPAN) and Wireless Body Area Networks (WBAN), etc. Another advantage of UWB radio is its excellent time resolution. High performance ranging, localization and tracking applications could be provided by the UWB radio systems. The applications include vehicular radar, indoor localization and tracking, and the radar imaging, such as ground penetration radar, wall radar imaging, and medical imaging, etc.

Within the scope of EUWB project, future applications based on UWB radio technology were sketched and investigated in four emerging areas, namely home entertainment, public transport, automotive, and heterogeneous access networks. In each area, interesting applications have been proposed and studied.

In home entertainment environment, both LDR and HDR UWB applications are serviceable. The ranging capable and localization aware features of UWB radio systems are also attractive to the home entertainment applications. In an intelligent building in the near future, most of the PC peripherals such as keyboards, mouse, and printer could be connected through wireless UWB radio to the host. These services are probably based on LDR applications, which have only very low power consumption. HDR applications, such as High Definition (HD) video streaming over wireless, wireless HD display devices, requiring very high data rate and reliable transmission, are also in great demand in home entertainment. Another interesting demand in home entertainment scenario is the location aware services, which means location of the network devices are expected, such as the controller and sensor in an interactive PC game system (like Kinect in Xbox 360 system), where the players could get true experiences when positions of them are known to the PC game system. Another example might be the home theatre system. The surround sound parameters could be adjusted accordingly to the position of the audience, so that vivid effects could be obtained. Therefore, both impulse based and OFDM based UWB radio could provide meaningful applications to the home entertainment environment.

Airplane In-Cabin UWB radio system is typical scenario of the applications in public traffic area. Low power emission and little interference to the other electronic systems is one of the advantages of UWB radio for airplane In-Cabin use. Applications in airplane In-Cabin of UWB radio mainly include cabin management system (CMS), passenger communication system and in-flight entertainment system. The current CMS does not have any wireless function and the network is based on a wired star topology [Bov08]. This implies a large number of cables and a high effort for the system installation and its maintenance. Extending the current CMS through a wireless infrastructure for the flexible wireless connection would enable an increased possibility to customize the cabin layout and the service available to the client specific requirements, and make possible at the same time a fast reconfiguration of the cabin layout to react to the passenger requests (e.g. increase the number of business class seats by removing economy class seats) [Bov08]. The UWB radio based passenger communication and in-flight entertainment system have the same advantages of little interference to the airplane's electronic systems. Besides, these systems could be seamlessly connected with the passenger's personal network device through UWB radio, and provide more convenient network access and on board services for the passengers.

In automotive area, UWB radio is also one of the attractive technologies. It is reported that in a car there are over 1000 meters long cable for controlling and entertainment systems, with an overall weight 80 Kg [Niu08]. For convenient and efficient deployments, some of the cables could be replaced by radio. UWB technology has its advantages to be deployed into vehicular environments, include the low power emission and little interference to the existing electronic and electrical systems of the car, the performance in ranging and localization. Different UWB applications been investigated in the automotive cluster within the scope of EUWB project [Has08].

In Heterogeneous access networks scenario, most of the smart network terminals support multiple communication standards. For example, one smart phone can have Universal Mobile Telecommunications System (UMTS) radio module for cellular network access, and it also has Bluetooth and Wi-Fi for short range communication. These multimode devices have already provided the customers very pleasant applications. In the future, the UWB radio module could also be integrated to the smart networks terminals. Three fields have been identified to perform the integration of UWB radio module into current and future heterogeneous networks, they are user devices, access network equipment and services based on location awareness [EUW08].

1.1.2.2 Potentials and Challenges to UWB

From the wide range of applications mentioned above, there is no doubt that the UWB radio could have bright future and a great market. The advantages come from the low power emission, accurate localization capability and high data rate transmission. However every coin has two sides, the low power emission level of UWB radio causes limited communication range. There are a lot of competitive technologies which make great challenges to UWB radio technology. In this part, the potential market and challenges to UWB radio technology are discussed.

Location-awareness is one of the most attractions in future wireless communication systems. With development of Internet-of-Things (IoT), more and more Location-based Services (LBS) are exploited, and the network terminals are expected to provide their locations. It is reported that only in China the market of LBS is about 3.8 Billion Yuan (500 Million €) [Abr10]. Professional localization systems, such as the Global Positioning System (GPS), are suitable for outdoor applications. Therefore the UWB based localization and tracking systems have the dominant position for the indoor use. There are a great demand to these high accuracy localization and tracking services, such as in a warehouse and by assembly line. The UWB based ranging systems have the absolute predominance in such local area LBS applications in indoor environments. Therefore, in the aforementioned four application areas, the advantages of the UWB radio in location and tracking applications are foreseen.

Another competitive point for the UWB radio technology to hold the market is its low power emission level and very high data rate transmission. The demand on data rate has increased exponentially with time for more than 20 years, when assuming the validity of Edholm's law of bandwidth for the next decade, data rate of several tens of Gigabit per second can be expected [Ars06]. The FCC-regulated frequency range from 3.1 GHz to 10.6 GHz already occupies 70% of whole available bandwidth below 10 GHz that is suitable for indoor environment. Therefore the UWB technology will be probability the best choice to fulfill such high data rate demand [Ars06]. From the application point of view, there are indeed great demands for such very high data rate transmission, especially for the consumer electronics market. Not only the high data rate, but also the low energy consumption, was the two key requirements of these consumer electronic devices. This is a coincidence with the feature of the UWB radio technology. Therefore UWB radio technology has great potential market in the consumer electronics market.

From the analysis above, one can notice that, accurate localization and tracking capability was the unique edge of UWB radio in indoor environments. However in the short range HDR applications, there are a lot of competitive technologies to UWB radio systems, such as such as IEEE 802.11g and IEEE 802.11n WLAN. The IEEE 802.11g/n system could also provide high data rate transmission up to hundreds Mbps, supporting a HD video streaming service. A brief comparison between WiMedia UWB system and the two IEEE 802.11 WLANs is listed in Table 1.1. From Table 1.1 one can observe that, compared to the IEEE 802.11 WLAN, the WiMedia UWB system has the advantages of less power consumption and localization and tracking capable, however communication range is the bottleneck.

Table 1.1 Comparison Short range Wireless Technology **[XUD11]**

	WiMedia	802.11g	802.11n
Packet PHY Date Rate	480Mbps	54Mbps	300Mbps
Typical PHY Data Rate	≈200Mbps	≈30Mbps	≈100Mb/s
Typical Power	40..80uW <400uW	~factor 10 over UWB	~factor 20 over UWB
Range in LoS Scenarios	Up 10m	≈40m	≈70m
LT accuracy	0.30m	not available	not available

The 60 GHz technology is another strong competitor to UWB radio technology, especially in very high data rate applications, such as uncompressed video streaming. The advantage of 60 GHz Radio is that there is no strictly restricted power emission level as in UWB radio specification. In the USA the regulation for the 60 GHz communication started in 1994. The FCC reserved 7 GHz bandwidth between 57 GHz and 64 GHz to be used with a maximal spectral power density of 13 dBm/MHz EIRP and 40 dBm EIRP transmit power [Fed95]. In Europe the 60 GHz communication between 57 GHz to 66 GHz is regulated by

the harmonized European norm EN 302 567, allowing a spectral power density of up to 13 dBm/MHz EIRP and a maximal transmit power of 40 dBm EIRP [ETS09]. The relative higher power emission level of 60 GHz technology promises a larger communication range. Therefore it is very competitive to the UWB technology. The current 60 GHz communication systems are listed below,

- IEEE 802.15.3c
- Wireless HD
- ECMA-367/ ISO/ICE 13156
- WiGig (Wireless Gigabit Alliance)
- IEEE 802.11 ad

However the 60 GHz radio has severe attenuation during propagation. The directional selective features of the 60 GHz channel also limited its wide applications. Besides, some of the 60 GHz technologies are derived from the OFDM based UWB radio, by up converting the baseband signal to the 60 GHz frequency. From a general definition of UWB, these 60 GHz technology are also UWB. Results of the conventional UWB studies could be adapted to 60 GHz. From this point of view, conventional UWB and 60 GHz are families.

In summary, the UWB technology has both great potential market and challenges. The issue is how to play up its strengths and avoid the weaknesses. Some advanced technologies, such as Multiple Antennas, cooperative diversity technologies, could be adapted to the UWB radio systems, and compensate the drawback due to the restrictive emission power.

1.1.3 UWB Regulation and Standardization

1.1.3.1 Organization

At a national wide level, the radio spectrum is managed by national administrations which adopt a national table of radio spectrum allocations, define a framework for its use and partition it among the different users via licenses or via license-free arrangements. [Dun11]. After the FCC released the first standardization of UWB technology for commercial use, the development of

UWB radio systems was accepted. UWB radio signal covers the lower part of Super-High-Frequency (SHF, 3-30 GHz) band [Par00], on which most of the civil and military systems are working. Therefore, UWB radio spectrum regulation and standardization is very important. In different countries and regions, the spectrum is differently used. European Union, China, Japan, Korea and Hong Kong have also specified their own UWB spectrum regulations according to the [FCC02]. In this part, the actual status of UWB spectrum regulations and standards in Europe as well as other counties are overviewed.

1.1.3.2 World Wide UWB Regulation

In USA the FCC approved UWB emission mask since 2002, specifying the emission mask for communications devices in an indoor environment. For generic UWB devices a maximum mean EIRP of -41.3 dBm/MHz and a peak power of 0 dBm measured in 50 MHz is authorized between 3.1 GHz and 10.6 GHz [Dun11]. Definition of UWB of FCC: An intentional radiator that, at any point in time, has a fractional bandwidth equal to or greater than 0.20 or has a UWB bandwidth equal to or greater than 500 MHz, regardless of the fractional bandwidth [FCC02].

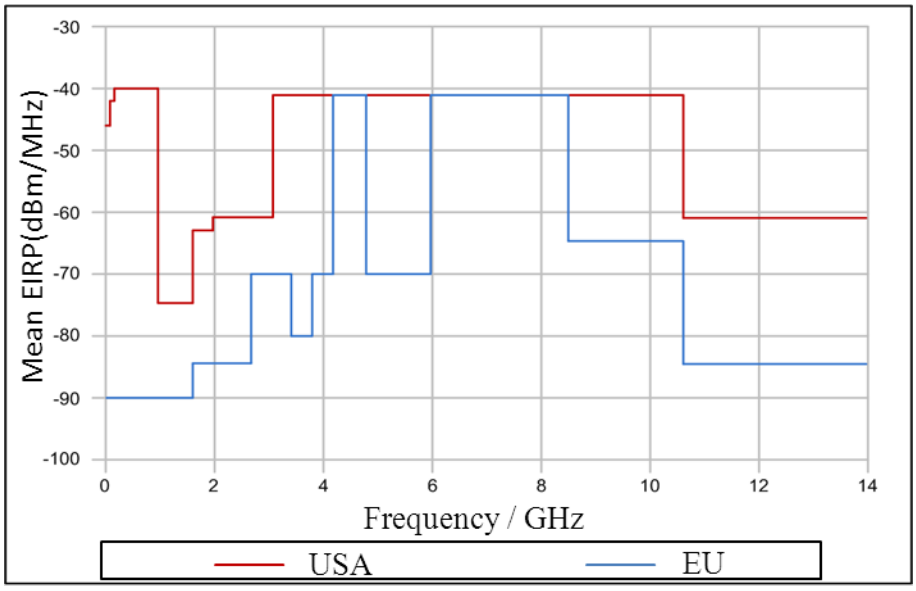

Figure 1.2 European spectrum mask of UWB compared to FCC regulation **[Dun11]**

At the European level, the European Commission (EC), the European Telecommunications Standards Institute (ETSI) and the Electronic Communications Committee (ECC) of the European Conference of Postal and Telecommunications Administrations (CEPT) cooperate on matters related to the regulatory environment for radio equipment and spectrum both at the EU level and at the wider intergovernmental level across Europe [Dun11]. Here the actual status (to April 2011) of the generic UWB spectrum regulation in Europe is collected. As shown in Figure 1.2, UWB devices can use the 6.0 to 8.5 GHz band with a maximum mean power spectral density of -41.3 dBm/MHz EIRP. This is the same level as specified in [FCC02]. The band from 3.4 to 4.8 GHz may also be used with a maximum mean power spectral density of -41.3 dBm/MHz EIRP, provided that a LDC mitigation technology is applied [Dun11].

In China the Ministry of Information and Industry (MII) has issued a public call for comments on the draft UWB regulation from May 28th, 2008 to September 30th, 2008. The UWB in band transmission is restricted to the frequency range from 4.2 to 4.8 GHz and from 6.0 to 9.0 GHz. The UWB transmission from 4.2 to 4.8 GHz is restricted to be used only indoors. The MII has already started DAA specification in 2011 in this spectrum range [MII11]. The UWB transmission from 6.0 to 9.0 GHz can be used indoors and outdoors [Hei08]. In Hong Kong the Office of Telecommunication Authority (OFTA) is responsible for the UWB regulation. In Hong Kong UWB devices are mainly used indoors. The maximum mean EIRP limits within the range of UWB band from 3.4 to 4.6 GHz is -41.3 dBm/MHz provided that of DAA technology is used. For UWB band from 6.0 to 8.5 GHz, maximum mean EIRP up to -41.3 dBm/MHz is acceptable [Dun11].

In Japan the Minister of Internal Affair and Communication is in charge of the radio spectrum specification [Hei08]. No final conclusion related to the definition of DAA has been reached between the UWB industry and the potential service operators. Thus the UWB band from 4.2 to 4.8 GHz is open without additional mitigation techniques until the end of 2013 [Dun11]. The maximum mean EIRP limits within the range of UWB band from 3.1 to 10.6 GHz is -41.3 dBm/MHz. For the frequency bands from 3.4 to 4.2 GHz, the limits are further reduced to less than -70 dBm/MHz.

In South Korea, first UWB regulation was done by Ministry of Information and Communication in July, 2006. The maximum mean EIRP limit within the range of UWB band from 3.1 to 10.6 GHz is -41.3 dBm/MHz. In the UWB band from 3.1

to 4.8 GHz DAA is required. In UWB band 7.2 to 10.2 GHz no interference mitigation is required.

Aside from the generic UWB spectrum specifications, EU is also active in standardizing the regulations of UWB for specific application environments with detailed rules. In Europe the responsibility for this regulatory framework is in the hands of the CEPT ECC working group TG3. In the past three years the ECC TG 3 has developed a regulatory UWB framework for Europe including a broad range of possible applications. These applications can range from sensor, surveillance and monitoring applications over radar application to high speed wireless multimedia distribution for in car entertainment systems. For further information about UWB specification please reference to [Dun11].

1.1.3.3 UWB System Standardization

The IEEE 802.15.3a Task Group was opened in December 2002, and it planned to standardize the high-speed UWB Physical (PHY) layer and Media Access Control (MAC) layer. At the beginning, there were 23 PHY proposals, two of which were selected as the candidate technologies. They were Multiple Band OFDM (MB-OFDM) and Direct Sequence Code Division Multiple Access (DS-CDMA) [Hei08]. Two camps were therefore formed, namely, MB-OFDM Alliance (MBOA) and UWB Forum. Unfortunately no further progress was achieved, and the process was hampered by the dichotomy in the history of the types of signal used in the two proposals [Hei08]. Neither group showed any willingness to compromise. Finally, on 19 January 2006, the IEEE P802.15 TG3a has been withdrawn. After the two camps of IEEE 802.15.3a decoupled, Motorola and Freescale left the group in 2006, and the UWB Forum was closed.

In March 2004, 802.15.4a became an official Task Group. The task of IEEE 802.15.4a is to provide alternate PHY standards that would allow for high aggregate throughput (lots of throughput over time) communications with a precision ranging capability (within 1 meter accuracy) and low power usage within the scope of the WPAN [IEE07]. In IEEE 802.15.4a two additional PHYs using Ultra-wideband (UWB) and chirp spread spectrum (CSS) are specified. Basically, both new PHYs added scalability to data rates, longer ranges, and lower power consumption into the standard, thus meeting the intent of the IEEE 802.15 standard to emphasize very low cost communications. The UWB PHY is designated frequencies in three ranges: below 1 GHz, between 3 and 5 GHz, and between 6 and 10 GHz. The CSS PHY is designated to the 2.450 GHz industrial,

scientific and medical (ISM) radio band. On the 22 March 2007 IEEE 802.15.4a was approved as a new amendment to IEEE 802.15.4-2006.

MBOA is the one camp from IEEE 802.15.3a work group. It later merged into WiMedia Alliance. WiMedia Alliance is a non-profit open industry association that promotes and enables the rapid adoption, regulation, standardization and multi-vendor interoperability of ultra-wideband (UWB) worldwide [WiM11]. The board member of WiMedia Alliance includes Samsung Electronics, Alereon and CSR. WiMedia submitted its first MB-OFDM UWB specification to European Computer Manufacturers Association (ECMA) in 2005. In December 2005 ECMA approved the PHY layer and MAC sub-layer specification and released ECMA-368 standard. Another WiMedia's MAC-PHY Interface (MPI) proposal has also been proved by ECMA and released as ECMA-369 standard. Both standards have been published by International Organization for Standardization (ISO) and ETSI. In December 2009, the WiMedia Alliance updated WiMedia PHY layer Specification (Version 1.5), WiMedia MAC layer specification (Version 1.5) and the WiMedia MAC-PHY Interface specification (Version 1.5).

1.2 State of the Art

In Section 1.1 the history, development and standardization of the UWB Radio technologies are reviewed. As already pointed out, UWB Radio technology faces the great challenges of limited communication range. To compensate this drawback, some advanced technologies could be applied. In this section, state of the art of OFDM based UWB technologies is surveyed. Status of key PHY technologies in an OFDM UWB system, for instance, channel coding schemes, multicarrier modulation technologies, multiple antenna technologies, cooperative diversity in UWB networks, as well as ranging and localization issues with OFDM UWB radio are examined.

- Channel Coding

In the WiMedia UWB standard, the Convolutional Codes (CC) and Low Density Parity Check (LDPC) Codes are the proposed channel codes. CC is a classic channel coding scheme in wireless communication systems. In WiMedia UWB specification, CC is proposed due to its simple implementation. Some variant of the CC have been also designed for OFDM UWB to improve the performance. In [Nyi06] concatenated Reed-Solomon (RS) Convolutional Codes for MB-OFDM UWB system has been proposed. The performance of 8-bit, 10-bit and 11-bit RS-

convolutional codes were investigated and evaluated. It was shown in [Nyi06] that concatenated codes perform better than single codes at high signal-to-noise ratio (SNR). Another powerful channel code based on CC is Turbo codes. The encoding and iterative decoding of Turbo codes were originally presented by Berrou in [Ber93], which allows reliable data transmission within a half decibel of the Shannon Limit. Turbo Trellis-Coded Modulation (TTCM) is an attractive scheme for higher data rate transmission, since it combines the impressive near Shannon limit error correcting ability of turbo codes with the high spectral efficiency property of TCM codes. Different schemes using TTCM have been presented in [LeG94] [Rob98]. Now the TTCMs are widely used, such as in UMTS and 3GPP Long Term Evolution (LTE) standards. In the OFDM UWB systems, high order Quadrature Amplitude Modulation (QAM) modulations are used, and TTCM could be applied. In [Wan05] studies of OFDM UWB system using TTCM with QAM constellation for higher data rate transmission have been carried out. Their results showed that with TTCM the OFDM UWB system can benefit much higher spectral efficiency.

LDPC codes were invented by Gallager in 1960s [Gal62], however it was forgotten because of the impractical implementation issues limited to the computing capacity until Gallager's work was discovered in 1996. LDPC code is also a Shannon capacity approaching channel code. In the space telecommunication, the advances of LDPC codes surpass turbo codes in terms of error floor and performance in the higher code rate range, leaving turbo codes better suited for the lower code rates only [Sni09]. There are already a lot of wired and wireless communication systems employing LDPC codes, such as Digital Video Broadcasting-Terrestrial (DVB-T), Digital Video Broadcasting-Satellite Second Generation (DVB-S2), and IEEE 802.11n WLANs. In the most recent released WiMedia PHY specification 1.5, LDPC code is also proposed. The LDPC code in the WiMedia UWB is based on the study of Ultra-Sparse LDPC (US-LDPC) code in [Bra07]. The US-LDPC codes with a codeword size of 1200 bits were designed and implemented. The performance of the US-LDPC codes in OFDM UWB system were compared with other standardized LDPC codes used in WiMax, IEEE 802.11g and IEEE 802.11n. Although all examined LDPC codes achieved the same performance gain of up to 4 dB compared to the convolutional code, the US-LDPC code gains up to 55% in VLSI area needed, using only 0.2 mm^2 after synthesis [Bra07].

From the literature review, we have noticed that the LDPC code and Turbo Code have good performance already very close to the Shannon capacity limit [Lin04]. It is difficult to invent innovative channel code for the OFDM UWB system. This

does not mean that there are no open issues in the channel coding areas for OFDM UWB system. For instance, performance evaluation in different channel environment, and practical problems in implementation are still under study. However the channel code designs are out of the main scope of this work.

- Fast Frequency Hopping in OFDM

The multicarrier modulation technique OFDM is one of the most popular transmission schemes in modern digital radio communication. The information carrying symbols are modulated on several orthogonal subcarriers which exist in parallel within the allocated bandwidth. In contrast to common single carrier frequency division multiplex (FDM) schemes, the multicarrier OFDM technology occupies the frequency more efficiently. The orthogonality between subcarriers allows the recovery of the information carrying symbols on the receiver side without complex equalization filters. Channel equalization is simplified because OFDM may be viewed as using many slowly modulated narrowband signals rather than one rapidly modulated wideband signal. The developments in digital signal processing allow an easy realization of those OFDM demodulators.

The origins of multicarrier techniques could date back to the 1950s. The so-called Kineplex system with 20 subcarriers each with a data rate of 150 bit/s, was presented [Doe57]. When using analogue signal processing, the multicarrier modulation scheme requires the use of expensive and complex circuits including oscillator banks for the systemization of carrier signals of transmitter and receiver side. Since the amount of filters and oscillators is considerable for a larger number of subcarriers, an efficient implementation of OFDM was proposed by using the Discrete Fourier Transform (DFT) or its more computationally efficient implementation, the Fast Fourier Transform (FFT) [Wei71]. The progress in semiconductor technology enabled the realization of an FFT for a high number of subcarriers up to several thousands. In consequence, OFDM gained much in significance.

Nowadays, OFDM is used in many mobile communication standards or considered for future standards. Future developments of OFDM usually target improvements of the transmission quality for high rate channel coding schemes. The exploitation of diversity is a mayor tool for this aim. Examples are the combination of the multicarrier scheme with code division multiple access (CDMA) [Jun96], [Van93], or the interleaved frequency division multiple access (IFDMA) [Sch98], which exploits the diversity of the mobile channel as well,

allowing a better transmission quality than conventional OFDM. Another diversity combining transmission scheme is FFH/OFDM [Sch05].

FFH/OFDM uses a cyclic frequency hopping pattern and allows the use of simple channel equalizers. The intrinsic diversity gain of FFH/OFDM enables high transmission quality for high rate data services. Compared with the other discussed diversity exploiting transmission schemes, FFH/OFDM gains from an easier implementation while reaching at least the same performance. A disadvantage of all discussed transmission schemes is the loss of orthogonality the information carrying symbols due to the multipath propagation. Hence the more complicated signal processing is required in the receiver. In [Sch05] two equalizer for the FFH/OFDM, namely Zero-Forcing (ZF) block linear equalizer and Minimum Mean Square Error (MMSE) block linear equalizer were given. It is shown that the FFH/OFDM exploits frequency diversity within one OFDM symbols in frequency selective channel. The FFH/OFDM method appied into WiMedia UWB systems is firstly reported in [Ber071]. In [Ber071] the FFH/OFDM UWB scheme combined with CC or US-LDPC code have been examined. The results showed that the FFH/OFDM could introduce transmission quality enhancement to WiMedia UWB system.

- Multiple Antenna with OFDM

Multiple antenna techniques are a favorite modern technique and have been researched widely and deeply. The basic idea behind multiple antenna techniques is to extend the signal processing behavior into space domain in communication system. This behavior will complement the signal processing in time and frequency domain and give some significant advance in system performance. When antenna arrays at the receiver and transmitter side are installed, a Multiple Input Multiple Output (MIMO) system is present.

In [Win87] the potentials of MIMO techniques in providing capacity increase to the wireless communication was shown. [Tel99] proved the fundamental results on the capacity of flat-fading MIMO channels. The first experimental testbed proving the potentials of MIMO communications was the Bell Laboratories layered space-time system (BLAST), developed at Bell Labs [Ser05]. In [Ala98] a simple transmit strategy to exploits spatial diversity was present. One of the advantages from the Alamouti scheme is that it can get the diversity gain with lower implementation complexity, only some linear signal processing at the receiver is required. Generally speaking, the common MIMO techniques have

been assigned into three categories, namely, spatial diversity, spatial multiplexing, and beamforming.

MIMO and OFDM are two promising technologies in the modern wireless communication system. OFDM technology has advantage of converting a wideband frequency-selective fading channel into numerous orthogonal narrow-band flat-fading channels. And MIMO can bring significant performance boost for wireless communication system under flat-fading channel. Combination MIMO with OFDM shows great potential in performance enhancement for the wireless systems. For instance MIMO-OFDM technology is adopted by next-generation cellular communications (LTE, Mobile WiMax) as well as IEEE 802.11n WLAN, and digital broadcasting systems. And it is also straightforward to introduce MIMO technologies to OFDM UWB systems. The potential benefits of MIMO with OFDM based UWB include greater coverage, higher data rate, interference rejection, etc.

In [Sir061] a general framework to characterize the performance of UWB-MIMO systems with multiband OFDM is proposed. In this study, a proper Space-Time-Frequency (STF) code design can exploit all of the spatial, temporal and frequency diversity and hence promise to yield high spectral efficiency and remarkable performance improvement. In [Kai09] a survey of UWB with MIMO were reported, including channel capacity, space-time coding and beamforming in both impulse based and OFDM based UWB systems. It is pointed that, the UWB-MIMO is still in its research infancy. In this survey the implementation of a testbed of 2×3 MIMO-OFDM UWB system with very high data rate were presented. In [Tra09] [Tra091] STF Codes for MB-OFDM UWB were also studied. Most of the studies ignored the unique feature of MB-OFDM UWB, time frequency hopping (TFC). However when TFC is applied, it is impossible to exploit space-time coding in the two adjacent the OFDM symbol, since the channel does not keep constant during two concatenated OFDM symbols due to the frequency hopping. This problem will be discussed in Section 3.3.4.

- Cooperative Communication in UWB Systems

MIMO techniques have shown great attractions to wireless communication systems for the benefits of spatial diversity or multiplexing gains. However due to the limited physical size or low cost consideration, it is not practical to set up multiple antennas to all network devices. One possible way to overcome this problem and to benefit from the performance enhancement introduced by MIMO techniques is the cooperative communication. Cooperative communications have

been aroused great research interests in recent years. The idea is to make use of available user terminals as relays that cooperate together as virtual antenna array to exploit the cooperative diversity. Most of the studies of cooperative communication are based on the two phase cooperative protocol proposed in [Lan02]. The interesting topics include, cooperative relay selection criteria, the distributed coding, and the relaying scheme, etc. UWB systems also face design challenges due to the limited transmit power and the low cost design. It is meaningful to exploit the cooperative diversity in UWB networks for coverage extension. In [Kim07] a hierarchical modulation and a suitable cooperative Space-Time block code (C-STBC) were proposed. Their method is free from the rate-loss and allows seamless cooperative communication while similar diversity gain is benefited. In [Tra08] the Space-Time-Frequency Coded MB-OFDM UWB in the cooperative manners are studied. In [Sir061] a decode-and-forward (DF) cooperative was designed, and optimum power allocation are provided. In [Che09] a cooperative communication in UWB body area networks (BANs) is explored, and the system diversity was analyzed under the body-centric multipath channel environment.

- Ranging with OFDM UWB signal

Accurate ranging and localization is one of the most fascinating applications of impulse based UWB radio technology. The high time resolution of impulse UWB radio makes it suitable for Time-of-Arrival (ToA) based ranging. It is reported that the accuracy of TOA measurements better than 40 ps has been achieved, which corresponds to 1.2 cm spatial uncertainty [She06]. There are already mature commercial ranging systems based on the impulse UWB radio technology. A ranging feature is also desired for OFDM based UWB systems in some applications. For instance, ToA based ranging method was defined as optional feature by WiMedia UWB specification [WiM09]. However, the definition of the ranging in [WiM09] is not thought to be thorough enough to provide a basis for a simple implementation. The definition is vague on the exact timing definition of the reception signal [Kra10]. Until now it has not been implemented by any manufacturer. Alternatively, one can use simply received signal strength (RSS) method. In department of communication technologies at the university of Duisburg-Essen, the RSS based ranging algorithms with WiMedia OFDM UWB system has been intensively examined and reported in [Wan10], [Waa101], and [Wan10]. RSS based ranging algorithms are very sensitive to the environment, and the ranging accuracy performance is not good. Therefore the fine ranging in the MB-OFDM UWB systems is still an interesting and unsolved topic.

1.3 Motivation and Contribution

1.3.1 Motivation and Objective

Motivated by the drawbacks of the current OFDM UWB techniques, this study is carried out. The objective of this thesis is to extend the communication range of an OFDM based UWB system, and to provide accurate ranging methods to the system. In such UWB systems, very high date rate services should be well supported, accurate localization and tracking services should be feasible, and the communication range should be also satisfying.

1.3.2 Tasks, Methodology and Contributions

To achieve this objective, the studies are divided into two directions, one focuses on the communication issues of the OFDM UWB technology, and the other is around the ranging problem with the OFDM UWB. Three tasks are unfolded: the first one is the study on the joint design of FFH/OFDM with SFBC in a multiple antenna MB-OFDM system, the second one is the study of distributed SFBC cooperative scheme in an MB-OFDM UWB based networks, and the third one is to develop accurate ranging methods for the MB-FODM UWB systems.

The above three tasks are carried out gradually from simple to complicated cases. We start the study with the FFH/OFDM in the single antenna system, then extend it to the SFBC-FFH case in a multi-antenna MB-OFDM UWB system, and finally cut into the cooperative protocol design. In developing the accurate ranging methods, firstly synchronization and channel estimation in an MB-OFDM system are reviewed, and then fine ToA detection method based on the synchronization and the estimated channel information are investigated, RTT measurement protocol is modified to facilitate the implementation of the proposed fine ToA detection method to the low cost UWB devices.

Innovative ideas and contributions of this thesis include,

1. Design and evaluation of the SFBC-FFH/OFDM scheme in the multiple antenna MB-OFDM UWB systems (Section 3.4),

2. Design of real-time distributed SFBC-TFC cooperative protocol in an MB-OFDM UWB relay networks (Section 4.3),

3. Fine ToA detection method for MB-OFDM UWB based on channel estimation (Section 5.3),

4. Modification to the RTT ranging protocol to WiMedia UWB to facilitate the implementation (Section 5.4).

1.4 Organization of the Dissertation

In Chapter 2 the UWB radio signal and its propagation characteristic are firstly introduced, and some basic descriptions of the wireless channel are reviewed. Then multipath channel modeling for UWB radio propagation is presented. The classic Saleh-Valenzuela (S-V) [Sal87] model is used to emulate the UWB propagation channel. The spatial UWB channel is also discussed. In addition, UWB radio propagation channel in specific scenarios, such as automotive environment and airplane In-cabin environment are parameterized.

In Chapter 3, the PHY layer of WiMedia OFDM UWB is firstly reviewed. Then two technologies that are dedicated to improving transmission quality of OFDM systems, the FFH/OFDM scheme and multiple antenna technology, are examined. Finally the joint design of FFH/OFDM and Alamouti SFBC scheme is developed and evaluated in a multiple antenna MB-OFDM UWB system. The proposed scheme shows good potential in improving the transmission quality, and accordingly extends the point-to-point communication range.

In Chapter 4, after a short review of cooperative communication, a distributed SFBC-TFC cooperative protocol for one-way relay system in the MB-OFDM UWB networks is designed. The proposed scheme is based on AF relaying scheme, and shows good real-time property. The distributed SFBC-TFC cooperative protocol shows good potential in extending the network coverage with a feasible low complex implementation. In addition, the proposed scheme is suitable for time-critical HDR applications.

In Chapter 5, accurate ranging method based on fine ToA detection in the MB-FODM UWB systems is reported. As the pre-knowledge to the fine ToA detection, the basic ranging schemes in the wireless communication systems, the synchronization and channel estimation issues in MB-OFDM UWB systems are firstly reviewed. Then the fine ToA detection method based on estimated channel impulse response (CIR) is invented. To facilitate the implementation, the RTT measurement protocol in [WiM09] is modified. It is proven that with the

combination of proposed fine ToA detection method and modified RTT protocol, accurate ranging capability as well as feasibility in implementation is provided to the MB-OFDM UWB systems.

In chapter 6 the brief summary of the accomplished work is presented and outlook of further researches in this area are discussed.

Chapter 2

UWB Radio Propagation Channel

2.1 Chapter Overview

To analyze and design UWB communication systems, in particular software simulators, investigating the localization of mobile tags or analyzing bit error ratios (BER), block error ratios (BLER), data rates and coverage, it is important to have accurate knowledge of the radio propagation channel. Due to its huge occupied spectrum band, UWB radio signal shows quite different characteristic in propagation from a narrowband signal. The main reason is the statistical features of the multipath arrival of the UWB signal are different from that of narrow band signal. Therefore understanding UWB propagation channel is vital prerequisite for the further studies of this work.

The chapter is organized as follows. In Section 2.2 the propagation characters of UWB radio signal is presented. Some important parameters describing a wireless channel are also reviewed. In Section 2.3, multipath UWB radio propagation channel based on S-V model is studied. The UWB spatial propagation channel is also discussed. In Section 2.4 UWB propagation channel for specific scenarios, automotive environment and airplane In-Cabin environment are parameterized. Section 2.5 summarized this chapter.

2.2 UWB Radio Propagation and Description

2.2.1 UWB Radio Propagation

In free space, the propagation of the UWB signal does not show significant difference with a narrowband signal, because in free space wireless channel is a linear time invariant system, and the wideband signal does not suffer frequency selective fading in this environment. From the Friis formula [Ped00], the transmitted power P_T and receive power P_R of the radio signal in free space has therefore the relationship

$$\frac{P_R}{P_T} = \frac{c^2 G_T G_R}{(4\pi f_c d)^2}, \tag{2.1}$$

where the f_c is the geometric mean value of the upper frequency f_u and lower frequency f_l of the transmitted UWB signal. G_T and G_R are transmit antenna gain and receive antenna gain, receptively. d is the signal propagation distance, and c is the speed of light in free space.

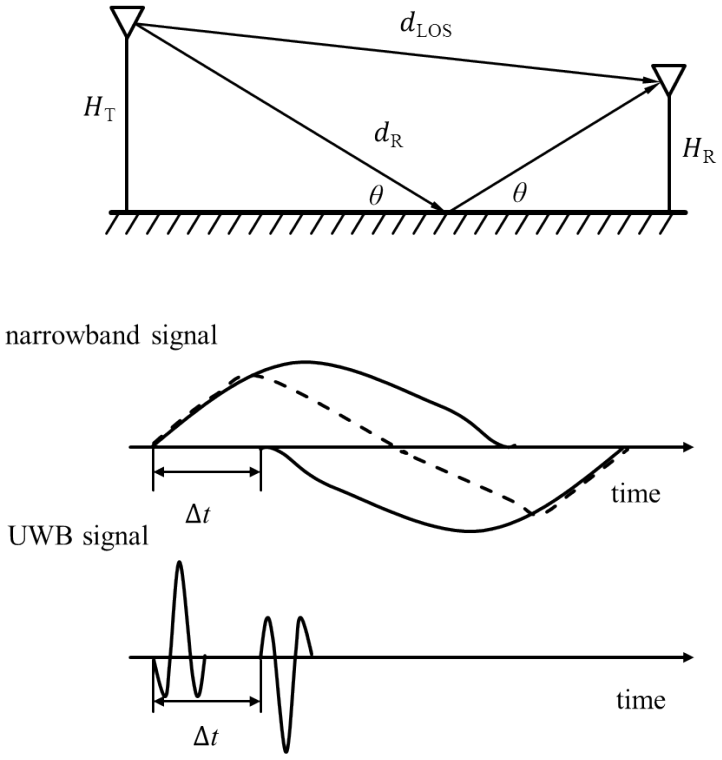

Figure 2.1 Direct and reflected radio signal propagation over a smooth ground

However, in practical scenarios UWB signals show quite different characters from narrowband signals. In Figure 2.1 radio propagates over a smooth ground is illustrated. The Line of Sight (LOS) component and reflected component has propagation path length of d_{LOS} and d_{R} , respectively. The propagation time difference between the two paths is $\Delta t = \left(d_{\mathrm{R}} - d_{\mathrm{LOS}}\right)/c$. For narrowband symbols in indoor environment, Δt is usually much smaller than symbol duration, which can be depicted by the middle diagram in Figure 2.1. Since the delay difference is shorter than symbol duration, in the receiver the received symbol is the superposition of the symbol from direct path and reflected path. Smooth ground has reflection coefficient around -1, and therefore the reflected signal has 180° degree phase jump. In some cases, the two waves could cancel each other. However situation for UWB signals is different, especially in the short range communication systems. The propagation deference Δt is probably larger than the UWB symbol duration, which means that the LOS component and reflected component do not overlap with each other. As illustrated by the lower diagram in Figure 2.1, they arrive one by one to the receiver, and are resolvable.

When extended to general scenarios, where there are not only one reflecting path from ground, but also some scatters around the transmitter and receiver, the multiple path propagation phenomena of radio could be discovered. In Figure 2.2 signal propagation in clusters of obstacles environment is illustrated. Confocal Ellipses describe the set of potential multipath components (MPCs) which have the same propagation delay from transmitter to receiver. The two neighboring ellipses stand for the bounds for the resolvable signals. There are a lot of interacting objects (such as, specular reflection, diffuse scattering, or diffraction, in [Ben06] the general term “interacting objects” is used) in the multiple path case, and superposition of these signals makes the received signal more complicated than the ideal scenarios mentioned above.

From Figure 2.2 one can observe that received signal is sum of scaled, phase shifted, delayed version of the transmitted signals. Signals arrive at the receiver within time window of symbol duration form one channel tap. In narrowband systems, symbol duration is so large that there are plenty of independent paths within one tap in rich scatter environment. According to the Central Limit Theorem, when a large number of statistically independent signals arrive in one channel tap, the envelope of received signal in this tap follows Rayleigh distribution. Take the Global System for Mobile Communications (GSM) with 200 KHz sub channel system in urban area as an example, the channel tap window length is 5 us, in other words, when two propagation paths have

difference less than 1500 m, the paths are regarded as in the same a tap. Therefore narrowband multipath channel is usually modeled by Rayleigh distribution

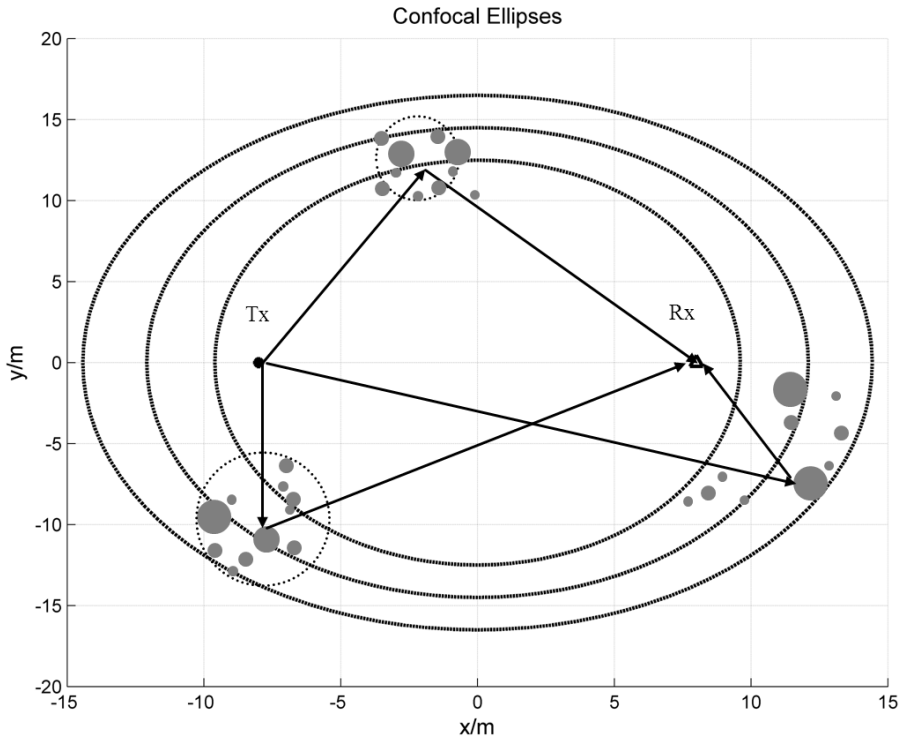

Figure 2.2 Illustration multiple-path propagation with Confocal Ellipses

Since the time duration of UWB symbol is much shorter, there are only limited MPCs fall into one channel tap. Take the WiMedia UWB symbol as an example, one symbol has length of 242 ns [WiM09], which is much shorter than one GSM symbol length. The corresponding unresolvable propagation path difference is about 60cm. It means that the multiple paths which have a propagation path difference smaller than 60cm do main contribute to the same channel tap, otherwise signals are resolvable. Since the number of the independent paths in one channel tap is not large enough and Central Limit Theorem is not fulfilled for UWB signals. This implies that the amplitude fading statistics for each tap are no longer Rayleigh distribution. Nakagami distribution, log-normal distribution were reported [Ars06]. This explains why the statistical character of UWB radio propagation is different from that of narrowband radio.

Due to the different propagation character, the Path-loss statistics of UWB signal is also different from the conventional signals in indoor environment. Principally

Path-loss model is used for system design (i.e., link budgets) in order to predict system coverage. In addition, based on the Path-loss model, the Received Signal Strength (RSS) could be applied for coarse ranging use. In [Gha02] a simple statistical model for evaluating the path loss in indoor environments was reported. In Section 5.2 the RSS ranging method based on Path-loss model is briefly introduced.

2.2.2 UWB Propagation Channel Description

In the last subsection, simplified physical illustration of UWB radio propagation in free space, smooth ground reflection and rich scattering environments are presented. In this subsection, the statistical description of UWB propagation channel is given. To better describe multipath propagation, some basic radio channel parameters are firstly reviewed.

- Delay Spread and Coherence Bandwidth

Delay Spread describes the time dispersive nature of the wireless propagation channel. It can be interpreted as the difference between the time of arrival of the earliest significant multipath component and the time of arrival of the latest multipath component. Delay spread limits the maximum data rate in an inter-symbol interference (ISI) free manner. ISI occurs when two symbols are transmitted with time interval smaller than the delay spread of the channel. Coherence Bandwidth is reciprocal to Delay Spread. It reflects approximate maximum bandwidth on which the channel is flat.

- Coherence Time and Doppler Spread

Coherence Time and Doppler Spread characterize the time varying nature of the propagation channel. Doppler Spread and Coherence Time are inversely proportional to one another. In most of the UWB scenarios mobility of a device is slight, therefore Doppler Spread is insignificant to system performance.

- Channel Impulse Response (CIR)

CIR is the time domain description of a radio propagation channel, whose Fourier transform is Channel Transfer Function (CTF). The continuous-time CIR for a multipath channel is given by

$$h(t,\tau)=\sum_{l}\alpha_l\delta(t-\tau_l), \tag{2.2}$$

where l is path index, t is the time variable, α_l denotes l-th path gain, and τ_l gives propagation delay of the l-th path, respectively. $\delta(\cdot)$ is Dirac delta function. In the digital communication analysis, normally discrete-time models are applied. Therefore the discrete-time CIR is driven. Let us assume that system have bandwidth W, and the sampling time $T_s = 1/W$. Substitute continuous time t with samples $t = m/W$. The discrete-time CIR is given by

$$h_i(m)=\sum_{l}\alpha_l \mathrm{sinc}\left(\frac{m}{W}-\tau_l\right), \tag{2.3}$$

with

$$\mathrm{sinc}=\frac{\sin(\pi t)}{\pi t}, \tag{2.4}$$

where h_i denotes the i-th channel tap of the discrete-time CIR, l is path index. There can be several paths fall into i-th tap and give main contribution to this tap.

Let us denote delay difference of adjacent path with $\Delta\tau = \tau_{i+1} - \tau_i$. Define two paths are unresolvable when their delay difference $\Delta\tau \le T_s$. In WiMedia UWB system, signal bandwidth is 528MHz [WiM09], and the corresponding tap space is less than 2 ns. The number of paths fall onto on channel tap is small. Again this mathematical model explains that the statically features of the UWB multipath propagation is different from a narrow band signal.

- Power Delay Profile (PDP)

PDP is defined as the squared magnitude of the CIR, averaged over the small-scale fading, and it is formulated as

$$P(\tau)=\mathrm{E}_t\left(\left|h(t,\tau)\right|^2\right). \tag{2.5}$$

where $\mathrm{E}_t(\cdot)$ is expectation function over time. The delay spread and power delay profile of UWB channel show quite different characters to the narrowband channel. In Figure 2.4 the PDP of the IEEE 802.15.3a reference channel, from CM1 to CM4 is shown. The character of the channels is analyzed in Section 2.3.1.

- Power Azimuth Spectrum (PAS)

The definition of Power Azimuth-Delay Spectrum of channel could be found in [Ped00],

$$P(\phi,\tau)=\mathrm{E}\left(\sum_{l}^{L}\left|a_l(t)\right|^2\delta\left(t-\tau_i(t)\right)\delta\left(\phi-\phi_l(t)\right)\right), \tag{2.6}$$

where $\mathrm{E}(\cdot)$ denotes expectation over time, and $|\cdot|$ denotes the absolute value of the argument. PAS is defined as the received signal power spectral density distribution over its arrival direction. It is the derived from integration of $P(\phi,\tau)$ over delay domain,

$$P_{\mathrm{A}}(\phi)=\int P(\phi,\tau)d\tau. \tag{2.7}$$

The PAS is useful in modeling spatial channel. In Section 2.3.2, the spatial UWB channel model is introduced. The typical PAS of the spatial channel measured in office environment in [Zha08] is adapted in Figure 2.3 to show the PAS property of UWB signal.

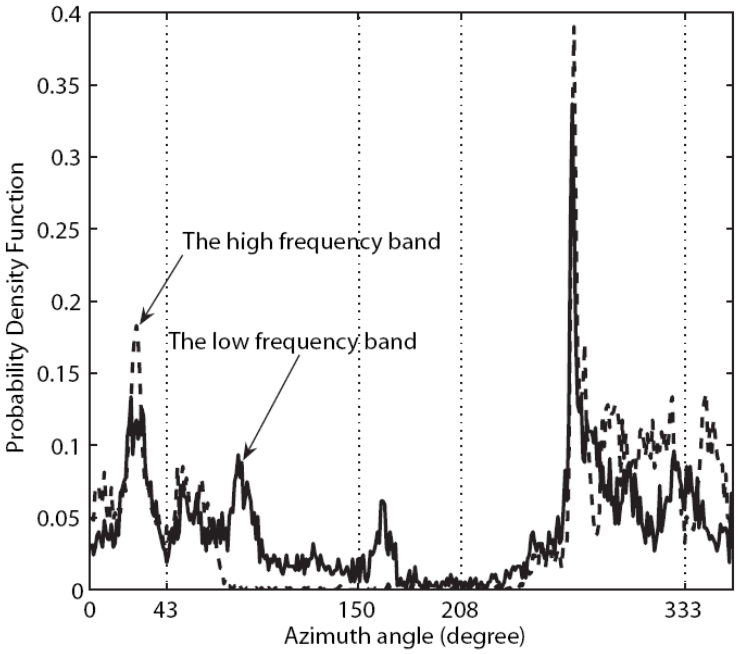

Figure 2.3 The probability density function of relative azimuth angle of arrival for LOS in office environment at the low frequency band from 3.1 to 4.85 GHz and high frequency band from 6.2 to 9.7 GHz. (Fig.6 from **[Zha08]**)

It is shown from the Figure 2.3 that, the Angle of Arrival (AoA) of the UWB signal is in cluster. Each peak of the curve denotes a main arrival direction of the signal. It is observed that there is strong branch signals come from the direction around 280° degree. This should be the LOS component. Signals from other direction are relative weak. They should arrive along the reflected or scattered paths [Zha08].

2.3 Multipath UWB Channel Model

There are typically two categories of methods describing the radio propagation channels. They are deterministic channel modeling and stochastic channel modeling [Ben06]. The classic method of deterministic modeling is Ray tracing. When complete information of the geometric and the electromagnetic properties of the surrounding are known, CIR can be predicted by Ray tracing. However it is with great computational complexity. The stochastic method models the typical properties of a wireless channel, without relating those properties to geometric information. For example, the Rayleigh or Rician distributions are used to describe the probability function of the envelope of the received narrowband signal.

In this section, the UWB channel based on S-V [Sal87] stochastic model is discussed, both the UWB channel without spatial and with spatial characters are presented.

2.3.1 S-V based UWB Channel

The S-V model [Sal87] was proposed as prototype for IEEE 802.15.3a reference channel [Foe03]. In S-V model the arrival of multipath signals are modeled as two-level, cluster arrival and ray arrival, cascaded Poisson process. One cluster is corresponding to a group of paths which arrive intensively one after the other, and after that there is a longer pause. One ray is the single path within the mentioned cluster. Figure 2.2 could be helpful to understand the so called cluster and ray.

A lognormal distribution is employed rather than a Rayleigh distribution for the gain of each channel tap, since UWB observations show that the lognormal distribution seems to better fit the measurement data [Foe03]. In addition, independent fading is assumed for each cluster as well as for each ray within the cluster. Therefore, the continuous-time CIR for the multipath UWB channel is given by,

$$h(t) = X\sum_{k=0}^{K-1}\sum_{l=0}^{L-1}\alpha_{k,l}\exp\left(\mathrm{j}\theta_{k,l}\right)\delta\left(t-T_l-\tau_{k,l}\right), \tag{2.8}$$

where T_l is the arrival time of the *l*-th cluster, $\tau_{k,l}$ is the delay of the *k*-th path relative to T_l. The phases $\theta_{k,l}$ are uniformly distributed in the range of $[0, 2\pi]$. The cluster arrival time and the ray arrival time are Poisson processes with arriving rate of Λ and λ, respectively.

$$\begin{aligned} p\left(T_l \mid T_{l-1}\right) &= \exp\left(-\Lambda\left(T_l - T_{l-1}\right)\right), l > 0 \\ p\left(\tau_{k,l} \mid \tau_{k-1,l}\right) &= \exp\left(-\lambda\left(\tau_{k,l} - \tau_{k-1,l}\right)\right), k > 0 \end{aligned} \tag{2.9}$$

$\alpha_{k,l}$ is the multipath gain coefficients of the *k*-th ray in the *l*-th cluster. When talking about lognormal distribution,

$$\log_{10}\left(\left|\alpha_{k,l}\right|^2\right) \sim \mathrm{N}\left(\mu_{k,l}, \sigma_1^2 + \sigma_2^2\right) \tag{2.10}$$

$\mathrm{N}\left(u, \sigma^2\right)$ describes a normal distribution. The mean value of $\alpha_{k,l}$ is $\mu_{k,l}$,

$$\mu_{k,l} = \frac{10\ln(\left|\overline{\alpha_{0,0}}\right|^2) - 10T_l / \Gamma - 10\tau_{k,l} / \gamma}{\ln(10)} - \frac{(\sigma_1^2 + \sigma_2^2)\ln(10)}{20}, \tag{2.11}$$

where $\left|\overline{\alpha_{0,0}}\right|^2$ the mean energy of the first path of the first cluster. The variance of $\alpha_{k,l}$ is $\sigma_1^2 + \sigma_2^2$. σ_1^2 and σ_2^2 are variance of the cluster decay ray decay process, respectively [IEE03]. *X* describes the log-normal shadowing fading of the total multipath, the standard deviation of X is denoted as σ_{SF}. For details of the S-V based UWB channel model please reference to [IEE03].

Based on (2.8), four different UWB channels are parameterized for indoor scenarios in [IEE03]. The parameters of the aforementioned random variables are listed in Table 2.1. There are at least the seven variables that are needed to describe the UWB multipath channel with the S-V model. The parameters are extracted from measurements mentioned in [IEE03]. CM1 channel model is based on LOS (0-4m) measurements, CM2 channel model is based on NLOS (0-4m) channel measurements, CM3 channel is also based on NLOS (4-10m) channel measurements, and CM4 channel model represents an extreme NLOS multipath channel [IEE03].

Table 2.1 Parameters of 802.15.3a reference channel **[IEE03]**

Parameter	CM1	CM2	CM3	CM4
Λ	0.0233	0.4	0.0667	0.0667
λ	2.5	0.5	2.1	2.1
Γ	7.1	5.5	14.00	24.00
γ	4.3	6.7	7.9	12
σ_1/dB	3.3941	3.3941	3.3941	3.3941
σ_2/dB	3.3941	3.3941	3.3941	3.3941
σ_{SF}/dB	3	3	3	3

Figure 2.4 represents the PDP of CM1, CM2, CM3 and CM4 with parameters listed in Table 2.1. The Y-axis represents the mean energy of MPCs in logarithmic scale, and the X-axis represents relative delay of the MPCs to the first arrival ray in the first arrival cluster in nanosecond. From Figure 2.4 one can get that the peak value of the PDP from CM2-CM4 does not appear at the firstly arrived path, which implies that the channel is NLOS, in contrast peak value the CM1 is at the firstly arrived path. From the PDP character, one can observe that the UWB channel shows quite different statically features with each other.

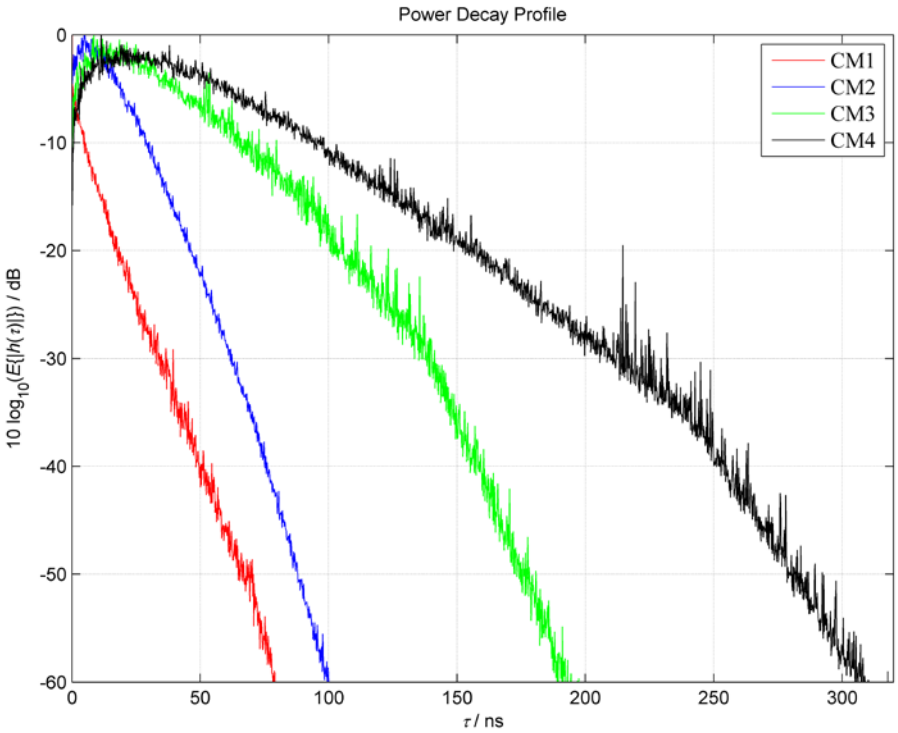

Figure 2.4 PDP of IEEE 802.15.3a reference Channel Model **[IEE03]**

2.3.2 Spatial UWB Channel

The conventional S-V UWB channel model in (2.8) could represent the multipath effects in a SISO system with the CIR. When examining the multiple antenna systems, the spatial features of the channel are also interested in modeling MIMO UWB channel. The spatial UWB channel, also termed as direction selective UWB channel in [Ali07], can be represented by the Directional CIR (DCIR),

$$h(\tau,t,\varphi) = X\sum_{l=1}^{L}\sum_{k=1}^{K_l}\alpha^{(k,l)}\exp\left(\mathrm{j}\theta_{k,l}\right) \delta\left(t-T_l-\tau_{k,l}\right)\delta\left(\varphi-\Phi_l-\varphi_{k,l}\right) \tag{2.12}$$

Compared with (2.8), the direction selectivity character is introduced to the channel by Dirac delta $\delta\left(\varphi-\Phi_l-\varphi_{k,l}\right)$ in Azimuth domain. This model was firstly proposed in [Spe00]. The Power Azimuth-Delay Spectrum depicted in (2.6) could be understood as the expectation of DCIR over time. In Figure 2.5 the DCIR of one realization of IEEE 802.15.3a CM3 channel generated with Spatial Mobile Channel (SMC) generation tool [Bla98] is presented. The Z-axis of

represents the amplitude of the DIR of the channel realization. X-axis repents the AoA of the path, and the Y-axis repents the delay feature of the path in the channel realization. From the DICR of this channel realization, one can observe that the main path of the multipath propagation comes from around -150 Degree.

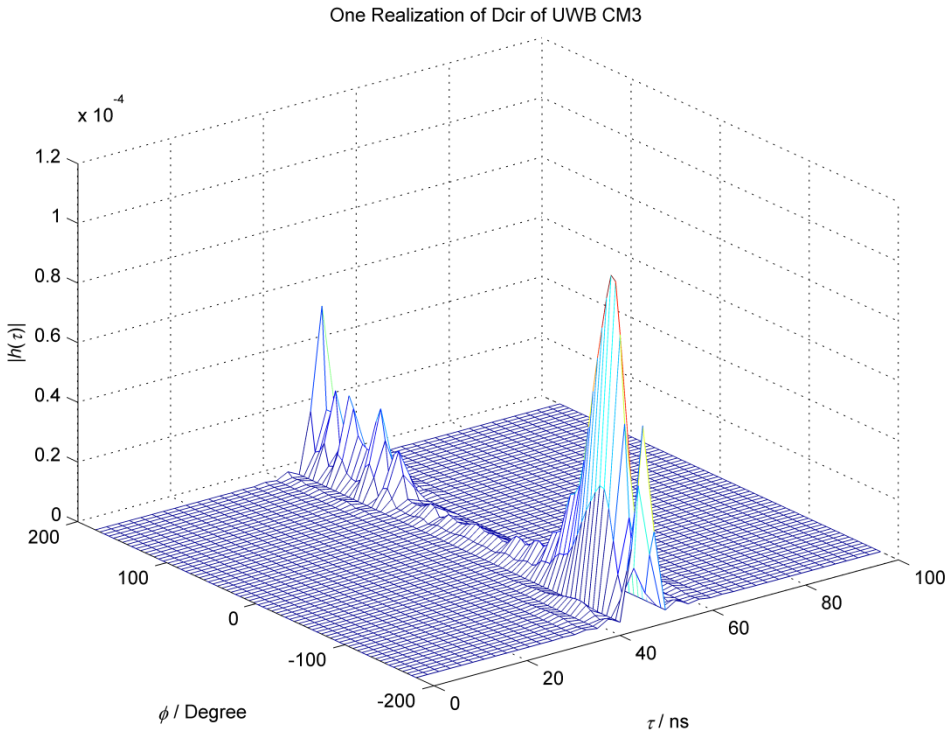

Figure 2.5 DCIR of UWB radio propagation channel (adapted from the IEEE 802.15.3a CM3 channel)

2.4 UWB Channel Parameterization in Specific Scenarios

The IEEE 802.15.3a reference channels are only suitable to indoor environments. In Section 1.1.2.1 it has been shown that there are a lot of applications for UWB in wide range scenarios. For instance the public traffic scenarios, and automotive environments. These UWB applications are close to our life and arouse great interests to both industry and academic. A realistic channel model for these environments must be based on field measurements. In this chapter, extracted from the measurements data, the UWB channel based on S-V channel model in automotive and airplane in cabin environment are parameterized.

The UWB channel parameters are extracted from the measurements in the frame of EUWB project and another industry financed project carried out by the project partners. The extracted parameters are used to generate UWB channel in the specific scenarios with the SMC tool [Bla98].

2.4.1 Automotive Scenario

The measurements of UWB channel in automotive environments were carried out and reported in [Gai09]. The parameters of the S-V channel model extracted from the measurement are listed in Table 2.2 . There are five different scenarios listed in Table 2.2, which are labeled from CM8201 to CM8025. The five scenarios belong to three different applications proposed in the automotive scenarios in [Gai09]. They are localization of a dedicated tag, detection and localization of passive non-cooperative objects, and two-way data communication.

CM8201-CM8203 is the channel for localizing a dedicated tag. UWB channels are measured between a mobile tag and an anchor node which is mounted to the car. CM8201 describes the scenario where mobile tag is inside a car in open space, CM8202 describes the channel when tag is outside the car in open space, and CM8203 depicts channel when tag is outside a car in a garage [Gai09] . CM8204 is the channel for detection and localization of passive non-cooperative objects application. Channel is measured between anchor nodes when there is intruder approaching, for instance when there is human coming from rear or side of the car, the channel between anchor nodes are affected [Gai09]. CM8205 is the channel measured in two-way data communication applications. Channel between stationary UWB nodes in the motor space and the cabin of the car [Gai09].

Figure 2.6 represents the PDP of the modeled channel from CM8201 to CM8205. It is shown that the CM8202 and CM8203 should have big delay spread. Since CM8202 and CM8203 the tag are outside of the car, and the signal undergoes more complicated channel from the anchor node mounded inside the car and the tag outside of the car. Compared with the indoor channel model shown in Figure 2.4, the UWB channel in automotive shows larger delay spread property. One reason to the large delay spread is the relative compact space of the car cabin and the metal material. Another reason comes from the surroundings of the car, when in the garage or along the street, there are also some unpredictable obstacles. In addition, the channel is time variant due to the mobility of devices during the measurements, specially the CM8204 channel. This also makes the channel in automotive more complicated than the indoor environment.

Table 2.2 Parameters for scenarios in Automotive Environment **[Gai09]**

Parameters	CM8201	CM8202	CM8203	CM8204	CM8205
Λ	0.0212	0.0226	0.014	0.0144	0.0143
λ	3.5985	3.1625	2.2487	2.5901	4.3032
Γ	11.2	22.8	14.9	8.2	8.1
γ	5.8	8.3	14.9	5.6	8.1
σ_1/dB	3.3941	3.3941	3.3941	3.3941	3.3941
σ_2/dB	3.3941	3.3941	3.3941	3.3941	3.3941
σ_{SF}/dB	3	3	3	3	3

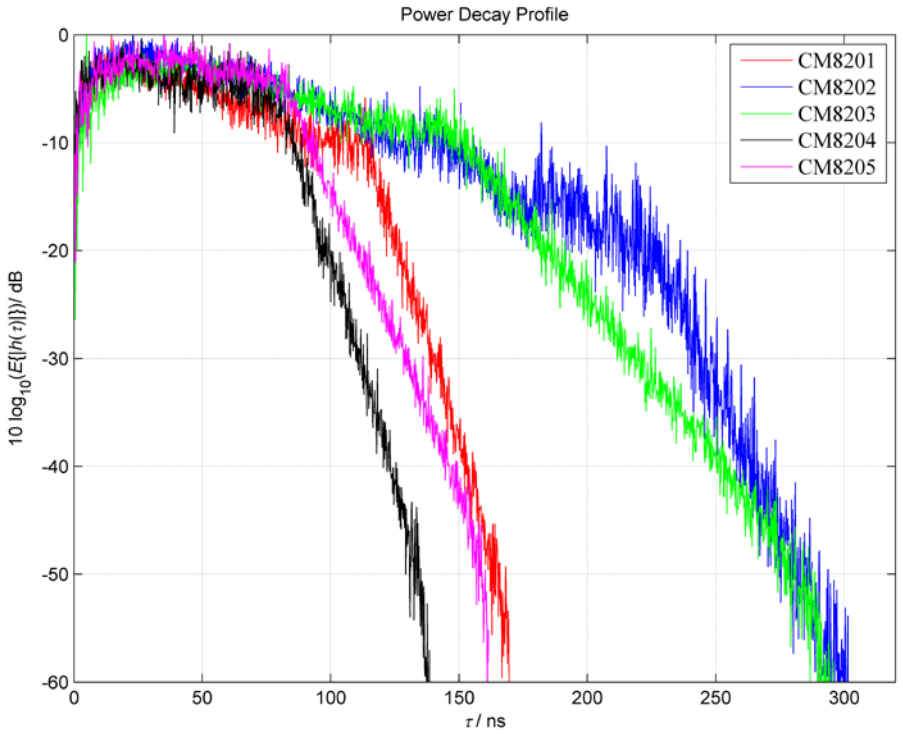

Figure 2.6 PDP of CM8201-CM8205 channel in Automotive Environment

2.4.2 Airplane In-cabin Scenario

The UWB channel model in airplane In-cabin is carried out in frame of an industry partner supported project. Similar to the parameterization in the automotive enrolments, the parameters of the UWB channel are extracted from the field measurements in Airbus A380 airplane cabins. The parameterization has been reported in [Bur09]. Some selected parameters are listed in Table 2.3.

Table 2.3 Selected Parameters Airplane in-cabin UWB Channel

Parameters	LOS	NLOS
Number of clusters	37	37
Λ	0.23 ns	0.22 /ns
Γ	4.82 ns	6 ns
γ	0.68 ns	0.48 ns

In Figure 2.7 the PDP of the emulated UWB channel with S-V model and the parameters list in Table 2.3 for the LOS and for the NLOS scenarios in an empty AIRBUS A380 cabin are shown. The PDP obtained by the S-V channel model is compared to the measured one. A good match between simulated and measured PDPs can be observed. Compared with the PDP of IEEE 802.15.3a indoor channel model CM1, the LOS UWB channel in AIRBUS A380 shows larger delay spread, even both are LOS scenarios. This is caused by the dimension difference between the airplane cabin and the office. The dimension of airplane cabin is narrower and lower than that of an ordinary office, and it is more like a long and narrow tunnel. The refection is severer by the airplane bulkhead than the wall in an office. Besides, the dense passenger seats could also introduce plenty of scatterings. However, the PDP shows less time dispersion than in the automotive environment. Since the measurement is carried out in an empty airplane, for real scenarios, when hundreds of passengers are on board, the In-cabin UWB channel should have severe multipath phenomena.

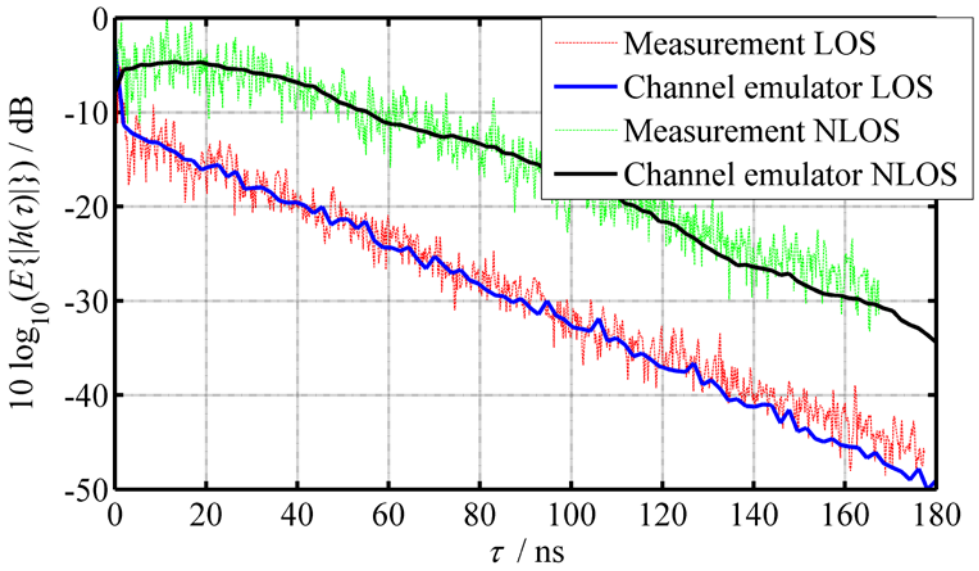

Figure 2.7 PDP in empty Airplane Cabin

2.5 Chapter Summary

In this chapter, the UWB propagation channel characters are examined, and the S-V based multipath UWB channel model is studied. The spatial UWB channel is also discussed. In addition, the UWB channel for specific scenarios, such as automotive environment and airplane In-cabin environment are parameterized and analyzed. These results are useful to the performance evaluation and network design for UWB applications in these specific scenarios.

This chapter is the basic of the study in the coming chapters, for instance in Chapter 4, based on the deep understating of the UWB channel features, the fine ToA detection method of OFDM UWB signal is invented.

Chapter 3

MB-OFDM UWB Systems

3.1 Chapter Overview

In this chapter, the WiMedia MB-OFDM UWB physical layer is reviewed firstly. The specific PHY technologies in the WiMedia UWB system, such as Dual Carrier Modulation (DCM), Zero-Padding Suffix OFDM (ZPS-OFDM) are presented. Then two technologies that are dedicated to improving transmission quality of OFDM systems, the FFH/OFDM scheme and multiple antenna technology, are examined.

Finally a combination of the FFH/OFDM and Alamouti SFBC schemes in a multiple antenna MB-OFDM UWB system is designed. The proposed SFBC-FFH/OFDM scheme is able to exploit the spatial and frequency diversity simultaneously in one OFDM symbol period, and introduces good performance enhancement to the MB-OFDM UWB systems. In addition to the good performance gain, the implementation complexity of proposed SFBC-FFH/OFDM scheme is comparable to the conventional Alamouti SFBC scheme.

The left of the chapter is organized as follows. In Section 3.2, physical layer of WiMedia UWB are briefly reviewed. In Section 3.3, the FFH/OFDM and multiple antenna technologies in OFDM systems are introduced in general. In Section 3.4, the SFBC-FFH/OFDM scheme is designed and evaluated. Section 3.5 summarizes this chapter.

3.2 WiMedia MB-OFDM UWB Physical Layer

3.2.1 WiMedia UWB Overview

In WiMedia UWB specifications, PHY layer, MAC layer and WiMedia Logic Link Control Protocol (WLP) for short range UWB radio communication systems are defined. In this study only the PHY specifications are interested.

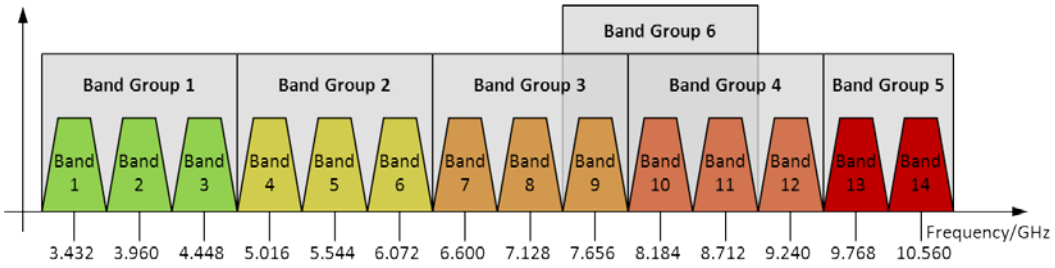

Figure 3.1 WiMedia UWB Bands and Band Groups **[WiM11]**

In WiMedia UWB's PHY specification, the physical layer technologies in baseband and radio frequency are defined. The utilized unlicensed frequency band (3.1 GHz~10.6 GHz) is divided into 14 bands, each with bandwidth of 528 MHz. The first twelve bands are grouped into fours band groups, each consists of three bands. The last two bands are grouped into the fifth band group, and band nine to band eleven forms the sixth band group. The bands and band groups of WiMedia UWB are illustrated in Figure 3.1.

WiMedia UWB PHY is based on OFDM modulation technique, whose sampling rate is 528 MHz and the number of subcarriers is 128. Out of which, 100 are data subcarriers, 10 are guard subcarriers, and 12 are pilot subcarriers, the left 6 are null tones. The separation between two neighboring subcarriers is 4.125MHz. Instead of cyclic prefix (CP) added to the front of each OFDM symbol after IDFT, ZPS with length of 37 samples is added to the end of each OFDM symbols to protect the signal from being destroyed by Inter Symbols Interference (ISI) caused by the multipath propagation. Therefore the total length of one ZPS-OFDM symbol is 165 samples, or 312.5 nana seconds. Some of the data rate dependent OFDM parameters of the WiMedia UWB are listed in Table 3.1.

Table 3.1 OFDM Parameters of WiMedia UWB **[WiM09]**

Parameter	Description	Value
f_s	Sampling rate	528MHz
Δf	Subcarrier frequency spacing	4.125MHz
N_{FFT}	Total number of subcarriers(FFT size)	128
T_{FFT}	IFFT and FFT period	242.42 ns
N_{ZPS}	Number of samples in ZPS	37
T_{ZPS}	Zero-padded suffix duration in time	70.08 ns
N_{sys}	$N_{FFT} + N_{ZPS}$	165

One of the most important characters of the MB-OFDM UWB is the multiple band time frequency hopping scheme. The hopping patterns are defined by the TFC in [WiM09]. In Figure 3.2 a WiMedia UWB packet transmitted over band group one with TFC 1 hopping pattern is illustrated. In [WiM09], 10 different hopping patterns are defined. With the time frequency hopping pattern specified by TFC 1, the first OFDM symbol is transmitted on the band 1, the second OFDM symbol on band 2, and the third OFDM symbol on band three. The process is repeated from the fourth OFDM symbol. This time frequency hopping scheme keeps the baseband sampling rate of 528 MHz and allows three times instantaneous transmit power, while the average transmitter power is still under the limit of the FCC specification. With this time frequency hopping pattern of TFC 1, 5 dB average transmitter power incensement compared with single band transmission is obtained. From the implementation point of view, the receiver should be fast enough to track the central frequency shift, and switch the local clock to the corrected one. All these signal processing should be finished within 9.47 ns or five sample length [Hei08].

A WiMedia UWB packet consists of three parts, Physical Layer Convergence Protocol (PLCP) preamble, PLCP header, and the payload. PLCP preamble is used to aid the receiver in timing synchronization, carrier-offset recovery, and channel estimation [WiM09]. PLCP preamble consists of synchronization

sequence and channel estimation sequence. Synchronization sequence is defined in time domain, and is real value sequence. It has length of 24 OFDM symbols (standard PLCP preamble) or 12 OFDM symbols (burst PLCP preamble). Channel estimation sequence is designed as frequency symbols, and it has duration of 6 OFDM symbols. PLCP header contains important information about the PHY and the MAC layer, which helps the receiver to decode the payload. For reliable transmission, it is firstly protected by Reed-Solomon code, and then transmitted with the lowest physical data rate (53.3Mbit/s) of WiMedia UWB.

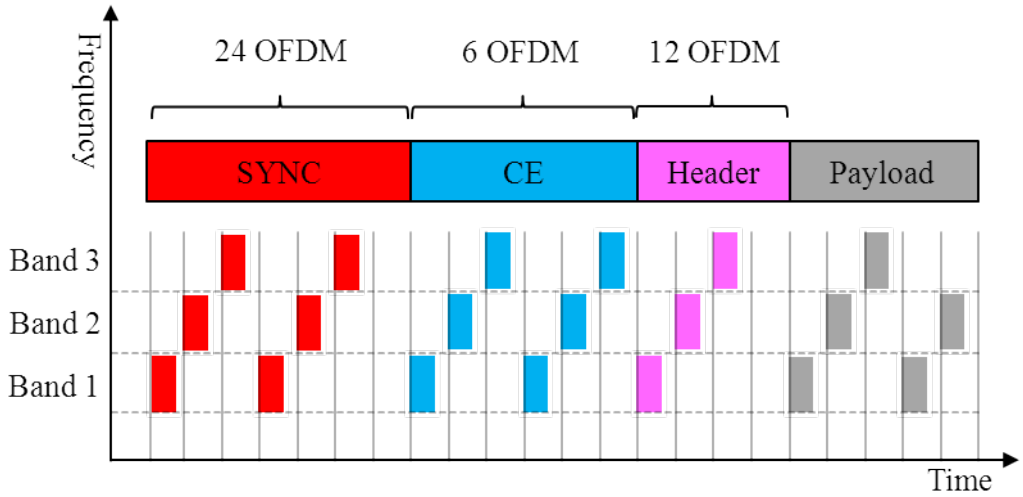

Figure 3.2 Example realization of transmitted RF signal using three bands

There are twelve available data rates from 53.3 Mbit/s up to 1024 Mbit/s proposed in the WiMedia UWB PHY specification [WiM09]. Support for transmitting and receiving data rates of 53.3 Mbit/s, 106.7 Mbit/s and 200 Mbit/s using convolutional code is mandatory [WiM09]. Compared with the former version PHY specification which has been standardized in ECMA-368 [ECM05], LDPC channel coding and Modified DCM (MDCM) modulation are newly supplemented in [WiM09]. With these modifications, data rates higher than 480 Mbit/s are possible. This enables the WiMedia UWB support high data rate transmission up to 1Gbit/s for distances around two meters.

3.2.2 Transmitter Structure

The diagram in Figure 3.3 illustrates the basic signal processing stages of the transmitter chain in the WiMedia UWB PHY. There are several stages in the transmitter chain from the information bits input to the radio frontend (RF). They

are channel coding module, interleaver module, constellation mapping module, OFDM transmitter module, Digital to Analog (D/A) converter and RF module.

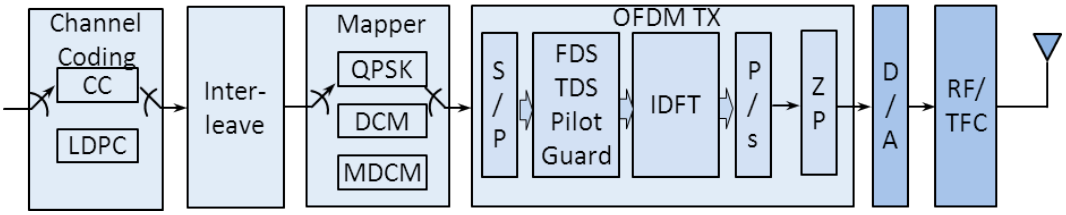

Figure 3.3 Diagram of Transmitter Chain for a WiMedia MB-OFDM

3.2.2.1 Channel Coding

Convolutional Code and LDPC are proposed in WiMedia UWB PHY [WiM09]. The Convolutional Code has basic code rate of 1/3 and with constrain length of 7 bits. Its generator polynomial is, $g_0 = 133_8$, $g_1 = 165_8$, and $g_2 = 171_8$ [WiM09]. More code rates, such as 1/2, 5/8 and 3/4 are achieved by puncturing the coded data with the basic code rate 1/3. In [WiM09] LDPC code is also proposed, with code rate 1/2, 3/4, 5/8, and 4/5, and the codeword has constant length with 1200 bits. LDPC code is a near Shannon limit channel code, and it is more powerful than convolutional code. Performance gain of up to 4 dB compared to the convolutional code is achieved by LDPC is reported [Bra07]. For details of the channel coding, please refer to Section 6.7 and 6.11 of [WiM09].

3.2.2.2 Interleaver

For data rates that use Convolutional Code, the coded and padded bit stream shall be interleaved prior to modulation to provide robustness against burst errors. The bit interleaving operation is performed in three distinct stages: symbol wise block interleaving, Intra-symbol tone interleaving, and Intra-symbol cyclic shifts. For details of the bit interleaving, please refer to Section 6.8 of [WiM09].

3.2.2.3 Constellation Mapping

There are three types of constellation mappings in WiMedia UWB PHY, namely, Quadrature Phase Shift Keying (QPSK), DCM and MDCM. For data rate 200 Mbits/s and lower, the interleaved coded binary bits shall be mapped to QPSK constellation. For data rate 320, 400 and 480 Mbits/s, the binary data shall be

mapped to DCM constellation. For data rate 640 Mbits/s and higher, the binary bits shall be mapped to MDCM constellation.

When mapping coded bits to QPSK, bits to QPSK symbol mapping are performed according to the Gray-coded constellation as

$$\underline{X}_k = \frac{1}{\sqrt{2}}\left(c_{2k} + \mathrm{j}c_{2k+1}\right), \quad k = 0,1,2\cdots \tag{3.1}$$

where $c_{2k}, c_{2k+1} \in \{+1,-1\}$, and $\underline{X}_k$ denotes the QPSK complex symbol.

When mapping coded bits to DCM symbol, every 200 coded binary bits are grouped into 50 groups, and each group forms a four bits vector [WiM09]

$$\left(c_{g(k)}, c_{g(k)+1}, c_{g(k)+50}, c_{g(k)+51}\right), \tag{3.2}$$

where

$$g(k) = \begin{cases} 2k, k \in [0,24] \\ 2k+50, k \in [25,49] \end{cases} \tag{3.3}$$

Each vector shall be mapped to two 16-QAM constellation symbols according to

$$\begin{bmatrix} \underline{X}_k \\ \underline{X}_{k+50} \end{bmatrix} = \frac{1}{\sqrt{10}} \begin{bmatrix} 2 & 1 \\ 1 & -2 \end{bmatrix} \begin{bmatrix} c_{g(k)} + \mathrm{j}c_{g(k)+50} \\ c_{g(k)+1} - \mathrm{j}c_{g(k)+51} \end{bmatrix}, k \in [0,49] \tag{3.4}$$

$\underline{X}_k$ denotes a DCM complex symbol that are modulated to the *k*-th subcarrier of OFDM. Finally 100 DCM complex symbols are generated from the 200 bits.

When mapping the coded bits to MDCM, each 400 bits are group into 50 groups, and each group is an eight bits vector, $\left(c_{8\times k}, \ldots c_{8\times k+7}\right)$. Intermediate value x_{a} is generated by the first four bits of the vector, and intermediate x_{b} is generated by the last four bits of the vector. Mapping from bits to intermediate value could refer to the looking up table in Table 3.2 [WiM09]. Each eight bits vector is mapped to two 256-QAM constellation symbols according to

$$\begin{bmatrix} \underline{X}_k \\ \underline{X}_{k+50} \end{bmatrix} = \frac{1}{\sqrt{170}} \begin{bmatrix} 4 & 1 \\ 1 & -4 \end{bmatrix} \begin{bmatrix} x_a \\ x_b \end{bmatrix}, k = 0, \ldots, 50. \tag{3.5}$$

Two symbols $\underline{X}_k$, $\underline{X}_{k+50}$ are therefore generated from the 8 coded bits. There are altogether 100 MDCM complex symbols generated from the 400 coded bits.

Table 3.2 Intermediate value looking up table **[WiM09]**

Bits	Symbol	Bits	Symbol	Bits	Symbol	Bits	Symbol
0000	-3-3j	0100	-1-3j	1000	3-3j	1100	1-3j
0001	-3-1j	0101	-1-1j	1001	3-1j	1101	1-1j
0010	-3+3j	0110	-1+3j	1010	3+3j	1110	1+3j
0011	-3+1j	0111	-1+1j	1011	3+1j	1111	1+1j
0000	-3-3j	0100	-1-3j	1000	3-3j	1100	1-3j
0001	-3-1j	0101	-1-1j	1001	3-1j	1101	1-1j

3.2.2.4 Zero-Padded Suffix OFDM

After constellation symbol mapping, the complex symbols are modulated to OFDM subcarriers. For the data rate services lower than 200 Mbits/s, Time Domain Spreading (TDS) and Frequency Domain Spreading (FDS) are introduced during the OFDM modulation. They introduce the redundancy in time domain and frequency domain to improve the transmission reliability. For the date rate of 320 Mbits/s and higher, no TDS or FDS is exploited. However one can observe from (3.4) and (3.5) that redundancy is introduced implicitly by DCM and MDCM.

To facilitate single-tap equalization as in regular OFDM, the deployment of ZPS in WiMedia UWB specification is proposed. Comparison between CP-OFDM and ZPS-OFDM could be found in [Muq02]. CP-OFDM is able to deal with ISI caused by multipath propagation by simply copy some samples in end of an OFDM symbol in to the front. However CP-OFDM causes ripples in the average power spectral density, which is not expected due to the strict emission constrains of UWB radio. Another drawback CP-OFDM is that symbol transmitted on the certain subcarrier cannot be recovered when it is hit by a channel zero (gain of this subcarrier is zero) [Muq02]. This limitation leads to a loss in frequency diversity.

When ZPS-OFDM is used, the ripples in the PSD can be reduced to zero, and the channel zero problem could also be overcome [Muq02].

3.2.3 Receiver Structure

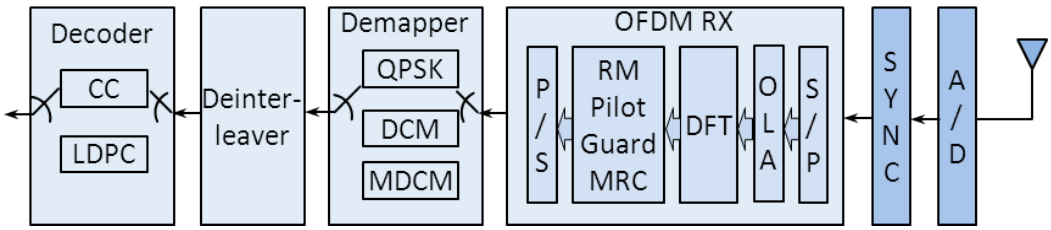

Figure 3.4 Diagram of Receiver chain structure for WiMedia UWB

The receiver chain of the WiMedia UWB system is an inverse process of the transmitter chain. The block diagram in Figure 3.4 represents the signal receiving process. The synchronization of MB-OFDM is a little more complicated than a conventional OFDM system where no time frequency hopping scheme is applied, since the receiver must detect the TFCs pattern applied to the received single from the synchronization sequence. In [Chi07] and [YeZ08] the synchronization of MB-OFDM is studied. In Section 5.2.2 the basics of the synchronization and channel estimation are introduced. After the signal is synchronized, an overlap–add scheme (OLA) shall be applied before the received samples sent to an OFDM demodulator. Principle idea of the OLA is, the first sample of the ZPS is added to the first sample of the OFDM symbol, the second sample of the ZPS to the second sample to the OFDM, and so forth. As long as the impulse response of the channel is shorter than ZPS length, this process recovers the energy loss to the filtering process. Further information of ZPS-OFDM receiver could be found in [Muq02] [Hei08].

3.2.4 Discrete-time baseband Model for OFDM UWB

Let the binary information to be transmitted in form of the data vector be

$$\boldsymbol{u} = \left(u_1, u_2 \cdots u_{\mathrm{N_s}}\right)^{\mathrm{T}}, \quad u_{\mathrm{n_s}} = \{1, 0\}, \; n_{\mathrm{s}} = 1 \cdots \mathrm{N_s}. \tag{3.6}$$

The generated information bits has length of $\mathrm{N_s}$, and encoded by either Convolutional encoder or LDPC encoder with code rate R_{c}, resulting in code bit streams comprising $N_{\mathrm{c}} = N_{\mathrm{s}}/R_{\mathrm{c}}$ coded bits $c_{\mathrm{n_c}}$, $n_{\mathrm{c}} = 1 \cdots N_{\mathrm{s}}/R_{\mathrm{c}}$.

$$\boldsymbol{c} = \left(c_1, c_2 \cdots c_{\mathrm{N_c}}\right)^{\mathrm{T}}, \quad c_{\mathrm{n_c}} = \{1, -1\}, \; n_{\mathrm{c}} = 1 \cdots \mathrm{N_s}/R_{\mathrm{c}} \tag{3.7}$$

The energy of uncoded bit equals to E_{b}, and energy of encoded bit is $E_{\mathrm{b}}R_{\mathrm{c}}$.

After constellation mapping (QPSK, DCM or MDCM), the complex symbols are grouped into consecutive frame, indexed by n, $n \in$. Let the transmitted energy of each symbol be E_{s}, and each data frame contains N_{D} complex symbols is given by

$$\underline{\boldsymbol{X}} = \left(\underline{X}_1, \underline{X}_2 \cdots \underline{X}_{N_{\mathrm{D}}}\right)^{\mathrm{T}}. \tag{3.8}$$

After inserting pilots and guard symbols, the data vector $\underline{\boldsymbol{d}}$ with length N_{FFT} is presented to the OFDM modulator like

$$\underline{\boldsymbol{d}}^{(n)} = \left(\underline{d}_0, \underline{d}_1 \cdots \underline{d}_{N_{\mathrm{FFT}}-1}\right)^{\mathrm{T}}. \tag{3.9}$$

Detail information of the pilot and guard mapping process can be found in [WiM09]. The *n*-th OFDM symbol is then given by

$$\underline{\boldsymbol{b}}^{(n)} = \underline{\boldsymbol{D}}\underline{\boldsymbol{d}}^{(n)}, \tag{3.10}$$

with its *l*-th element

$$\underline{b}_l^{(n)} = \sum_{k=0}^{N_{\mathrm{FFT}}-1} d_k^{(n)} \exp\left(\frac{\mathrm{j}2\pi kl}{N_{\mathrm{FFT}}}\right), k, l = 0, \cdots N_{\mathrm{FFT}} - 1. \tag{3.11}$$

$\underline{\boldsymbol{D}}$ is defined as the Inverse Discrete Fourier Transform (IDFT) matrix,

$$\underline{\boldsymbol{D}} = \frac{1}{\sqrt{N_{\mathrm{FFT}}}} \begin{bmatrix} 1 & 1 & \cdots & 1 \\ 1 & \exp\left\{\mathrm{j}2\pi \frac{1}{N_{\mathrm{FFT}}} \cdot 1\right\} & \cdots & \exp\left\{\mathrm{j}2\pi \frac{1}{N_{\mathrm{FFT}}} \cdot \left(N_{\mathrm{FFT}} - 1\right)\right\} \\ \vdots & \vdots & \ddots & \vdots \\ 1 & \exp\left\{\mathrm{j}2\pi \frac{N_{\mathrm{FFT}} - 1}{N_{\mathrm{FFT}}} \cdot 1\right\} & \cdots & \exp\left\{\mathrm{j}2\pi \frac{N_{\mathrm{FFT}} - 1}{N_{\mathrm{FFT}}} \cdot \left(N_{\mathrm{FFT}} - 1\right)\right\} \end{bmatrix}. \tag{3.12}$$

The columns of $\underline{\boldsymbol{D}}$ are associated with a particular subcarrier, and the rows of $\underline{\boldsymbol{D}}$ refer to the sampling time. Since $\underline{\boldsymbol{D}}$ is a unitary matrix, its inverses matrix (DFT matrix) is given by $\underline{\boldsymbol{D}}^{-1} = \underline{\boldsymbol{D}}^{\mathrm{H}}$.

The $\underline{\boldsymbol{b}}^{(n)}$ is then serialized to obtain the time-domain symbols, and N_{zp} trailing zeros are padded, yielding a $N_{\mathrm{SYS}} \times 1$ transmit vector $\underline{\tilde{\boldsymbol{b}}}^{(n)}$ as

$$\begin{aligned}\underline{\tilde{\boldsymbol{b}}}^{(n)} &= \left(\underline{b}_1^{(n)}, \underline{b}_2^{(n)} \cdots \underline{b}_{N_{\mathrm{FFT}}}^{(n)}, \underbrace{0, 0 \cdots 0}_{N_{\mathrm{zp}}}\right)^{\mathrm{T}} \\ &= \begin{pmatrix} \underline{\boldsymbol{D}} & \mathbf{0} \\ \mathbf{0} & \mathbf{0} \end{pmatrix} \begin{pmatrix} \underline{\boldsymbol{d}}^{(n)} \\ \mathbf{0} \end{pmatrix} \\ &= \underline{\boldsymbol{D}}_{\mathrm{zp}} \underline{\boldsymbol{d}}_{\mathrm{zp}}^{(n)}.\end{aligned} \tag{3.13}$$

The signal $\underline{\tilde{\boldsymbol{b}}}^{(n)}$ is the OFDM symbols with ZPS, and it is transmitted over UWB propagation channel to the receiver. The channel impulse response (CIR) of the L tap channel after padded with zero to an $N_{\mathrm{FFT}} \times 1$ column vector is given by

$$\underline{\boldsymbol{h}}^{(n)} = \left(\underline{h}_0^{(n)}, \underline{h}_1^{(n)}, \ldots, \underline{h}_{L-1}^{(n)}, 0, \ldots, 0\right)^{\mathrm{T}}. \tag{3.14}$$

Let $\underline{\boldsymbol{H}}_{\mathrm{t}}^{(n,k)}$ denote the $N_{\mathrm{FFT}} \times N_{\mathrm{FFT}}$ circular convolutional matrix of the multi-path channel after OLA operation in the receiver. It is a Toeplitz matrix and is always guaranteed to be invertible.

$$\underline{\boldsymbol{H}}_{\mathrm{t}}^{(n)} = \begin{bmatrix} \underline{h}_0^{(n)} & 0 & \cdots & 0 & 0 & \underline{h}_{\mathrm{L}-1}^{(n)} & \cdots & \underline{h}_1^{(n)} \\ \underline{h}_1^{(n,k)} & \underline{h}_0^{(n)} & 0 & \cdots & 0 & 0 & \ddots & \vdots \\ \vdots & \underline{h}_1^{(n)} & \underline{h}_0^{(n)} & 0 & 0 & \cdots & 0 & \underline{h}_{\mathrm{L}-1}^{(n)} \\ \underline{h}_{\mathrm{L}-1}^{(n)} & \ddots & \underline{h}_1^{(n,k)} & \ddots & \vdots & \cdots & 0 & 0 \\ 0 & \underline{h}_{\mathrm{L}-1}^{(n)} & \ddots & \ddots & \underline{h}_0^{(n)} & \cdots & \ddots & 0 \\ \vdots & 0 & \underline{h}_{\mathrm{L}-1}^{(n)} & \ddots & \underline{h}_1^{(n,k)} & \underline{h}_0^{(n)} & 0 & 0 \\ \vdots & \vdots & 0 & \ddots & \ddots & \ddots & \ddots & 0 \\ 0 & 0 & \cdots & 0 & \underline{h}_{\mathrm{L}-1}^{(n)} & \cdots & \underline{h}_1^{(n)} & \underline{h}_0^{(n)} \end{bmatrix}^{\mathrm{T}} \tag{3.15}$$

$\underline{\boldsymbol{H}}_{\mathrm{f}}^{(n,k)}$ is the CTF matrix of the multipath channel, and it is a $N_{\mathrm{FFT}} \times N_{\mathrm{FFT}}$ diagonal matrix, whose diagonal entries are DFT of (3.14). Since subcarriers of an OFDM symbols are orthogonal to each other, only diagonal entries are none zero.

$$\underline{\boldsymbol{H}}_{\mathrm{f}}^{(n)} = \begin{bmatrix} \underline{H}_{\mathrm{f},0}^{(n)} & 0 & \cdots & 0 \\ 0 & \underline{H}_{\mathrm{f},1}^{(n)} & \cdots & 0 \\ \vdots & \vdots & \ddots & \vdots \\ 0 & 0 & \cdots & \underline{H}_{\mathrm{f},\mathrm{N_{FFT}}}^{(n)} \end{bmatrix} \tag{3.16}$$

3.3 Enhancement to MB-OFDM UWB

3.3.1 Principle Idea

As already discussed in Section 1.2, different techniques could be adapted to MB-OFDM UWB systems to improve the transmission quality and extend communication range, such as advanced channel coding (Turbo Code and LDPC Code), FFH/OFDM and multiple antenna technologies. The actual channel coding schemes are already approaching Shannon channel capacity limit. Therefore we will not investigate channel coding in this work. The FFH/OFDM and aultiple antenna technologies are studied in this section.

FFH/OFDM is introduced in 3.3.2, and different MIMO technologies for exploration of spatial diversity are viewed in Section 3.3.3. Then the potential improvements by combining the FFH/OFDM and multiple antenna technology are discussed in Section 3.3.4. The SFBC Alamouti scheme is chosen to jointly design with FFH/OFDM in a multiple antenna MB-OFDM UWB system.

3.3.2 FFH/OFDM

The FFH/OFDM scheme was first proposed in [Sch05]. It is a good strategy to achieve frequency diversity in frequency selective channel within one OFDM symbol period. The first study introducing FFH/OFDM scheme in WiMedia UWB system is found in [Ber071]. The FFH/OFDM shows good performance compared with the conventional OFDM in the WiMedia UWB system. In what follows, the concept of FFH/OFDM is introduced, and the statistical character of the received signal SNR with FFH/OFDM scheme and a conventional OFDM is analyzed.

Frequency hopping inherits the potential to either provide interferer diversity or frequency diversity or both [Bru04]. In order to mathematically model FFH/OFDM, we shall set out from the standard IDFT matrix in (3.12). When

FFH/OFDM is applied, the frequency of the *m*-th subcarrier associated with a particular data symbol $d_m^{(n)}$ changes every T_s second within one OFDM modulation. Therefore, the frequency of this particular subcarrier is not modulated by fixed, but rather a function of the time instant, denoted by $l = 0 \cdots N_{\mathrm{FFT}} - 1$ [Bru04]. Let denote the frequency associated with this particular subcarrier m at time l as $\left[\boldsymbol{\Phi}\right]_{l,m}$, $l = 0 \cdots N_{\mathrm{FFT}} - 1$. The real-valued $N_{\mathrm{FFT}} \times N_{\mathrm{FFT}}$ FFH patterns matrix is then given to present the frequency information,

$$\boldsymbol{\Phi} = \begin{pmatrix} \left[\boldsymbol{\Phi}\right]_{0,0} & \left[\boldsymbol{\Phi}\right]_{0,1} & \cdots & \left[\boldsymbol{\Phi}\right]_{0,N_{\mathrm{FFT}}-1} \\ \left[\boldsymbol{\Phi}\right]_{1,0} & \left[\boldsymbol{\Phi}\right]_{1,1} & \cdots & \left[\boldsymbol{\Phi}\right]_{1,N_{\mathrm{FFT}}-1} \\ \vdots & \vdots & \ddots & \vdots \\ \left[\boldsymbol{\Phi}\right]_{N_{\mathrm{FFT}}-1,0} & \left[\boldsymbol{\Phi}\right]_{N_{\mathrm{FFT}}-1,1} & \cdots & \left[\boldsymbol{\Phi}\right]_{N_{\mathrm{FFT}}-1,N_{\mathrm{FFT}}-1} \end{pmatrix}. \tag{3.17}$$

The real value elements $\Phi_{l,m}$ denote the quasi-instantaneous frequency associated with $\underline{d}_m^{(n)}$ at sampling time *l*. With (3.17) the FFH/OFDM matrix is

$$\underline{\boldsymbol{D}}_{\mathrm{H}} = \begin{bmatrix} \left[\underline{\boldsymbol{D}}_{\mathrm{H}}\right]_{0,0} & \left[\underline{\boldsymbol{D}}_{\mathrm{H}}\right]_{0,1} & \cdots & \left[\underline{\boldsymbol{D}}_{\mathrm{H}}\right]_{0,N_{\mathrm{FFT}}-1} \\ \left[\underline{\boldsymbol{D}}_{\mathrm{H}}\right]_{1,0} & \left[\underline{\boldsymbol{D}}_{\mathrm{H}}\right]_{1,1} & \cdots & \left[\underline{\boldsymbol{D}}_{\mathrm{H}}\right]_{1,N_{\mathrm{FFT}}-1} \\ \vdots & \vdots & \ddots & \vdots \\ \left[\underline{\boldsymbol{D}}_{\mathrm{H}}\right]_{N_{\mathrm{FFT}}-1,0} & \left[\underline{\boldsymbol{D}}_{\mathrm{H}}\right]_{N_{\mathrm{FFT}}-1,1} & \cdots & \left[\underline{\boldsymbol{D}}_{\mathrm{H}}\right]_{N_{\mathrm{FFT}}-1,N_{\mathrm{FFT}}-1} \end{bmatrix}, \tag{3.18}$$

with the elements

$$\left[\underline{\boldsymbol{D}}_{\mathrm{H}}\right]_{l,m} = \frac{1}{\sqrt{N_{\mathrm{FFT}}}} \left(\exp\left\{ \mathrm{j}2\pi \frac{(l-1)}{N_{\mathrm{FFT}}} \cdot \left[\Phi\right]_{l,m} \right\} \right). \tag{3.19}$$

It is reported in [Bru04] that FFH operation can be regarded as linear pre-coding $\underline{\boldsymbol{U}}$ applied to $\underline{\boldsymbol{d}}^{(n)}$ before the IDFT operation. In other words, the FFH/OFDM matrix $\underline{\boldsymbol{D}}_{\mathrm{H}} = \underline{\boldsymbol{D}}\underline{\boldsymbol{U}}$, which is actually a shuffled version of the IDFT matrix $\underline{\boldsymbol{D}}$. The *n*-th OFDM symbol with FFH/OFDM modulation is given by

$$\begin{aligned} \underline{\boldsymbol{b}}_{\mathrm{H}}^{(n)} &= \underline{\boldsymbol{D}}\underline{\boldsymbol{U}}\underline{\boldsymbol{d}}^{(n)} \\ &= \underline{\boldsymbol{D}}_{\mathrm{H}}\underline{\boldsymbol{d}}^{(n)}. \end{aligned} \tag{3.20}$$

Without FFH, the frequencies of the subcarriers at a certain time instant *l* are arranged in an ascending order, setting out from 0 and ending at $N_{\mathrm{FFT}} - 1$.This leads to a regular OFDM, and $\underline{\boldsymbol{U}}$ is an identity matrix. Each symbol in $\underline{\boldsymbol{d}}^{(n)}$ is

always modulated to the same subcarrier at any sampling time *l*. Thus, the real-valued $N_{\mathrm{FFT}} \times N_{\mathrm{FFT}}$ FFH patterns matrix defined in (3.17) becomes

$$\boldsymbol{\Phi} = \begin{pmatrix} 0 & 1 & \cdots & N_{\mathrm{FFT}}-1 \\ 0 & 1 & \cdots & N_{\mathrm{FFT}}-1 \\ \vdots & \vdots & \cdots & \vdots \\ 0 & 1 & \cdots & N_{\mathrm{FFT}}-1 \end{pmatrix}. \tag{3.21}$$

In this case, the frequencies associated with of all subcarriers at a certain time instant *l* are fixed. $\underline{\boldsymbol{D}}_{\mathrm{H}}$ and $\underline{\boldsymbol{D}}$ are identical.

The cyclic FFH patterns proposed in [Sch05] has the structure of

$$\left[\boldsymbol{\Phi}\right]_{l,m} = \mathrm{mod}\left(f_l + m - 1, M \right), \quad l, m = 0 \cdots N_{\mathrm{FFT}} - 1. \tag{3.22}$$

With the Cyclic FFH pattern, the frequency associated with subcarrier $m = 0$ is defined by $\left[\boldsymbol{\Phi}\right]_{l,0} = f\left(l\right), l = 1 \cdots N_{\mathrm{FFT}} - 1$, $f\left(l\right)$ is a random shuffled sequence of $\left[0, \cdots N_{\mathrm{FFT}} - 1\right]$. All other subcarrier frequencies are arranged in ascending order derived from $\left[\boldsymbol{\Phi}\right]_{l,0}$, as defined in (3.22). In the case of Cyclic FFH patterns, FFH/OFDM matrix $\underline{\boldsymbol{D}}_{\mathrm{H}}$ is unitary matrix. Therefore the (3.20) could be expressed as

$$\begin{aligned} \underline{\boldsymbol{b}}_{\mathrm{H}}^{(n)} &= \underline{\boldsymbol{D}}_{\mathrm{H}} \underline{\boldsymbol{d}}^{(n)} \\ &= \underbrace{\underline{\boldsymbol{D}}\underline{\boldsymbol{U}}\underline{\boldsymbol{D}}^{\mathrm{H}}}_{\underline{\boldsymbol{\Delta}}} \underline{\boldsymbol{D}}\underline{\boldsymbol{d}}^{(n)}. \end{aligned} \tag{3.23}$$

$\underline{\boldsymbol{\Delta}}$ is a diagonal matrix, each diagonal entry has unit value . The original IDFT described by the matrix multiplication $\underline{\boldsymbol{D}}\underline{\boldsymbol{d}}^{(n)}$ in (3.10) can be used to generate $\underline{\boldsymbol{b}}_{\mathrm{H}}^{(n)}$ in time domain. The matrix multiplication in (3.20) is simplified by weighting the samples of OFDM symbol $\underline{\boldsymbol{D}}\underline{\boldsymbol{d}}^{(n)}$ with a vector, and the computational complexity is reduced. With this cyclic FFH patterns, hardware accelerators designed for DFT/IDFT can be used without change. At the transmitter side, FFH/OFDM implementation is done by applying phase shifting to the IFFT output [Bru04].

At the receiver side, the *n*-th received signal in frequency domain is given by

$$\underline{\boldsymbol{e}}_{\mathrm{f}}^{(n)} = \underline{\boldsymbol{H}}_{\mathrm{f}}^{(n)} \underline{\boldsymbol{U}}\underline{\boldsymbol{d}}^{(n)} + \underline{\boldsymbol{n}}_{\mathrm{f}}^{(n)}, \tag{3.24}$$

$\underline{\boldsymbol{H}}_{\mathrm{f}}^{(n)}$ is the CTF matrix of the multipath channel defined in (3.16), $\underline{\boldsymbol{n}}_{\mathrm{f}}^{(n)}$ is the Additive White Gaussian Noise (AWGN) vector in frequency domain. ZF and MMSE block linear equalizer proposed in [Sch05] can be applied to (3.24).

$$\hat{\underline{\boldsymbol{d}}}_{\mathrm{ZF}}^{(n)} = \underline{\boldsymbol{D}}^{\mathrm{H}} \underline{\boldsymbol{\Delta}}^{*} \underline{\boldsymbol{D}} \underline{\boldsymbol{H}}_{\mathrm{f}}^{-1} \underline{\boldsymbol{e}}_{\mathrm{f}} \tag{3.25}$$

and

$$\begin{aligned} \hat{\underline{\boldsymbol{d}}}_{\mathrm{MMSE}}^{(n)} &= \underline{\boldsymbol{D}}^{\mathrm{H}} \underline{\boldsymbol{\Delta}}^{*} \underline{\boldsymbol{D}} \left(\underline{\boldsymbol{H}}_{\mathrm{f}} + \frac{\left(\underline{\boldsymbol{H}}_{\mathrm{f}}{}^{\mathrm{H}} \right)^{-1}}{\left(\mathrm{E}\left\{ \left| \underline{d}_m^{(n)} \right|^2 \right\} \Big/ N_0 \right)} \right)^{-1} \underline{\boldsymbol{e}}_{\mathrm{f}} \\ &= \underline{\boldsymbol{H}}_{\mathrm{E\_MMSE}} \underline{\boldsymbol{e}}_{\mathrm{f}} \end{aligned} \tag{3.26}$$

In (3.25) and (3.26), $\underline{\boldsymbol{\Delta}}^{*}$ is the conjugate matrix to $\underline{\boldsymbol{\Delta}}$, and is also a diagonal matrix. $\left| \underline{d}_m^{(n)} \right|^2$ in (3.26) is the average energy of the data symbol $\underline{d}_m^{(n)}$, N_0 is the noise power spectral density.

When cyclic FFH/OFDM is applied to transmit data symbols, best frequency diversity exploitation can be achieved from the frequency selective channel. The reason is that each data symbol is modulated to the available frequency ergodically throughout the OFDM band. Advantage of the FFH/OFDM is that the SNR of the received signal is averaged after equalization.

For a regular OFDM UWB system, the post-processing SNR of the received signal is calculated by

$$\begin{aligned} \mathrm{SNR}_{\mathrm{OFDM}} &= \frac{E_{\mathrm{s}}}{\mathrm{E}\left(\underline{\boldsymbol{H}}_{\mathrm{f}}^{-1} \underline{\boldsymbol{n}}_{\mathrm{f}} \left(\underline{\boldsymbol{H}}_{\mathrm{f}}^{-1} \underline{\boldsymbol{n}}_{\mathrm{f}} \right)^{\mathrm{H}} \right)} \\ &= \frac{1}{\left(\underline{\boldsymbol{H}}_{\mathrm{f}}^{-1} \left(\underline{\boldsymbol{H}}_{\mathrm{f}}^{-1} \right)^{\mathrm{H}} \right)} \frac{E_s}{N_0} \end{aligned} \tag{3.27}$$

where N_0 is the noise power spectral density. $\mathrm{E}(\cdot)$ is expectation of the argument. The post-processing SNR of the equalized signal with ZF equalizer is calculated as

$$\begin{aligned} \mathrm{SNR}_{\mathrm{FFH\_ZF}} &= \frac{\mathrm{E}\left(\left(\underline{\boldsymbol{U}}^{\mathrm{H}}\boldsymbol{H}_{\mathrm{f}}^{-1}\boldsymbol{H}_{\mathrm{f}}\underline{\boldsymbol{U}\boldsymbol{d}}\right)\left(\underline{\boldsymbol{U}}^{\mathrm{H}}\boldsymbol{H}_{\mathrm{f}}^{-1}\boldsymbol{H}_{\mathrm{f}}\underline{\boldsymbol{U}\boldsymbol{d}}\right)^{\mathrm{H}}\right)}{\mathrm{E}\left(\underline{\boldsymbol{U}}^{\mathrm{H}}\underline{\boldsymbol{H}}_{\mathrm{f}}^{-1}\underline{\boldsymbol{n}}_{\mathrm{f}}\left(\underline{\boldsymbol{U}}^{\mathrm{H}}\underline{\boldsymbol{H}}_{\mathrm{f}}^{-1}\underline{\boldsymbol{n}}_{\mathrm{f}}\right)^{\mathrm{H}}\right)} \\ &= \frac{1}{\left(\underline{\boldsymbol{U}}^{\mathrm{H}}\underline{\boldsymbol{H}}_{\mathrm{f}}^{-1}\left(\underline{\boldsymbol{H}}_{\mathrm{f}}^{-1}\right)^{\mathrm{H}}\underline{\boldsymbol{U}}\right)}\frac{E_s}{N_0} \end{aligned} \tag{3.28}$$

The post-processing SNR of the equalized signal with MMSE equalizer can be calculated from

$$\mathrm{SNR}_{\mathrm{FFH\_MMSE}} = \frac{\mathrm{E}\left(\left(\boldsymbol{H}_{\mathrm{E\_MMSE}}\boldsymbol{H}_{\mathrm{f}}\underline{\boldsymbol{U}\boldsymbol{d}}\right)\left(\boldsymbol{H}_{\mathrm{E\_MMSE}}\boldsymbol{H}_{\mathrm{f}}\underline{\boldsymbol{U}\boldsymbol{d}}\right)^{\mathrm{H}}\right)}{\mathrm{E}\left(\boldsymbol{H}_{\mathrm{E\_MMSE}}\underline{\boldsymbol{n}}_{\mathrm{f}}\left(\boldsymbol{H}_{\mathrm{E\_MMSE}}\underline{\boldsymbol{n}}_{\mathrm{f}}\right)^{\mathrm{H}}\right)} \tag{3.29}$$

In Figure 3.5 the Probability Density Function (PFD) of the post-processing SNR of a regular OFDM signal, FFH/OFDM signal with the ZF block linear equalizer and FFH/OFDM signal with the MMSE block linear equalizer is compared. The curves are derived from simulation in UWB CM4 channel, the QPSK complex symbols are transmitted with the E_s/N_0 of 20 dB. The Y-axis is the probability density function of the received signal power, and X-axis is the SNR value of the received signal in logarithmic scale. The red curve represents the SNR distribution of the received regular OFDM signal, the green curve represents the post-processing SNR of the FFH/OFDM signal with ZF block linear equalizer, and the blue curve represents the FFH/OFDM signal with MMSE block linear equalizer. It is obvious that the distribution of the post-processing SNR of the received FFH/OFDM signal is quite different from that of a regular OFDM signal. The distribution of the post-processing SNR for regular OFDM looks like a two order chi-square distribution, while the distribution of the post-processing SNR with the MMSE block linear equalizer looks like Gaussian. The distribution of post-processing SNR is dependent to the channel features and the FFT size of the OFDM. In Figure 3.6 the Cumulative Distribution Function (CDF) of the post-processing SNR corresponding to PDF in Figure 3.5 is given. From the CDF we can estimate that, the FFH/OFDM with MMSE block linear equalizer should have the best uncoded BER performance due to the high probability with higher SNR realization.

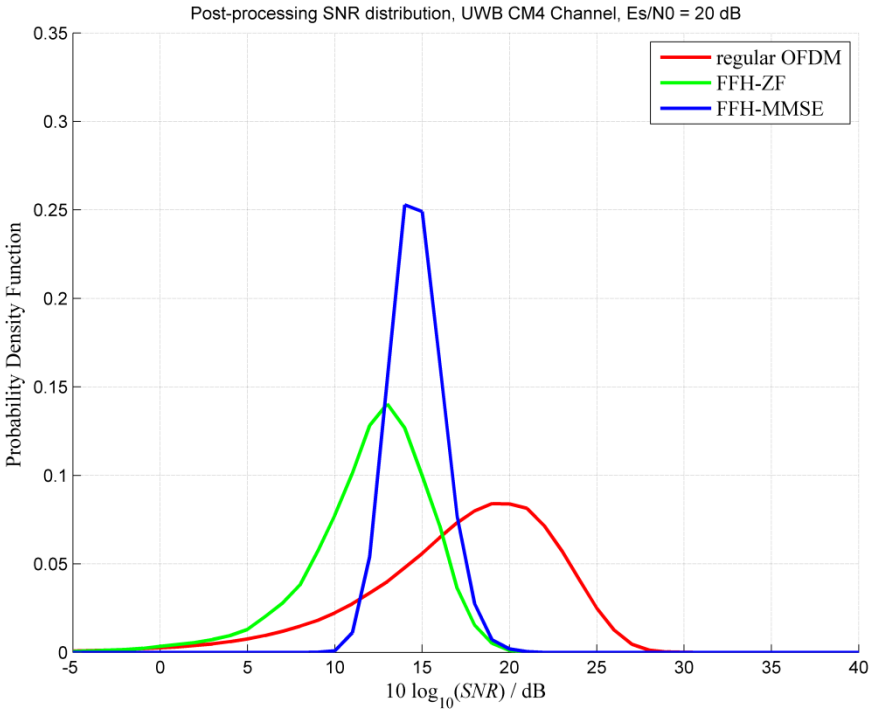

Figure 3.5 PDF of post-processing SNR

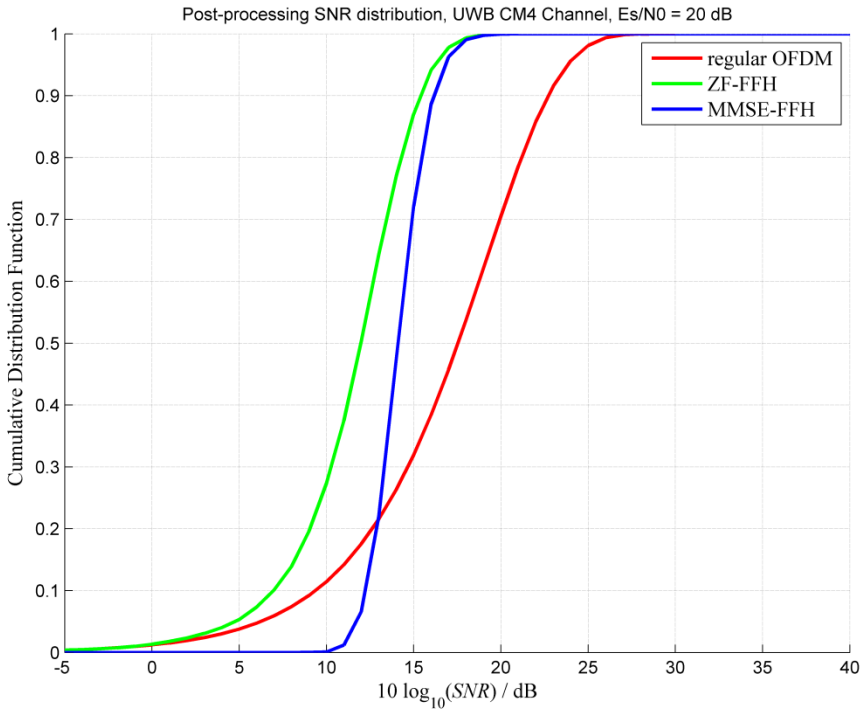

Figure 3.6 CDF of post-processing SNR

3.3.3 Multiple Antenna with OFDM

As already discussed in Section 1.2, multiple antenna techniques could be applied to exploit spatial diversity in the multipath UWB propagation channel. In this work, the objective is to improve the data transmission quality and extend the communication range. Therefore exploiting spatial diversity with multiple antenna technologies is interested. In what follows, three different schemes for the spatial diversity exploitation are reviewed. They are receiver combining, Alamouti scheme, and transmit beamforming.

3.3.3.1 Receiver Combining

Receiver combining is a classic adaptive array processing method in the receiver. There are several types of combining strategies, such as the Maximal-Ratio Receive Combining (MRRC) scheme, Equal Gain Combining, and Switched Combining. The MRRC is examined in in [Ala98], and is the optimal one among the three. Let us assume that K_{R} RX antenna elements installed on the receiver, and only one TX antenna element on transmitter. A $1\times K_{\mathrm{R}}$ SIMO system is presented. Let us denote $\underline{d}_m^{(n)}$ as the transmitted signal on *m*-th subcarrier of the *n*-th OFDM symbol, $\underline{h}_{\mathrm{f},m}^{(n,k_{\mathrm{R}})}$ as the channel transfer function of *m*-th subcarrier associated with the channel between TX antenna and the k_{R} -th RX antenna element, $\underline{n}_{\mathrm{f}}^{(n,k_{\mathrm{R}})}$ as AWGN on the k_{R} -th RX antenna. The equivalent system model is given by

$$\underline{\boldsymbol{e}}_{\mathrm{f}}^{(n)} = \underline{\boldsymbol{h}}_{\mathrm{f},m}^{(n)} \underline{d}_m^{(n)} + \underline{\boldsymbol{n}}_{\mathrm{f}}^{(n)}, \tag{3.30}$$

where

$$\underline{\boldsymbol{h}}_{\mathrm{f},m}^{(n)} = \left(\underline{h}_{\mathrm{f},m}^{(n,k_1)}, \ldots \underline{h}_{\mathrm{f},m}^{(n,k_{\mathrm{R}}-1)}, \underline{h}_{\mathrm{f},m}^{(n,k_{\mathrm{R}})} \right)^{\mathrm{T}} \tag{3.31}$$

is $K_{\mathrm{R}} \times 1$ column vector, denoting the CTF of the *k*-th subcarrier on each RX antenna element. The AWGN added on the RX antenna array is given by

$$\underline{\boldsymbol{n}}_{\mathrm{f}}^{(n)} = \left(\underline{n}^{(n,k_1)}, \ldots \underline{n}^{(n,k_{\mathrm{R}}-1)}, \underline{n}^{(n,K_{\mathrm{R}})} \right)^{\mathrm{T}}. \tag{3.32}$$

In the receiver, the MRRC scheme is carried out with

$$\hat{\underline{d}}_m^{(n)} = \left(\underline{\boldsymbol{h}}_{\mathrm{f},m}^{(n)}\right)^{\mathrm{H}} \underline{\boldsymbol{e}}_{\mathrm{f}}^{(n)} = \left\|\underline{\boldsymbol{h}}_{\mathrm{f},m}^{(n)}\right\|^2 \underline{d}_m^{(n)} + \left(\underline{\boldsymbol{h}}_{\mathrm{f},m}^{(n)}\right)^{\mathrm{H}} \underline{\boldsymbol{n}}_{\mathrm{f}}^{(n)}, \tag{3.33}$$

The SNR of combined signal after MRRC is given by,

$$SNR = \left\|\underline{\boldsymbol{h}}_m^{(n)}\right\|^2 = \sum_{k_{\mathrm{R}}=1}^{K_{\mathrm{R}}} \left|\underline{h}_{\mathrm{f},m}^{(n,k_{\mathrm{R}})}\right|^2 \frac{E_{\mathrm{s}}}{N_0}. \tag{3.34}$$

E_{s} denotes the transmitted signal power of the symbol $\underline{d}_m^{(n)}$, N_0 is the noise power spectral density. $|\cdot|$ is operator of absolute value for a scalar, and $\|\cdot\|$ returns inner product of an vector. The SNR of the received signal after MRRC scheme has been improved by the diversity order of K_{R}.

3.3.3.2 Transmit Beamforming

Compared to the receiver combing technology, the transmit beamforming can exploit the spatial diversity on the transmitter side. The signal processing for UWB beamforming can either be carried out in the time domain or in the frequency domain. The time domain method is suitable for impulse based UWB radios, whereas the frequency domain method is suitable for OFDM based UWB systems.

Let us assume the UWB transmitter has a smart antenna with K_{T} antenna elements, and the receiver has one antenna element. Without loss of generality, assuming Uniform Linear Array (ULA) on TX is applied. The array elements are located along a straight line with a spacing of Δd. Let the first element in one end of the antenna be the reference point of the array with index $k_{\mathrm{T}} = 1$, the distance between the k_{T}-th element to the reference element is $\left(k_{\mathrm{T}} - 1\right)\Delta d$. Let us assume that signal arrives at the antenna array on one plane with K_{C} main directions termed $\alpha^{(k_{\mathrm{C}})}$. This is also the Angle of Arrival (AoA) of the received signal. $\alpha^{(k_{\mathrm{C}})}$ is initially unknown and must be determined during the channel estimation.

When talking about the *m*-th subcarrier, the wavelength dependent phase correlation of the arrived signal from direction $\alpha^{(k_{\mathrm{C}})}$ between the k_{T}-th antenna element and the reference element is given by [Gio11],

$$\Psi_{\mathrm{T}}\left(k_{\mathrm{T}}, \lambda_m, k_{\mathrm{C}}\right) = 2\pi \frac{k_{\mathrm{T}} \Delta d}{\lambda_m} \cos\left(\alpha^{(k_{\mathrm{C}})}\right), k_{\mathrm{T}} = 1, \ldots K_{\mathrm{T}} \tag{3.35}$$

Δd is the space between two antenna elements, λ_m is the wavelength of the *m*-th subcarrier, and it is the reciprocal to the $f_c + m\Delta f$, where f_c and Δf are the carrier frequency and subcarrier separation of OFDM, respectively. m is index of the subcarrier. It is proposed that Δd is selected as half wavelength of the highest frequency of all the subcarriers. The transmit beamforming for the *m*-th subcarrier in the k_C-th direction is given by [Gio11]

$$\underline{\boldsymbol{\omega}}_T^{(k_C,\lambda_n)} = \frac{1}{\sqrt{K_T}}\left(\exp\left(j\Psi_T\left(1,k_C,\lambda_m\right)\right),\ldots,\ \exp\left(j\Psi_T\left(K_T,k_C,\lambda_m\right)\right)\right)^T \tag{3.36}$$

$\underline{\boldsymbol{\omega}}_T^{(k_T,\lambda_n)}$ is a $K_T \times 1$ column vector, let us assume that the number of antenna elements is bigger than K_C. The beamforming strategy for all the K_C directions can be described by a $K_T \times K_C$ matrix.

$$\underline{\boldsymbol{W}} = \frac{1}{\sqrt{K_C}}\left(\underline{\boldsymbol{\omega}}_T^{(1,\lambda_m)}, \underline{\boldsymbol{\omega}}_T^{(2,\lambda_m)}\ldots, \underline{\boldsymbol{\omega}}_T^{(K_C,\lambda_m)}\right) \tag{3.37}$$

Each column of beamforming matrix $\underline{\boldsymbol{W}}$ corresponds to one steering vector in one direction. For the simplest case $K_C = 1$, which means from one main direction the received signal comes. The system with transmit beamforming is given by

$$\underline{e}_f^{(n)} = \underline{\boldsymbol{h}}_{f,m}^{(n)}\underline{\boldsymbol{\omega}}_T^{(1,\lambda_m)}\underline{d}_m^{(n)} + \underline{n}_f^{(n)}, \tag{3.38}$$

where

$$\underline{\boldsymbol{h}}_{f,m}^{(n)} = \left(\underline{h}_{f,m}^{(n,k_1)},\ldots \underline{h}_{f,m}^{(n,k_T-1)}, \underline{h}_{f,m}^{(n,k_T)}\right) \tag{3.39}$$

is the $1\times K_T$ row channel vector associated with the *m*-th subcarrier. With the transmitter beamforming strategy, SNR of the received signal is given by

$$SNR = \left\|\underline{\boldsymbol{h}}_{f,m}^{(n)}\underline{\boldsymbol{\omega}}_T^{(1,\lambda_m)}\right\|^2 \frac{E_s}{N_0}. \tag{3.40}$$

The more spatial correlation feature the channel vector $\underline{\boldsymbol{h}}_{f,m}^{(n)}$ has, the better performance of the transmitter beamforming can achieve.

3.3.3.3 Alamouti Scheme

Alamouti scheme is proposed in [Ala98]. It is a spatial diversity exploitation method in the transmitter when channel information is unknown. Compared with MRRC and transmit beamforming schemes, advantage of the Alamouti scheme is its simple implementation, no channel state information (CSI) is required in the transmitter and only linear signal processing shall be performed in the receiver. It can exploit the same order spatial diversity gain as the MRRC and transmitter beamforming.

Let us assume that there are two antenna elements deployed in the TX antenna array, and K_{R} antennas elements deployed in RX antenna array. The Alamouti transmit strategy can be generalized by the 2×2 encoding matrix

$$\underline{\boldsymbol{S}} = \begin{bmatrix} \overset{\rightarrow \text{Time / Frequency}}{\underline{s}^{(n)}} & -\underline{s}^{(n+1)*} \\ \underline{s}^{(n+1)} & \underline{s}^{(n)*} \end{bmatrix} \downarrow \text{Space/TX Antennas.} \tag{3.41}$$

Each row of the matrix denotes the symbol transmitted on orthogonal time slot or frequency (subcarrier in an OFDM). Each column denotes the symbol transmitted on the different antenna elements. When STBC is considered, orthogonal time slot are used. It is postulated that channel is time invariant over the two symbol periods in $\underline{\boldsymbol{S}}$, namely, $\underline{h}_{k_{\mathrm{R}},k_{\mathrm{T}}}^{(n)} = \underline{h}_{k_{\mathrm{R}},k_{\mathrm{T}}}^{(n+1)}$. When SFBC is considered, the two subcarriers in an OFDM are chosen to build (3.41). And it is postulated that channel associated with the two concatenated subcarriers have identical frequency response.

In the following, the classic STBC Alamouti is presented. The $2\times K_{\mathrm{R}}$ MIMO system model is given by

$$\left(\underline{\boldsymbol{e}}^{n}, \underline{\boldsymbol{e}}^{n+1}\right) = \underline{\boldsymbol{H}} \cdot \underline{\boldsymbol{S}} + \underline{\boldsymbol{N}}, \tag{3.42}$$

$\underline{\boldsymbol{e}}_{\mathrm{t}}^{n}$, $\underline{\boldsymbol{e}}_{\mathrm{t}}^{n+1}$ denotes the received signal on the RX antenna array of in the n-th and n+1-th time slot, respectively. $\underline{\boldsymbol{H}}$ denotes the $K_{\mathrm{R}}\times 2$ MIMO channel matrix, the first column of $\underline{\boldsymbol{H}}$ represents the received signal transmitted via the first TX antenna element, and the second column of $\underline{\boldsymbol{H}}$ represents the received signal transmitted via the second TX antenna element. Since channel is assumed constant over n-th and n+1-th time slot, $\underline{\boldsymbol{H}} = \underline{\boldsymbol{H}}_{n} = \underline{\boldsymbol{H}}_{n+1}$ is given by

$$\underline{\boldsymbol{H}} = \left(\underline{\boldsymbol{h}}_1, \underline{\boldsymbol{h}}_2\right) = \begin{bmatrix} \underline{h}_{1,1} & \underline{h}_{1,2} \\ \underline{h}_{2,1} & \underline{h}_{2,2} \\ \vdots & \vdots \\ \underline{h}_{K_R,1} & \underline{h}_{K_R,1} \end{bmatrix}. \tag{3.43}$$

AWGN added on the RX antenna array in *n*-th and *n*+1-th time slot is given by

$$\underline{\boldsymbol{N}} = \left(\underline{\boldsymbol{n}}^n, \underline{\boldsymbol{n}}^{n+1}\right) = \begin{bmatrix} \underline{n}_0^n & \underline{n}_0^{n+1} \\ \underline{n}_1^n & \underline{n}_1^{n+1} \\ \vdots & \vdots \\ \underline{n}_{K_R-1}^n & \underline{n}_{K_R-1}^{n+1} \end{bmatrix}. \tag{3.44}$$

In the receiver, combining scheme to the STBC transmit strategy is given by

$$\begin{aligned} \begin{bmatrix} \hat{\underline{s}}^n \\ \hat{\underline{s}}^{n+1} \end{bmatrix} &= \begin{bmatrix} \underline{\boldsymbol{h}}_1^{\mathrm{H}} \cdot \underline{\boldsymbol{e}}^n + \left(\underline{\boldsymbol{h}}_2^{\mathrm{H}} \cdot \underline{\boldsymbol{e}}^{n+1}\right)^{\mathrm{H}} \\ \underline{\boldsymbol{h}}_2^{\mathrm{H}} \cdot \underline{\boldsymbol{e}} \; - \left(\underline{\boldsymbol{h}}_1^{\mathrm{H}} \cdot \underline{\boldsymbol{e}}^{n+1}\right)^{\mathrm{H}} \end{bmatrix} \\ &= \begin{bmatrix} \underline{\boldsymbol{h}}_1^{\mathrm{H}} \cdot \underline{\boldsymbol{e}}^n + \underline{\boldsymbol{e}}_{n+1}^{\mathrm{H}} \cdot \underline{\boldsymbol{h}}_2 \\ \underline{\boldsymbol{h}}_2^{\mathrm{H}} \cdot \underline{\boldsymbol{e}}^n - \underline{\boldsymbol{e}}_{n+1}^{\mathrm{H}} \cdot \underline{\boldsymbol{h}}_1 \end{bmatrix}. \end{aligned} \tag{3.45}$$

The SNR of the combined signal through Alamouti scheme is therefore given by,

$$SNR = \left(\left\|\underline{\boldsymbol{h}}_1\right\|^2 + \left\|\underline{\boldsymbol{h}}_2\right\|^2\right)\frac{E_S}{N_0}. \tag{3.46}$$

It is known from (3.46) that Alamouti scheme is able to introduce SNR gain with a diversity order of $2 \times K_R$ to the received signal.

3.3.4 Proposals for MB-OFDM UWB

It is already proven that the Alamouti scheme is a simple way to exploit the spatial diversity in multiple antenna systems. Therefore the Alamouti scheme is preferable to the UWB systems in the consideration of low cost implementation. STBC or SFCB can be employed according to the statistic feature of the propagation channel. In general the STBC scheme is suitable to time invariant channel, and the SFBC could be deployed when the frequency selectivity is not severe. From the literature review in Section 1.2, one can notice that, most of the studies discussed the STBC schemes for the multiple antenna MB-OFDM UWB systems, study of SFBC in MB-OFDM UWB system is seldom reported. It is

clear that in the indoor environment, the UWB propagation channel is almost time invariant. However in the MB-OFDM UWB systems the time frequency hopping scheme is applied, as shown in Figure 3.2. This implies that in two neighboring symbol period, the channel cannot keep time invariant since the frequency band is changing. In other words, the fundamental assumption for the combination scheme presented in (3.45) does not establish anymore. To solve this problem, the Alamouti STCB encoding should be jointly designed with the TFCs patterns. Take the transmission shown in Figure 3.2 as an example, where in the data transmission TFC 1 is applied. At the first time slot and fourth time slot, the transmission is on the same band, which means that the transmitted symbol on these two time slots undergoes the same channel. The Alamouti STBC encoding matrix in (3.41) should select two symbols according the TFC patterns as a pair, rather simply find the two adjacent symbols.

Alternatively, SFBC could be considered. The advantage of the SFBC is it can exploit the spatial diversity within one OFDM system period, and it will be not affected by the time frequency hopping scheme. In Section 3.4, the combination of FFH/OFDM and SFBC scheme is studied.

3.4 SFBC/FFH MB-OFDM

3.4.1 System Model

Let us assumed that K_{T} antenna elements are installed on the TX antenna array, and K_{R} antenna elements are installed on the RX antenna array. In the case of $K_{\mathrm{T}} = 2$, a $2 \times K_{\mathrm{R}}$ MIMO system is present. The frequency domain signal coded by Alamouti scheme to the FFH/OFDM symbol is given by

$$\begin{aligned} \underline{\boldsymbol{d}}^{(n,1)} &= \underline{\boldsymbol{U}}\underline{\boldsymbol{d}}^{(n)} \\ \underline{\boldsymbol{d}}^{(n,2)} &= \boldsymbol{C}\left(\underline{\boldsymbol{U}}\underline{\boldsymbol{d}}^{(n)}\right)^{*} \end{aligned} \tag{3.47}$$

where $\underline{\boldsymbol{d}}^{(n)}$ is the n-th complex vector to be transmitted, and $\underline{\boldsymbol{d}}^{(n,k_{\mathrm{T}})}$ denotes the n-th complex vector transmitted via the k_{T} -th TX antenna element. And the transmitted FFH/OFDM symbol via the first TX antenna element is given by

$$\begin{aligned} \underline{\boldsymbol{b}}^{(n,1)} &= \underline{\boldsymbol{D}}\underline{\boldsymbol{d}}^{(n,1)} \\ &= \underline{\boldsymbol{\Delta}}\underline{\boldsymbol{D}}\underline{\boldsymbol{d}}^{(n)}, \end{aligned} \tag{3.48}$$

and *n*-th signal transmitted via the second TX antenna element is the FFH/OFDM symbol coded by Alamouti SFBC scheme

$$\begin{aligned}\underline{\boldsymbol{b}}^{(n,2)} &= \underline{\boldsymbol{D}}\underline{\boldsymbol{d}}^{(n,2)} \\ &= \underline{\boldsymbol{D}}\boldsymbol{C}\left(\underline{\boldsymbol{U}}\underline{\boldsymbol{d}}^{(n)}\right)^{*} \\ &= \underline{\boldsymbol{D}}\boldsymbol{C}\left(\underline{\boldsymbol{D}}^{\mathrm{H}}\underline{\boldsymbol{D}}\underline{\boldsymbol{U}}\underline{\boldsymbol{d}}^{(n)}\right)^{*} \\ &= \underline{\boldsymbol{D}}\boldsymbol{C}\underline{\boldsymbol{D}}\left(\underline{\boldsymbol{D}}\underline{\boldsymbol{U}}\underline{\boldsymbol{d}}^{(n)}\right)^{*} \\ &= \underbrace{\underline{\boldsymbol{D}}\boldsymbol{C}\underline{\boldsymbol{D}}\ \underline{\boldsymbol{\Delta}}^{*}}_{\boldsymbol{\Delta}_{\text{SFBC-FFH}}}\left(\underline{\boldsymbol{D}}\underline{\boldsymbol{d}}^{(n)}\right)^{*}\end{aligned} \tag{3.49}$$

$\boldsymbol{C}$ is real value matrix defined in (3.50) to switch position and sign of the vector elements,

$$\boldsymbol{C} = \begin{pmatrix} \boldsymbol{c} & 0 & \cdots & 0 \\ 0 & \boldsymbol{c} & \cdots & 0 \\ \vdots & \vdots & \ddots & \vdots \\ 0 & 0 & \cdots & \boldsymbol{c} \end{pmatrix}, \text{ where } \boldsymbol{c} = \begin{bmatrix} 0 & 1 \\ -1 & 0 \end{bmatrix}. \tag{3.50}$$

$\underline{\boldsymbol{D}}$ is IDFT matrix, and $\underline{\boldsymbol{U}}$ is the FFH pre-coding matrix which are defined in Section 3.3.2, $\underline{\boldsymbol{U}}^{*}$ is conjugated matrix of $\underline{\boldsymbol{U}}$. In the case of $\underline{\boldsymbol{U}}$ is an identical matrix, the (3.49) then describes the conventional SFBC signal. Comparing with the $\boldsymbol{\Delta}$ in (3.23), $\underline{\boldsymbol{D}}\boldsymbol{C}\underline{\boldsymbol{D}}\ \underline{\boldsymbol{\Delta}}^{*}$ is not a diagonal matrix any more, however it is still a very sparse matrix, whose row vector has maximum two none zero elements. Therefore this matrix multiplication could also be realized by the complex weighting operations to the IDFT output in time domain, but two weighting vectors are required. Compared with the FFH/OFDM symbol generation, the computational complexity in generating the SFBC coded FFH/OFDM symbol is doubled. However it is still much simpler than matrix multiplication. The low cost implementation of the SFBC-FFH encoded is feasible.

In the receiver, the frequency domain signal of the *n*-th received FFH/OFDM symbol on the k_{R} -th antenna element is given by

$$\underline{\boldsymbol{e}}_{\mathrm{f}}^{(n,k_{\mathrm{R}})} = \underline{\boldsymbol{H}}_{\mathrm{f}}^{(k_{\mathrm{R}},1)}\underline{\boldsymbol{U}}\underline{\boldsymbol{d}}^{(n)} + \underline{\boldsymbol{H}}_{\mathrm{f}}^{(k_{\mathrm{R}},2)}\boldsymbol{C}\left(\underline{\boldsymbol{U}}\underline{\boldsymbol{d}}^{(n)}\right)^{*} + \boldsymbol{n}_{\mathrm{f}}^{(n,k_{\mathrm{R}})} \tag{3.51}$$

The system model of the $2\times K_{\mathrm{R}}$ MIMO system is presented as

$$\begin{pmatrix} \underline{\boldsymbol{e}}_{\mathrm{f}}^{(n,1)} \\ \underline{\boldsymbol{e}}_{\mathrm{f}}^{(n,2)} \\ \vdots \\ \underline{\boldsymbol{e}}_{\mathrm{f}}^{(n,K_{\mathrm{R}})} \end{pmatrix} = \begin{pmatrix} \underline{\boldsymbol{H}}_{\mathrm{f}}^{(1,1)} \underline{\boldsymbol{U}\boldsymbol{d}}^{(n)} + \underline{\boldsymbol{H}}_{\mathrm{f}}^{(1,2)} \boldsymbol{C}\left(\underline{\boldsymbol{U}\boldsymbol{d}}^{(n)}\right)^{*} \\ \underline{\boldsymbol{H}}_{\mathrm{f}}^{(2,1)} \underline{\boldsymbol{U}\boldsymbol{d}}^{(n)} + \underline{\boldsymbol{H}}_{\mathrm{f}}^{(2,2)} \boldsymbol{C}\left(\underline{\boldsymbol{U}\boldsymbol{d}}^{(n)}\right)^{*} \\ \vdots \\ \underline{\boldsymbol{H}}_{\mathrm{f}}^{(K_{\mathrm{R}},1)} \underline{\boldsymbol{U}\boldsymbol{d}}^{(n)} + \underline{\boldsymbol{H}}_{\mathrm{f}}^{(K_{\mathrm{R}},2)} \boldsymbol{C}\left(\underline{\boldsymbol{U}\boldsymbol{d}}^{(n)}\right)^{*} \end{pmatrix} + \begin{pmatrix} \boldsymbol{n}_{\mathrm{f}}^{(n,1)} \\ \boldsymbol{n}_{\mathrm{f}}^{(n,2)} \\ \vdots \\ \boldsymbol{n}_{\mathrm{f}}^{(n,K_{\mathrm{R}})} \end{pmatrix}. \tag{3.52}$$

$\underline{\boldsymbol{H}}_{\mathrm{f}}^{(k_{\mathrm{R}},k_{\mathrm{T}})}$ is the CTF matrix of the OFDM channel between the k_{T}-th TX antennas element on and the k_{R}-th RX antennas element. $\underline{H}_{\mathrm{f},m}^{(k_{\mathrm{R}},k_{\mathrm{T}})}$ is the complex channel gain of m-th subcarrier. $\boldsymbol{n}_{\mathrm{f}}^{(n,k_{\mathrm{R}})}$ is the AWGN vector added to antennas element array in frequency domain.

$$\underline{\boldsymbol{H}}_{\mathrm{f}}^{(k_{\mathrm{t}},k_{\mathrm{r}})} = \begin{bmatrix} \underline{H}_{\mathrm{f},1}^{(k_{\mathrm{R}},k_{\mathrm{T}})} & 0 & \cdots & 0 \\ 0 & \underline{H}_{\mathrm{f},2}^{(k_{\mathrm{R}},k_{\mathrm{T}})} & \cdots & 0 \\ \vdots & \vdots & \ddots & \vdots \\ 0 & \cdots & 0 & \underline{H}_{\mathrm{f},N_{\mathrm{FFT}}}^{(k_{\mathrm{R}},k_{\mathrm{T}})} \end{bmatrix} \tag{3.53}$$

It is observed from (3.51) that the received signal on the RX is superposition of the signals transmitted from all the TX antenna elements. Let us assume that, the channel is perfectly known to the receiver. Let us assume that

$$\underline{H}_{\mathrm{f},2m}^{(k_{\mathrm{R}},k_{\mathrm{T}})} = \underline{H}_{\mathrm{f},2m+1}^{(k_{\mathrm{R}},k_{\mathrm{T}})}, m = 0,1,\cdots,\frac{N_{\mathrm{FFT}}}{2}-1. \tag{3.54}$$

The channel equalizer for decoding the SFBC is defined as

$$\begin{aligned} \underline{\boldsymbol{H}}_{\mathrm{fe}}^{(k_{\mathrm{R}},1)} &= \underline{\boldsymbol{H}}_{\mathrm{f}}^{(k_{\mathrm{R}},1)*}, \\ \underline{\boldsymbol{H}}_{\mathrm{fe}}^{(k_{\mathrm{R}},2)} &= \underline{\boldsymbol{H}}_{\mathrm{f}}^{(k_{\mathrm{R}},2)} \boldsymbol{C}^{\mathrm{T}}. \end{aligned} \tag{3.55}$$

Firstly we tread the whole $\underline{\boldsymbol{U}\boldsymbol{d}}^{(n)}$ as a whole. The received signal on different TX antenna elements shall be combined with the following rule

$$
\begin{aligned}
\underline{\boldsymbol{s}}^{(n)} &= \sum_{k_{\mathrm{R}}=1}^{K_{\mathrm{R}}} \underline{\boldsymbol{H}}_{\mathrm{fe}}^{(k_{\mathrm{R}},1)} \underline{\boldsymbol{e}}^{(n,k_{\mathrm{R}})} + \underline{\boldsymbol{H}}_{\mathrm{fe}}^{(k_{\mathrm{R}},2)} \underline{\boldsymbol{e}}^{(k_{\mathrm{R}},2)*} \\
&= \sum_{k_{\mathrm{R}}=1}^{K_{\mathrm{R}}} \begin{pmatrix} \underline{\boldsymbol{H}}_{\mathrm{f}}^{(k_{\mathrm{R}},1)*} \left(\underline{\boldsymbol{H}}_{\mathrm{f}}^{(k_{\mathrm{R}},1)} \underline{\boldsymbol{U}}\underline{\boldsymbol{d}}^{(n)} + \underline{\boldsymbol{H}}_{\mathrm{f}}^{(k_{\mathrm{R}},2)} \boldsymbol{C} \left(\underline{\boldsymbol{U}}\underline{\boldsymbol{d}}^{(n)} \right)^* + \boldsymbol{n}_{\mathrm{f}}^{(n,k_{\mathrm{R}})} \right) \\ + \underline{\boldsymbol{H}}_{\mathrm{f}}^{(k_{\mathrm{R}},2)} \boldsymbol{C}^{\mathrm{T}} \left(\underline{\boldsymbol{H}}_{\mathrm{f}}^{(k_{\mathrm{R}},1)} \underline{\boldsymbol{U}}\underline{\boldsymbol{d}}^{(n)} + \underline{\boldsymbol{H}}_{\mathrm{f}}^{(k_{\mathrm{R}},2)} \boldsymbol{C} \left(\underline{\boldsymbol{U}}\underline{\boldsymbol{d}}^{(n)} \right)^* + \boldsymbol{n}_{\mathrm{f}}^{(n,k_{\mathrm{R}})} \right)^* \end{pmatrix} \\
&= \sum_{k_{\mathrm{R}}=1}^{K_{\mathrm{R}}} \begin{pmatrix} \underline{\boldsymbol{H}}_{\mathrm{f}}^{(k_{\mathrm{R}},1)*} \underline{\boldsymbol{H}}_{\mathrm{f}}^{(k_{\mathrm{R}},1)} \underline{\boldsymbol{U}}\underline{\boldsymbol{d}}^{(n)} + \underline{\boldsymbol{H}}_{\mathrm{f}}^{(k_{\mathrm{R}},1)*} \underline{\boldsymbol{H}}_{\mathrm{f}}^{(k_{\mathrm{R}},2)} \boldsymbol{C} \left(\underline{\boldsymbol{U}}\underline{\boldsymbol{d}}^{(n)} \right)^* + \underline{\boldsymbol{H}}_{\mathrm{f}}^{(k_{\mathrm{R}},1)*} \boldsymbol{n}_{\mathrm{f}}^{(n,k_{\mathrm{R}})} \\ + \underline{\boldsymbol{H}}_{\mathrm{f}}^{(k_{\mathrm{R}},2)} \boldsymbol{C}^{\mathrm{T}} \underline{\boldsymbol{H}}_{\mathrm{f}}^{(k_{\mathrm{R}},1)*} \left(\underline{\boldsymbol{U}}\underline{\boldsymbol{d}}^{(n)} \right)^* + \underline{\boldsymbol{H}}_{\mathrm{f}}^{(k_{\mathrm{R}},2)} \boldsymbol{C}^{\mathrm{T}} \underline{\boldsymbol{H}}_{\mathrm{f}}^{(k_{\mathrm{R}},2)*} \boldsymbol{C} \underline{\boldsymbol{U}}\underline{\boldsymbol{d}}^{(n)} + \underline{\boldsymbol{H}}_{\mathrm{fe}}^{(k_{\mathrm{R}},2)} \boldsymbol{C}^{\mathrm{T}} \left(\boldsymbol{n}_{\mathrm{f}}^{(n,k_{\mathrm{R}})} \right)^* \end{pmatrix} \\
&= \sum_{k_{\mathrm{R}}=1}^{K_{\mathrm{R}}} \begin{pmatrix} \left\| \underline{\boldsymbol{H}}_{\mathrm{f}}^{(k_{\mathrm{R}},1)} \right\|^2 \underline{\boldsymbol{U}}\underline{\boldsymbol{d}}^{(n)} + \left\| \underline{\boldsymbol{H}}_{\mathrm{f}}^{(k_{\mathrm{R}},2)} \right\|^2 \underline{\boldsymbol{U}}\underline{\boldsymbol{d}}^{(n)} + \underline{\boldsymbol{H}}_{\mathrm{f}}^{(k_{\mathrm{R}},1)*} \underline{\boldsymbol{H}}_{\mathrm{f}}^{(k_{\mathrm{R}},2)} \left(\boldsymbol{C} + \boldsymbol{C}^{\mathrm{T}} \right) \left(\underline{\boldsymbol{U}}\underline{\boldsymbol{d}}^{(n)} \right)^* \\ \underline{\boldsymbol{H}}_{\mathrm{f}}^{(k_{\mathrm{R}},1)*} \boldsymbol{n}_{\mathrm{f}}^{(n,k_{\mathrm{R}})} + \boldsymbol{C}^{\mathrm{T}} \underline{\boldsymbol{H}}_{\mathrm{f}}^{(k_{\mathrm{R}},2)} \boldsymbol{C}^{\mathrm{T}} \left(\boldsymbol{n}_{\mathrm{f}}^{(n,k_{\mathrm{R}})} \right)^* \end{pmatrix} \\
&= \sum_{k_{\mathrm{R}}=1}^{K_{\mathrm{R}}} \begin{pmatrix} \left(\left\| \underline{\boldsymbol{H}}_{\mathrm{f}}^{(k_{\mathrm{R}},1)} \right\|^2 + \left\| \underline{\boldsymbol{H}}_{\mathrm{f}}^{(k_{\mathrm{R}},2)} \right\|^2 \right) \underline{\boldsymbol{U}}\underline{\boldsymbol{d}}^{(n)} \\ + \underline{\boldsymbol{H}}_{\mathrm{f}}^{(k_{\mathrm{R}},1)*} \boldsymbol{n}_{\mathrm{f}}^{(n,k_{\mathrm{R}})} - \underline{\boldsymbol{H}}_{\mathrm{f}}^{(k_{\mathrm{R}},2)} \boldsymbol{C} \left(\boldsymbol{n}_{\mathrm{f}}^{(n,k_{\mathrm{R}})} \right)^* \end{pmatrix}
\end{aligned}
\tag{3.56}
$$

where $\|\cdot\|$ returns the absolute value of each element of the input.

Secondly, the FFH/OFDM decoding processing should be carried out. Let us define equivalent channel gain as

$$
\boldsymbol{H}_{\mathrm{f,FFH}}^{(n)} = \sum_{k_{\mathrm{R}}=1}^{K_{\mathrm{R}}} \left(\left(\left\| \underline{\boldsymbol{H}}_{\mathrm{f}}^{(k_{\mathrm{R}},1)} \right\|^2 + \left\| \underline{\boldsymbol{H}}_{\mathrm{f}}^{(k_{\mathrm{R}},2)} \right\|^2 \right) \right). \tag{3.57}
$$

And the equivalent noise is defined as

$$
\underline{\boldsymbol{n}}_{\mathrm{f,FFH}}^{(n)} = \sum_{k_{\mathrm{R}}=1}^{K_{\mathrm{R}}} \left(\underline{\boldsymbol{H}}_{\mathrm{f}}^{(k_{\mathrm{R}},1)*} \boldsymbol{n}_{\mathrm{f}}^{(n,k_{\mathrm{R}})} - \boldsymbol{C} \underline{\boldsymbol{H}}_{\mathrm{fe}}^{(k_{\mathrm{R}},2)} \left(\boldsymbol{n}_{\mathrm{f}}^{(n,k_{\mathrm{R}})} \right)^* \right). \tag{3.58}
$$

To decode $\underline{\boldsymbol{d}}^{(n)}$ the, combined signal in (3.59) should be equalized. MMSE block linear equalizer (3.26) is recommended.

$$
\underline{\boldsymbol{s}}^{(n)} = \boldsymbol{H}_{\mathrm{f,FFH}}^{(n)} \underline{\boldsymbol{U}}\underline{\boldsymbol{d}}^{(n)} + \underline{\boldsymbol{n}}_{\mathrm{f,FFH}}^{(n)} \tag{3.59}
$$

Comparing with the STBC, the SFBC Alamouti scheme has the advantage to exploit spatial diversity within one OFDM symbol period. Disadvantage is sometimes the assumption for SFBC is not perfectly fulfilled. Especially in the server multipath environment, adjacent subcarriers do not have same frequency responses character.

3.4.2 Performance Evaluation

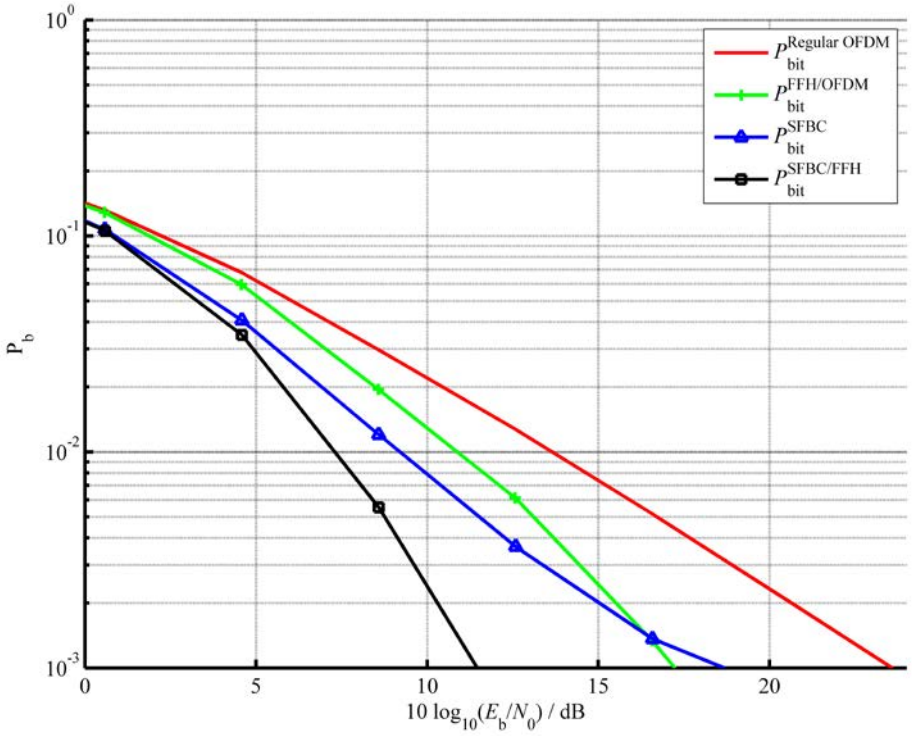

Figure 3.7 Uncoded BER Performance in IEEE 802.15.3a CM1 Channel

The uncoded BER performance of the proposed SFBC-FFH scheme is evaluated by simulation. The OFDM parameters in the simulation are listed in Table 3.1. In all the simulations, information bits are mapped to QPSK symbols. IEEE 802.15.3a CM1 and CM4 channels are used.

At desirably low BER values below 10^{-2}, the proposed SFBC/FFH scheme outperforms the regular OFDM, the conventional SFBC, and the FFH/OFDM by 6.5 dB, 4 dB and 2 dB, respectively. This is due to the SFBC/FFH scheme could exploits the spatial diversity and also considerable frequency diversity in the frequency selective channel. In the lower E_s/N_0 area, the conventional Alamouti SFBC is better than the FFH/OFDM scheme, since the FFH scheme introduces interference cross subcarrier. In the higher E_s/N_0 area, the FFH/OFDM exploits good frequency diversity, and the FFH/OFDM scheme begins outperforming the conventional SFBC scheme at the E_s/N_0 value around 17 dB. The proposed SFBC/FFH shows the best performance in the all listed schemes.

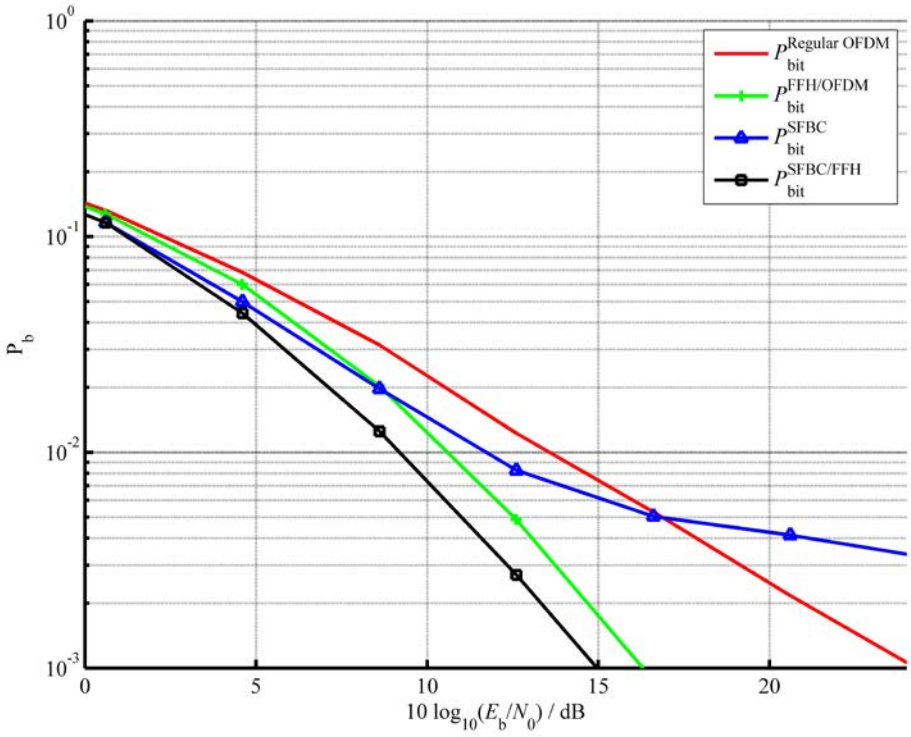

Figure 3.8 Uncoded BER Performance in IEEE 802.15.3a CM4 Channel

In Figure 3.8 the simulation results in IEEE 802.15.3a CM4 channel are presented. It is observed that the conventional Alamouti SFBC shows worst performance, even worse than the regular OFDM cases without applying the Alamouti scheme. This performance degradation is due to the severe multipath propagation in CM4 channel. Since the two concatenated subcarriers do not have identical frequency response in such a severe multipath channel, therefore the condition for Alamouti SFBC is not fulfilled any more. This leads to an even worse performance. At desirably low BER values below 10^{-2}, the proposed SFBC-FFH scheme outperforms the regular OFDM, the conventional SFBC, and the FFH/OFDM by about 4.5 dB, 3.5 dB, and 1.8 dB, respectively. Compared with performance in CM1 channel, performance gain introduced by the SFBC/FFH over other schemes in CM4 channel is smaller. However the proposed SFBC/FFH scheme still outperforms the other schemes.

3.5 Chapter Summary

Studies in this chapter are focusing on the first objective of this work, namely, to improve data transmission quality and accordingly extend the point-to-point communication range. The first task presented in Section 1.3.2 is solved.

In this chapter, the joint design of Alamouti SFBC scheme and the FFH/OFDM in a multiple antennas MB-OFDM UWB system is carried out. The implementation complexity of the proposed SFBC/FFH scheme is comparable to the same order Alamouti SFBC scheme. In the transmitter, the OFDM symbols are generated by complex vector weighting to the IFFT output, and complicated matrix multiplication is avoided. In the receiver, only one extra step for FFH/OFDM symbol equalization is required after a standard SFBC decoding. Simulation results show that the proposed SFBC/FFH scheme can introduce considerable improvements over the conventional MB-OFDM in IEEE 802.15.3a CM1 channel, and also acceptable performance gain in the CM4 channel. This performance gain comes from the jointly design of the Alamouti SFBC and FFH/OFDM schemes, which is able to exploit the spatial diversity and frequency diversity within one OFDM symbol period.

Chapter 4

Cooperative Communication in MB-OFDM UWB Systems

4.1 Chapter Overview

In Chapter 3, MIMO technology has been applied to MB-OFDM UWB systems to extend the point-to-point communication range. Usually it is not practical to have multiple antennas installed in some low cost UWB devices. In order to benefit from the performance enhancement introduced by MIMO technology, the cooperative communication between several single antenna UWB devices could be applied. In this chapter, studies of extending the communication range by exploiting the cooperative diversity in the network scenarios are discussed.

In Section 4.2 the principle of cooperative communication is introduced, and then the feasibility and advantages of cooperative communication in an MB-OFDM based UWB system are analyzed. In Section 4.3 the cooperative protocol in one-way relay MB-OFDM UWB system is designed. In the proposed protocol, SFBC is encoded in a distributed manner, and the TFC time frequency hopping feature of the MB-OFDM UWB system also is applied. Therefore, the proposed scheme is termed as distributed SFBC-TFC cooperative protocol. Performance of the designed cooperative protocol is evaluated in both LOS and NLOS scenarios. In Section 4.4 the chapter is summarized.

4.2 Cooperative Communication

4.2.1 Cooperative Diversity

To overcome performance degradation caused by multipath fading effects during the radio propagation, diversity technology could be used. There are many ways to obtain diversity, for instance diversity over time can be obtained via coding and interleaving, diversity over frequency can be exploited by frequency hopping, like the FFH/OFDM in [Sch05], and diversity over space can be obtained by STBC or SFBC code. Recently, cooperative commination was applied to exploit the cooperative diversity. The cooperative diversity was defined as space diversity using a collection of distributed antennas belonging to multiple users through jointly transmission in a distribute manner [Lan02]. Through cooperative diversity, sets of wireless terminals benefit by relaying messages for each other to propagate redundant signals over multiple paths in the wireless networks.

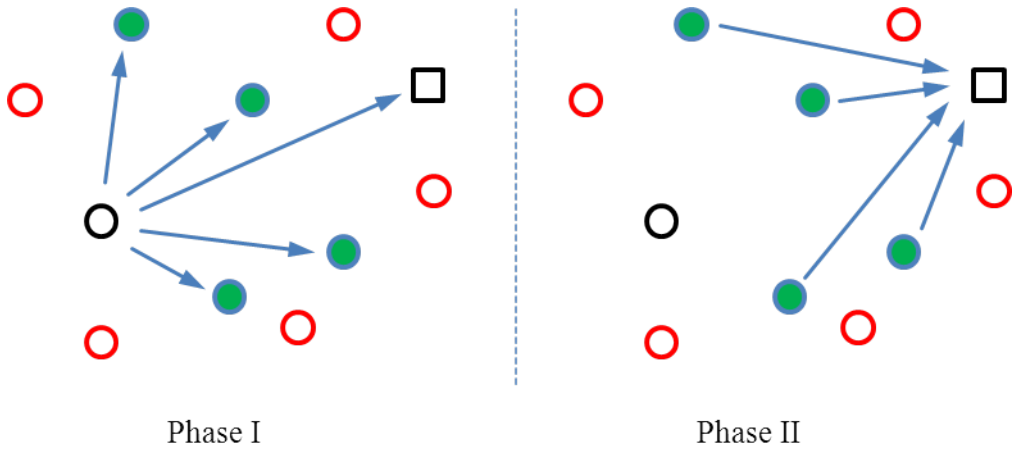

Figure 4.1 Illustration of the two phases of repetition-based and space–time-coded cooperative diversity algorithms (Adapted from **[Lan02]**).

In [Lan02] the two-phase cooperative protocol was designed. As shown in Figure 4.1, the black circle represents information source, the green ones represent the selected relays, the black circle represents the information source and the red cycles denote the other devices which are not involved in this cooperation. In the first phase, the source sends the message to destination. Thanks to the broadcasting feature of the radio channel, other devices could overhear this message, and some of them are selected as relays to assist the transmission. There are various strategies that can be applied to the overheard signal. In the simplest

case, the relays just amplify the received signal with analog signal processing and forward it. In more complicated cases, the received signal shall be demodulate and even decoded, and then a total new message is regenerated for forwarding. In the second phase, the selected relays forward the processed signal to the destination. Many strategies could be performed during this forwarding process, such as, simply repetition, or distributed coding schemes.

During the two-phase cooperative protocol, following problems are interesting, for instance, which devices are selected to be cooperated, how does one selected device deal with its received messages, and how do the selected devices cooperate with each other. These problems arouse the great research interests in the following topics.

- Relay selection

It is shown in Figure 4.1 that there are several available relay candidates around the source. The question is when to select a cooperators and which one shall be selected. There are various schemes to choose the best relay among a collection of available relays in the literature. In [Zha05], a location based relay selection method based on the geographic random forwarding (GeRaF) protocol proposed in [Zor031] and [Zor03] was presented. The relay selection criterion could also depend on the received SNR quality or CSI. For instance, in [Luo04] relay that has received the transmitted data from the source correctly and has the highest mean SNR to the destination node, is chosen to forward the source's data. In [Ibr08] availability of CSI at the source and the relays is used for relay selection. A properly designed relay selection criteria could improve the efficiency of the cooperative communication considerably, and reduce the overall power consumption of devices in the network.

- Forwarding Schemes

Regarding to signal processing to the received signal on the relay, different forwarding schemes could be applied. The most commonly talked forward schemes are, AF and DF. In an AF scheme, the received signal is amplified and then forwarded to the destination. However the noise is also amplified, therefore the AF scheme is not expected has good performance when the receiver works at low SNRs. It is studied in [Lin07] given an equal transmission power at source and relay, the performance of AF depends on the position of relay to the source and destination. Optimum relay location is the mid-point with respect to the source and destination. In DF scheme, relays apply some form of detection and/or

decoding algorithms to their received signals and re-encode the information and forward. When the channel quality between source and relay is good, the DF scheme outperforms the AF scheme. When the channel quality between source and relay is bad, in DF scheme relay does not decode the received message correctly, after re-encoding the incorrect bits, the error will be propagated to destination and leads to worse performance than the AF scheme [LiY09].

- Distributed Coding

In the second phase of the cooperative protocol illustrated Figure 4.1, instead of simply forwarding the received signal in a repetition manner separately, the distributed coding schemes could be applied. There are a wide range of distributed coding schemes, such as distributed STBC (D-STBC), distributed Turbo Code (DTC), and distributed LDPC code (D-LDPC), etc. In contrast to the conventional coding scheme, the distributed coding constructs the whole codeword in a distributed manner among the selected relays and source in the two-phase cooperative system [LiY09]. Different parts of the codeword of the distributed coding scheme are transmitted from different relays, and signal undergoes different fading. Therefore the distributed coding shows larger degree of freedom compared to the conventional coding schemes. The greatest challenges of the distributed coding are the practical issues during implementation, for instance, the synchronization between the cooperative devices, the error propagation problems, etc.

Aside from the general and theoretical studies mentioned above, specific and practical cooperative communication systems have been also investigated. IEEE 802 standards have already started working on incorporating cooperative techniques into current standards. In [Fit06] the IEEE 802 standardization activities that address cooperative techniques across the different Working Groups is surveyed. Some practical issues in different layer, such as, mesh networks, cooperative or multi-hop relay, spectrum sharing, and cognitive radio techniques are reviewed.

Cooperative techniques have only recently received considerable attentions. There are still a lot of theoretic as well as practical open issues.

4.2.2 Cooperative Communication in MB-OFDM UWB Systems

Similar to the other wireless communication systems, the throughput enhancement, coverage extension and spectral efficiency improvement can be also benefited from applying the cooperative communication schemes to the MB-OFDM UWB systems. The state-of-the-art of the cooperative communication in the MB-OFDM UWB systems has been reviewed in the Section 1.2. In this part, we only discuss the advantages of the MB-OFDM UWB system in applying the cooperative communication technologies.

One of the advantages of the cooperative communication in MB-OFDM systems is due to the OFDM technique. OFDM can convert the multipath channel into parallel single tap channel, which eases the signal equalization, and also raise the feasibility of implementation the cooperative scheme. Compared with the impulse based UWB systems, the MB-OFDM UWB systems are more suitable to perform the cooperative communication in the signal processing point of view.

Another advantage for MB-OFDM UWB systems to perform cooperative communication is its time frequency hopping scheme. As shown in Figure 3.1, in an MB-OFDM UWB system, multiple orthogonal physical resources, namely, the multiple frequency bands are available. The orthogonal frequency band could be used simultaneously in a hopping manner defined by the TFCs. This provides more flexible multiple access scheme to the selected relays, and reduce the complexity in signal detection during the cooperation. This is a unique feature of MB-OFDM UWB systems over the other wireless communication. With this feature, the source and relay can transmit via orthogonal band or the same band in the second phase of the cooperative relay protocol illustrate by Figure 4.1. When different band is used on different relays, the destination can easily separate the received signal from multiple relay, since they do not interface with each other due to the orthogonal bands. The receiver just combine them from different receive band. However this demands bigger memory to store temporally the revived signals for each band. Alternatively, the same frequency band can be used by different relays. In this case, the signal received at the destination is the superposition of signal forwarded by different relays, and distributed coding shall be applied to ease the signals processing on the designation.

By utilizing time frequency hopping feature in MB-OFDM UWB system, in Section 4.3 the distributed SFBC-TFC cooperative protocol is designed.

4.3 Distributed SFBC-TFC Protocol

In this section, a real-time cooperative protocol in one-way relay system based on MB-OFDM UWB is presented. This protocol is designed to extend the coverage of the MB-OFDM UWB networks, and is especially suitable to the delay-critical HDR applications, such as the HD video streaming over large distance. In this protocol, the TFCs time frequency hopping and the Alamouti SFBC scheme are jointly designed. Different from the classic Alamouti SFBC scheme in a multiple antenna MB-OFDM UWB system, the construction of Alamouti SFBC code in the proposed protocol is in a distributed manner. Both the conventional Alamouti SFCB [Ala98] and the proposed SFBC/FFH scheme in Section 3.4 could be applied. For less reduplicate expression, we describe the protocol with a classic Alamouti SFBC scheme. The formulation with SFBC/FFH scheme could be similarly derived by referencing to Section 3.4.1.

In Section 4.3.1, the one-way cooperative relay system model is illustrated. In Section 4.3.2, the distributed SFBC-TFC protocol is designed. And In Section 4.3.3, the performance of the proposed cooperative protocol is analyzed.

4.3.1 System Model

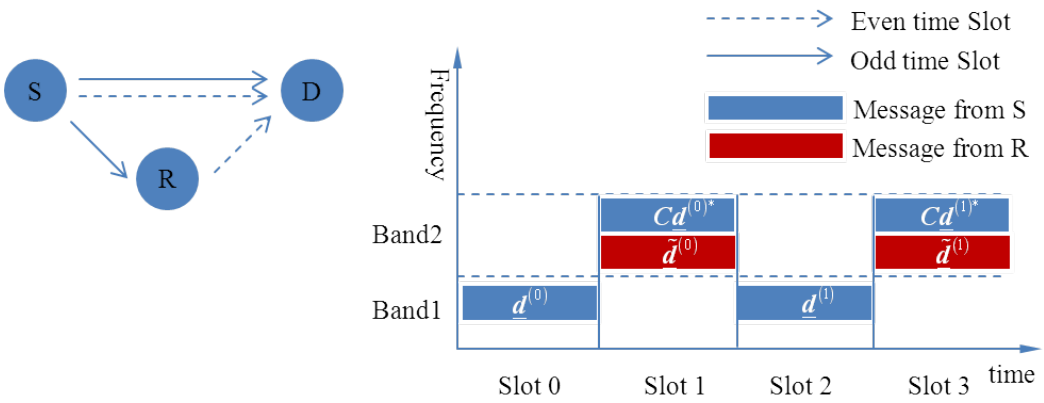

Figure 4.2 Three node relay strategy with distributed SFC-TFC-OFDM

In Figure 4.2 the distributed SFBC-TFC protocol in a one-way relay system is shown. There are three MB-OFDM UWB devices in the relay system, labeled as source (S), relay (R) and destination (D), respectively. When S and D are spaced by large distance, the transmission quality from S directly to D is bad. Therefore the information generated by S is transmitted to D with the aid of R.

4.3.2 Protocol Design

Let us assume that, on S, the time frequency hopping code TFC 8 [WiM09] is applied, TDS is also applied for reliable data transmission. In the 2*n*-th time slot, S broadcasts the message over band 1, and in the 2*n*+1-th time slot, S encodes the same message with SFBC code, and broadcasts it on band 2.

For R, in the 2*n*-th time slot, it receives signal from S, and in the 2*n*+1-th time slot it forwards the re-generated signal to D. The signal could be re-generated with either DF or AF scheme. When a DF scheme is applied, some complicated signal processing is required. For instance, converting the received time domain signal into frequency domain symbols, and demodulating the symbols with hard decision technique, etc. Then the detected symbols should be re-modulated to time domain samples again. During this process, DFT and IDFT operation should be performed each once, and hard decisions are made to all the frequency domain symbols. Expect for the computational complexity, the time for processing is also limited. Therefore it is really a challenge for the relay to do the DF during one OFDM symbol period. Alternatively the AF based method could be considered. Based on AF scheme, received signals on R are just scaled and forwarded. Therefore the AF based scheme is much simpler from the implementation point of view.

For D, in the 2*n*-th time slot, it receives the message from the direct link between S and D without interference. In the 2*n*+1-th time slot, it receives the superposition of signals from S and R. The superposition signals are encoded with distributed SFBC scheme between S and R, and the Alamouti decoding method discussed in Section 3.4.1 could be used to decode the superposition signals.

Referencing to (3.47), the signal transmitted by S is given by

$$\begin{cases} \underline{\boldsymbol{d}}^{(n)}, 2n \\ \boldsymbol{C}\underline{\boldsymbol{d}}^{(n)*}, 2n+1 \end{cases} \tag{4.1}$$

$\underline{\boldsymbol{d}}^{(n)}$ is transmitted in the 2*n*-th time slot with power α. $\boldsymbol{C}\underline{\boldsymbol{d}}^{(n)*}$ is transmitted in the 2*n*+1-th time slot with power β, which is the one part of the distributed SFBC codeword.

The received signal on R in the 2*n*-th time slot is given by

$$\underline{\boldsymbol{e}}_{\mathrm{f,r}}^{(2n)} = \sqrt{\alpha}\,\underline{\boldsymbol{H}}_{\mathrm{f,sr}}^{(2n)}\underline{\boldsymbol{d}}^{(n)} + \underline{\boldsymbol{n}}_{\mathrm{f,r}}^{(2n)}, \tag{4.2}$$

and the re-generated frequency domain signal by R with AF scheme is given by

$$\begin{aligned}\underline{\tilde{\boldsymbol{d}}}^{(n)} &= \boldsymbol{A}\left(\underline{\boldsymbol{e}}_{\mathrm{f,r}}^{(2n)}\right), \\ &= \sqrt{\alpha}\boldsymbol{A}\left(\underline{\boldsymbol{H}}_{\mathrm{f,sr}}^{(2n)}\underline{\boldsymbol{d}}^{(n)} + \underline{\boldsymbol{n}}_{\mathrm{f,r}}^{(2n)}\right) \\ &= \sqrt{\alpha}\boldsymbol{A}\underline{\boldsymbol{H}}_{\mathrm{f,sr}}^{(2n)}\underline{\boldsymbol{d}}^{(n)} + \boldsymbol{A}\underline{\boldsymbol{n}}_{\mathrm{f,r}}^{(2n)},\end{aligned} \tag{4.3}$$

where

$$\boldsymbol{A} = \left(\alpha\left\|\underline{\boldsymbol{H}}_{\mathrm{f,sr}}^{(2n)}\right\|^2 + N_0 \cdot \boldsymbol{I}\right)^{-1/2} \tag{4.4}$$

is a scaling matrix used to normalize the power of re-generated signal, N_0 is noise power spectral density, $\|\cdot\|$ returns the absolute value of each element of the input. $\underline{\boldsymbol{H}}_{\mathrm{f,sr}}^{(2n)}$ represents the CTF matrix of channel between S and R in the 2*n*-th time slot, and $\underline{\boldsymbol{n}}_{\mathrm{f,r}}^{(2n)}$ represents the frequency domain AWGN noise added to the received signal in the 2*n*-th time slot. This re-generated signal is forwarded to D in the 2*n*+1-th time slot in band 2 with transmit power of γ, it is another part of the distributed SFBC codeword. This forwarded signal and the signal transmitted by S in the 2*n*+1-th time slot are in the same band, they construct the whole distributed SFBC codeword.

The received signal on D in the 2*n*-th time slot is given by

$$\underline{\boldsymbol{e}}_{\mathrm{f,d}}^{(2n)} = \sqrt{\alpha}\underline{\boldsymbol{H}}_{\mathrm{f,sd}}^{(2n)}\underline{\boldsymbol{d}}^{(n)} + \underline{\boldsymbol{n}}_{\mathrm{f,d}}^{(2n)}, \tag{4.5}$$

where $\underline{\boldsymbol{H}}_{\mathrm{f,sd}}^{(2n)}$ represents the CTF matrix of channel between S and D in the 2*n*-th time slot, $\underline{\boldsymbol{n}}_{\mathrm{f,d}}^{(2n)}$ represents the frequency domain AWGN noise added to the received signal.

The received signal on D in the 2*n*+1-th time slot is given by

$$\begin{aligned}\underline{\boldsymbol{e}}_{\mathrm{f,d}}^{(2n+1)} &= \sqrt{\gamma}\underline{\boldsymbol{H}}_{\mathrm{f,rd}}^{(2n+1)}\underline{\tilde{\boldsymbol{d}}}^{(n)} + \sqrt{\beta}\underline{\boldsymbol{H}}_{\mathrm{f,sd}}^{(2n+1)}\boldsymbol{C}\underline{\boldsymbol{d}}^{(n)*} + \boldsymbol{n}_{\mathrm{f,d}}^{(2n+1)} \\ &= \sqrt{\gamma}\underline{\boldsymbol{H}}_{\mathrm{f,rd}}^{(2n+1)}\left(\sqrt{\alpha}\boldsymbol{A}\underline{\boldsymbol{H}}_{\mathrm{f,sr}}^{(2n)}\underline{\boldsymbol{d}}^{(n)} + \boldsymbol{A}\underline{\boldsymbol{n}}_{\mathrm{f,r}}^{(2n)}\right) + \sqrt{\beta}\underline{\boldsymbol{H}}_{\mathrm{f,sd}}^{(2n+1)}\boldsymbol{C}\underline{\boldsymbol{d}}^{(n)*} + \boldsymbol{n}_{\mathrm{f,d}}^{(2n+1)} \\ &= \sqrt{\alpha}\sqrt{\gamma}\boldsymbol{A}\underline{\boldsymbol{H}}_{\mathrm{f,rd}}^{(2n+1)}\underline{\boldsymbol{H}}_{\mathrm{f,sr}}^{(2n)}\underline{\boldsymbol{d}}^{(n)} + \sqrt{\beta}\underline{\boldsymbol{H}}_{\mathrm{f,sd}}^{(2n+1)}\boldsymbol{C}\underline{\boldsymbol{d}}^{(n)*} + \sqrt{\gamma}\boldsymbol{A}\underline{\boldsymbol{H}}_{\mathrm{f,rd}}^{(2n+1)}\underline{\boldsymbol{n}}_{\mathrm{f,r}}^{(2n)} + \boldsymbol{n}_{\mathrm{f,d}}^{(2n+1)} \\ &= \underbrace{\sqrt{\alpha}\sqrt{\gamma}\boldsymbol{A}\underline{\boldsymbol{H}}_{\mathrm{f,rd}}^{(2n+1)}\underline{\boldsymbol{H}}_{\mathrm{f,sr}}^{(2n)}}_{\underline{\boldsymbol{H}}_{\mathrm{f,eq1}}}\underline{\boldsymbol{d}}^{(n)} + \underbrace{\sqrt{\beta}\underline{\boldsymbol{H}}_{\mathrm{f,sd}}^{(2n+1)}}_{\underline{\boldsymbol{H}}_{\mathrm{f,eq2}}}\boldsymbol{C}\underline{\boldsymbol{d}}^{(n)*} + \underbrace{\sqrt{\gamma}\boldsymbol{A}\underline{\boldsymbol{H}}_{\mathrm{f,rd}}^{(2n+1)}\underline{\boldsymbol{n}}_{\mathrm{f,r}}^{(2n)} + \boldsymbol{n}_{\mathrm{f,d}}^{(2n+1)}}_{\underline{\boldsymbol{n}}_{\mathrm{f,eq}}}\end{aligned} \tag{4.6}$$

$\underline{\boldsymbol{H}}_{\mathrm{f,sd}}^{(2n+1)}$ represents the CTF matrix of channel between S and D in the $2n$+1-th time slot, $\underline{\boldsymbol{H}}_{\mathrm{f,sd}}^{(2n+1)}$ is different from and $\underline{\boldsymbol{H}}_{\mathrm{f,sd}}^{(2n)}$ since different frequency band is used. $\underline{\boldsymbol{H}}_{\mathrm{f,rd}}^{(2n+1)}$ is the CTF matrix of channel between R and D in the $2n$+1-th time slot. $\underline{\boldsymbol{n}}_{\mathrm{f,d}}^{(2n+1)}$ represents the frequency domain AWGN noise added to the received signal in the $2n$+1-th time slot.

The equivalent baseband model of the cooperative system is given by

$$\begin{aligned}\begin{pmatrix}\underline{\boldsymbol{e}}_{\mathrm{f,d}}^{(2n)}\\ \underline{\boldsymbol{e}}_{\mathrm{f,d}}^{(2n+1)}\end{pmatrix}&=\begin{bmatrix}\sqrt{\alpha}\boldsymbol{H}_{\mathrm{f,sd}}^{(2n)} & 0\\ \sqrt{\alpha}\sqrt{\gamma}\boldsymbol{A}\underline{\boldsymbol{H}}_{\mathrm{f,sr}}^{(2n)}\boldsymbol{H}_{\mathrm{f,rd}}^{(2n+1)} & \sqrt{\beta}\boldsymbol{H}_{\mathrm{f,rd}}^{(2n+1)}\end{bmatrix}\begin{bmatrix}\underline{\boldsymbol{d}}^{(n)}\\ \boldsymbol{C}\underline{\boldsymbol{d}}^{(n)*}\end{bmatrix}\\&+\begin{bmatrix}\underline{\boldsymbol{n}}_{\mathrm{f,d}}^{(2n)}\\ \sqrt{\gamma}\boldsymbol{A}\underline{\boldsymbol{H}}_{\mathrm{f,rd}}^{(2n+1)}\underline{\boldsymbol{n}}_{\mathrm{f,r}}^{(2n)}+\underline{\boldsymbol{n}}_{\mathrm{f,d}}^{(2n+1)}\end{bmatrix}\end{aligned}\tag{4.7}$$

Let us define

$$\underline{\boldsymbol{H}}_{\mathrm{f,eq1}}=\sqrt{\alpha}\sqrt{\gamma}\boldsymbol{A}\underline{\boldsymbol{H}}_{\mathrm{f,rd}}^{(2n+1)}\underline{\boldsymbol{H}}_{\mathrm{f,sr}}^{(2n)}\tag{4.8}$$

as the equivalent CTF matrix of the channel undergoes by the first part of the distributed Alamouti SFBC codeword, and define

$$\underline{\boldsymbol{H}}_{\mathrm{f,eq2}}=\sqrt{\beta}\underline{\boldsymbol{H}}_{\mathrm{f,sd}}^{(2n+1)}\tag{4.9}$$

as the equivalent CTF matrix of the channel by the second part of the distributed SFBC codeword, and define

$$\underline{\boldsymbol{n}}_{\mathrm{f,eq}}=\sqrt{\gamma}\boldsymbol{A}\underline{\boldsymbol{H}}_{\mathrm{f,rd}}^{(2n+1)}\underline{\boldsymbol{n}}_{\mathrm{f,r}}^{(2n)}+\boldsymbol{n}_{\mathrm{f,d}}^{(2n+1)}\tag{4.10}$$

as the equivalent noise added to the whole STBC codeword.

According to (3.55), the following equalizer is designed

$$\begin{aligned}\underline{\boldsymbol{H}}_{\mathrm{fe,eq1}}&=\underline{\boldsymbol{H}}_{\mathrm{f,eq1}}^{*}\\ \underline{\boldsymbol{H}}_{\mathrm{fe,eq2}}&=\underline{\boldsymbol{H}}_{\mathrm{f,eq2}}\boldsymbol{C}^{\mathrm{T}}.\end{aligned}\tag{4.11}$$

The decoding process is the same as presented in Section 3.4.1. After Alamouti SFBC decoding, the combined signal in the $2n$+1-th time slot is given by

$$\begin{aligned}\underline{\boldsymbol{s}}^{(2n+1)} &= \underline{\boldsymbol{H}}_{\text{fe,eq1}}\underline{\boldsymbol{e}}_{\text{f,d}}^{(2n+1)} + \underline{\boldsymbol{H}}_{\text{fe,eq2}}\underline{\boldsymbol{e}}_{\text{f,d}}^{(2n+1)*} \\ &= \left(\left\|\underline{\boldsymbol{H}}_{\text{f,eq1}}\right\|^2 + \left\|\underline{\boldsymbol{H}}_{\text{f,eq2}}\right\|^2\right)\underline{\boldsymbol{d}}^{(n)} + \underline{\boldsymbol{H}}_{\text{f,eq1}}^{*}\boldsymbol{n}_{\text{f,eq}} - \underline{\boldsymbol{H}}_{\text{f,eq2}}\boldsymbol{C}\boldsymbol{n}_{\text{f,eq}}^{*} \\ &= \left(\alpha\gamma\left\|\underline{\boldsymbol{H}}_{\text{f,sr}}^{(2n)}\right\|^2 \cdot \left\|\underline{\boldsymbol{H}}_{\text{f,rd}}^{(2n+1)}\right\|^2 \left(\alpha\left\|\underline{\boldsymbol{H}}_{\text{f,sr}}^{(2n)}\right\|^2 + N_0\boldsymbol{E}\right)^{-1} + \beta\left\|\underline{\boldsymbol{H}}_{\text{f,sd}}^{(2n+1)}\right\|^2\right)\underline{\boldsymbol{d}}^{(n)} \\ &\quad + \sqrt{\alpha}\sqrt{\gamma}\left(\alpha\left\|\underline{\boldsymbol{H}}_{\text{f,sr}}^{(2n)}\right\|^2 + N_0\boldsymbol{E}\right)^{-1}\underline{\boldsymbol{H}}_{\text{f,sr}}^{(2n)*}\underline{\boldsymbol{H}}_{\text{f,rd}}^{(2n+1)*}\boldsymbol{n}_{\text{f,eq}} - \sqrt{\beta}\boldsymbol{C}\underline{\boldsymbol{H}}_{\text{f,sd}}^{(2n+1)}\boldsymbol{n}_{\text{f,eq}}^{*}\end{aligned} \tag{4.12}$$

For the finial detection, the (4.12) and (4.5) should be firstly combined, and then decoded in the following way,

$$\begin{aligned}\hat{\underline{\boldsymbol{d}}}^{(n)} &= \frac{\underline{\boldsymbol{s}}^{(2n+1)} + \sqrt{\alpha}\underline{\boldsymbol{H}}_{\text{f,sd}}^{(2n)*}\underline{\boldsymbol{e}}_{\text{f,d}}^{(2n)}}{\beta\left\|\underline{\boldsymbol{H}}_{\text{f,sd}}^{(2n+1)}\right\|^2 + \alpha\gamma\left\|\underline{\boldsymbol{H}}_{\text{f,sr}}^{(2n)}\right\|^2 \cdot \left\|\underline{\boldsymbol{H}}_{\text{f,rd}}^{(2n)}\right\|^2 \left(\alpha\left\|\underline{\boldsymbol{H}}_{\text{f,sr}}^{(2n)}\right\|^2 + N_0\boldsymbol{E}\right)^{-1} + \alpha\left\|\underline{\boldsymbol{H}}_{\text{f,sd}}^{(2n)}\right\|^2} \\ &= \frac{\underline{\boldsymbol{s}}^{(2n+1)} + \alpha\left\|\underline{\boldsymbol{H}}_{\text{f,sd}}^{(2n)}\right\|^2\underline{\boldsymbol{d}}^{(n)} + \sqrt{\alpha}\underline{\boldsymbol{H}}_{\text{f,sd}}^{(2n)*}\underline{\boldsymbol{n}}_{\text{f,d}}^{(2n)}}{\beta\left\|\underline{\boldsymbol{H}}_{\text{f,sd}}^{(2n+1)}\right\|^2 + \alpha\gamma\left\|\underline{\boldsymbol{H}}_{\text{f,sr}}^{(2n)}\right\|^2 \cdot \left\|\underline{\boldsymbol{H}}_{\text{f,rd}}^{(2n)}\right\|^2 \left(\alpha\left\|\underline{\boldsymbol{H}}_{\text{f,sr}}^{(2n)}\right\|^2 + N_0\boldsymbol{E}\right)^{-1} + \alpha\left\|\underline{\boldsymbol{H}}_{\text{f,sd}}^{(2n)}\right\|^2} \\ &= \underline{\boldsymbol{d}}^{(n)} + \frac{\sqrt{\alpha}\sqrt{\gamma}\left(\alpha\left\|\underline{\boldsymbol{H}}_{\text{f,sr}}^{(2n)}\right\|^2 + N_0\boldsymbol{E}\right)^{-1}\underline{\boldsymbol{H}}_{\text{f,sr}}^{(2n)*}\underline{\boldsymbol{H}}_{\text{f,rd}}^{(2n+1)*}\boldsymbol{n}_{\text{f,eq}} - \sqrt{\beta}\boldsymbol{C}\underline{\boldsymbol{H}}_{\text{f,sd}}^{(2n+1)}\boldsymbol{n}_{\text{f,eq}}^{*} + \sqrt{\alpha}\underline{\boldsymbol{H}}_{\text{f,sd}}^{(2n)*}\underline{\boldsymbol{n}}_{\text{f,d}}^{(2n)}}{\beta\left\|\underline{\boldsymbol{H}}_{\text{f,sd}}^{(2n+1)}\right\|^2 + \alpha\gamma\left\|\underline{\boldsymbol{H}}_{\text{f,sr}}^{(2n)}\right\|^2 \cdot \left\|\underline{\boldsymbol{H}}_{\text{f,rd}}^{(2n)}\right\|^2 \left(\alpha\left\|\underline{\boldsymbol{H}}_{\text{f,sr}}^{(2n)}\right\|^2 + N_0\boldsymbol{E}\right)^{-1} + \alpha\left\|\underline{\boldsymbol{H}}_{\text{f,sd}}^{(2n)}\right\|^2}\end{aligned} \tag{4.13}$$

The post-processing SNR of the combined signal in (4.13)is given by,

$$SNR = \left(\alpha\left\|\underline{\boldsymbol{H}}_{\text{f,sd}}^{(2n)}\right\|^2 + \beta\left\|\underline{\boldsymbol{H}}_{\text{f,sd}}^{(2n+1)}\right\|^2 + \gamma\left\|\underline{\boldsymbol{H}}_{\text{f,rd}}^{(2n+1)}\right\|^2 \cdot \frac{\alpha\left\|\underline{\boldsymbol{H}}_{\text{f,sr}}^{(2n)}\right\|^2}{\alpha\left\|\underline{\boldsymbol{H}}_{\text{f,sr}}^{(2n)}\right\|^2 + N_0\boldsymbol{E}}\right)\frac{E_s}{N_0} \tag{4.14}$$

In the 2*n*-th time slot, when the received signals on the R have high SNR,

$$\alpha\left\|\underline{\boldsymbol{H}}_{\text{f,sr}}^{(2n)}\right\|^2 + N_0\boldsymbol{E} \approx \alpha\left\|\underline{\boldsymbol{H}}_{\text{f,sr}}^{(2n)}\right\|^2 \tag{4.15}$$

The (4.14) becomes

$$SNR \approx \left(\beta\left\|\underline{\boldsymbol{H}}_{\text{f,sd}}^{(2n+1)}\right\|^2 + \gamma\left\|\underline{\boldsymbol{H}}_{\text{f,rd}}^{(2n+1)}\right\|^2 + \alpha\left\|\underline{\boldsymbol{H}}_{\text{f,sd}}^{(2n)}\right\|^2\right)\frac{E_s}{N_0} \tag{4.16}$$

It is shown from (4.16) that, the distributed SFBC-TFC protocol could introduce a diversity order of three.

When in the 2*n*-th time slot, the received signals on R have low SNR, the (4.14) becomes,

$$SNR \approx \left(\alpha \left\| \underline{\boldsymbol{H}}_{\mathrm{f,sd}}^{(2n)} \right\|^2 + \beta \left\| \underline{\boldsymbol{H}}_{\mathrm{f,sd}}^{(2n+1)} \right\|^2 \right) \frac{E_s}{N_0}. \tag{4.17}$$

The distributed SFBC-TFC protocol could still introduce a diversity order of two. In other words, the proposed distributed SFBC-TFC cooperative protocol could benefit at least a diversity order of two.

4.3.3 Performance Analysis

One of the advantages of the distributed SFBC-TFC cooperative protocol is its real time feature. Once R receives one OFDM symbol, it forwards immediately. The proposed protocol is able to improve the data transmission quality without introducing any latency. Therefore it is suitable for the delay-critical applications.

Another advantage of the distributed SFBC-TFC cooperative protocol is its feasibility in implementation. In realizing proposed SFBC-TFC protocol, only a little modification to the standard WiMedia UWB devices is required. On the D side, a standard linear decoding scheme for the Alamouti SFBC is required. On the S side, the SFBC encoding is needed, as already discussed in (3.49), the SBFC encoding could be realized by weighting to the time domain signal with two complex vector, no matrix multiplication required. On the R side, only the low cost AF scheme is needed. Therefore, the proposed SFBC-TFC cooperative protocol could be adapted to the standard WiMedia UWB devices with only a little modification.

In addition, higher instantaneous transmit power is allowed on S and R in the proposed protocol. As already discussed in Section 3.2.1, in the MB-OFDM UWB system, when time frequency hopping is applied, higher instantaneous transmit power is allowed. In the protocol, S applies TFC 8, 3 dB transmitter power increase is allowed. R only transmits in half time, therefore 3 dB transmitter power increase is also allowed.

The uncoded BER performances of SFBC-TFC cooperative relay with FFH/OFDM scheme are evaluated through simulation. Two simulation scenarios are carried out. In the first scenario, the LOS MPCs between the each two device among S, R and D exist. We emulate this scenario by applying IEEE 802.15.3a

CM1 channel to model $\underline{\boldsymbol{H}}_{\mathrm{f,sr}}^{(2n)}$, $\underline{\boldsymbol{H}}_{\mathrm{f,sd}}^{(2n)}$, $\underline{\boldsymbol{H}}_{\mathrm{f,sd}}^{(2n+1)}$ and $\underline{\boldsymbol{H}}_{\mathrm{f,rd}}^{(2n+1)}$. In the second scenario, the channel between S and D is assumed to be NLOS, and channel between S and R, R and D is assumed to be LOS. In this scenario, $\underline{\boldsymbol{H}}_{\mathrm{f,sd}}^{(2n)}$ and $\underline{\boldsymbol{H}}_{\mathrm{f,sd}}^{(2n+1)}$ are modeled with IEEE 802.15.3a CM4 channel, and $\underline{\boldsymbol{H}}_{\mathrm{f,sr}}^{(2n)}$ and $\underline{\boldsymbol{H}}_{\mathrm{f,rd}}^{(2n+1)}$ are modeled with IEEE 802.15.3a CM1 channel. Let all the transmission on S, R have the same transmit power, namely, $\alpha = \beta = \gamma = P/3$, P denotes the total transmit power. In Figure 4.3, the red curve represents BER performance of naive transmission without cooperation from S to D in CM1 channel. The green curve represents the BER performance of transmission in the first scenario, and the black curve shows the BER performance of transmission in the second scenario. At desirably low BER values below 10^{-2}, the proposed SFBC-TFC cooperative scheme could introduce 5 dB and 3.5 dB gain over the naive transmission in the LOS scenario and the scenario when S to D link is NLOS. In the second scenario, although there is no LOS MPC between S and D, the performance transmission does not have much degradation compared to first scenarios. This is because the relay links are LOS, and the good condition relay link improves the overall transmission quality. This performance gain benefits from the higher order of freedom exploitation of the proposed SFBC-TFC cooperative protocol.

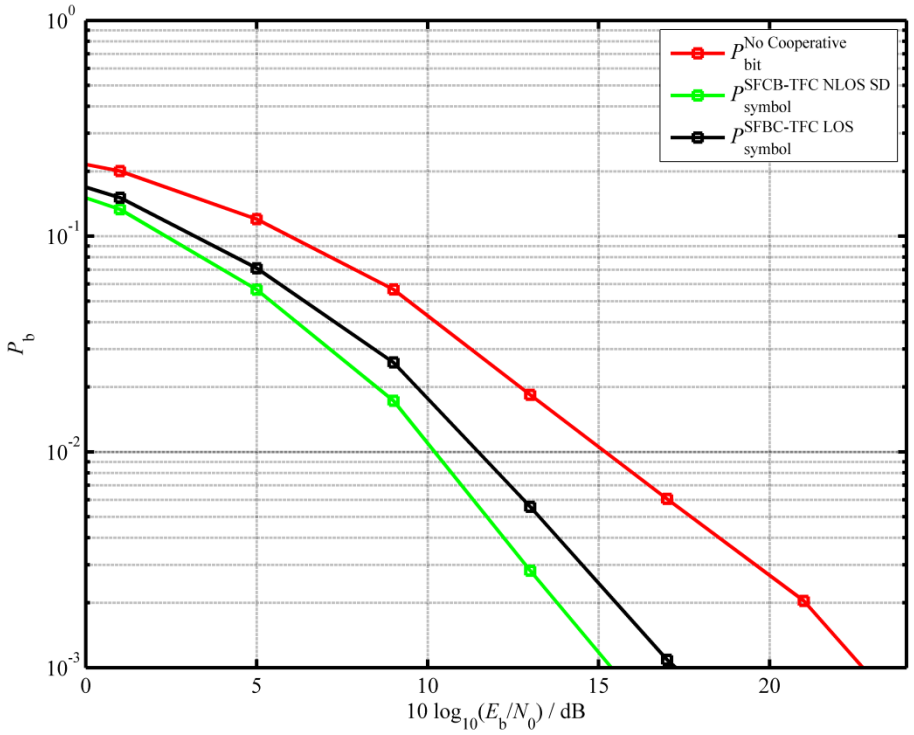

Figure 4.3 BER performance of the SFC-TFC-OFDM

4.4 Chapter Summary

Same as the Chapter 3, studies in this chapter are also focusing on extending the communication range of the MB-OFDM UWB systems. Network coverage can be improved by the distributed SFBC-TFC cooperative protocol in MB-OFDM based UWB systems. The second task of the thesis presented in Section 1.3.2 is finished.

It is analyzed that a diversity order of at least two is introduced through proposed cooperative protocol. With this higher order of freedom, more robust transmission is provided. Simulation results show that, the distributed SFBC-TFC cooperative protocol works well in both LOS and NLOS environments and it is suitable to improve the transmission quality and extend network coverage.

In addition to the outperformance, the distributed SFBC-TFC scheme shows other good features, including good real-time property, flexible and feasible in implementation, etc. And it is suitable to support delay-critical HDR services in the MB-FODM UWB networks.

Chapter 5

Accurate Ranging in MB-OFDM UWB Systems

5.1 Chapter Overview

In this chapter, accurate ranging methods in an MB-OFDM UWB system are developed. Although the OFDM based UWB system is not customized for ranging applications, it is still possible to provide ToA based ranging services due to the huge bandwidth of the OFDM symbols. There is a full definition of the RTT ranging protocol in [WiM09]. However ambiguities still exist in the specification, for instance, the ToA detection [Kra10] is not clear. To solve these problems, an accurate ToA detection method based on estimated channel information is designed. For the purpose of a feasible implementation, the RTT ranging protocol has been modified. With this modified RTT (MRTT) ranging protocol, complicated computational tasks are delivered to one side device, which is relative powerful in the ranging device pair. The proposed accurate ToA detection method and the MRTT protocol have introduced great promotion to the ranging performance of the MB-OFDM UWB system.

This chapter is organized as follows, in Section 5.2 different ranging technologies in wireless communication system and basics of the timing synchronization of MB-OFDM system are reviewed. In Section 5.3 the proposed accurate ToA detection method is presented. In Section 5.4 the MRTT protocol is designed and its performance is evaluated. Section 5.5 4 finalizes this chapter.

5.2 Basics to Radio Ranging and OFDM Timing Synchronization

5.2.1 Overview of Ranging Technology

Ranging is a measurement to get physical distance between two separated devices. There are professionally designed radio systems for ranging and localizations, for instance, the satellite positioning and navigation systems. Until now there are four such systems in operation or under development. They are GPS from USA, GLONASS (Globalnaya Navigatsionnaya Sputnikovaya Sistema) system from Russia, Galileo from European Union, and BeiDou (Compass) from China. Different from the professional satellite positioning and navigation systems, ranging and localization are secondary applications in most civil used wireless communication system. As discussed in Chapter 1, there are more and more LBS applications in wireless cellular networks, WLAN and wireless sensor networks (WSNs). In these wireless communication systems, ranging schemes based on AoA, RSS, and Time-of-Flight (ToF) are commonly applied.

- RSS based Method

The idea of RSS based method is to calculate the distance between a receiver and a transmitter from the signal strength attenuation during its propagation. The signal strength attenuation could be calculated when both transmit and receive power of the signal is known. Based on an appropriate propagation channel Path-loss model and the detected RSS, the propagation distance could be estimated. The Path-loss of UWB radio propagation channel is already mentioned in Section 2.2.2. In the department of communication technologies at the university of Duisburg-Essen, the RSS based ranging algorithms with WiMedia OFDM UWB devices have been intensively examined and reported in [Wan10], [Waa10], and [Waa101].

RSS based method has the lowest implementation complexity among the three mentioned schemes. It does not require any extra hardware support from the devices, since in most of the wireless communication systems RSS information is available. Therefore the RSS based ranging method is attractive to the some low cost systems, such as WSNs and WLANs. The performance of the RSS based method relies on the Path-loss model of the propagation channel which is determined by the environment around transmitter and receiver. Therefore RSS based ranging method is very sensitive to the surroundings. The performance is

not guaranteed when moving the RSS based ranging system from one place to another. Aside from the instability, the ranging accuracy performance is also not good.

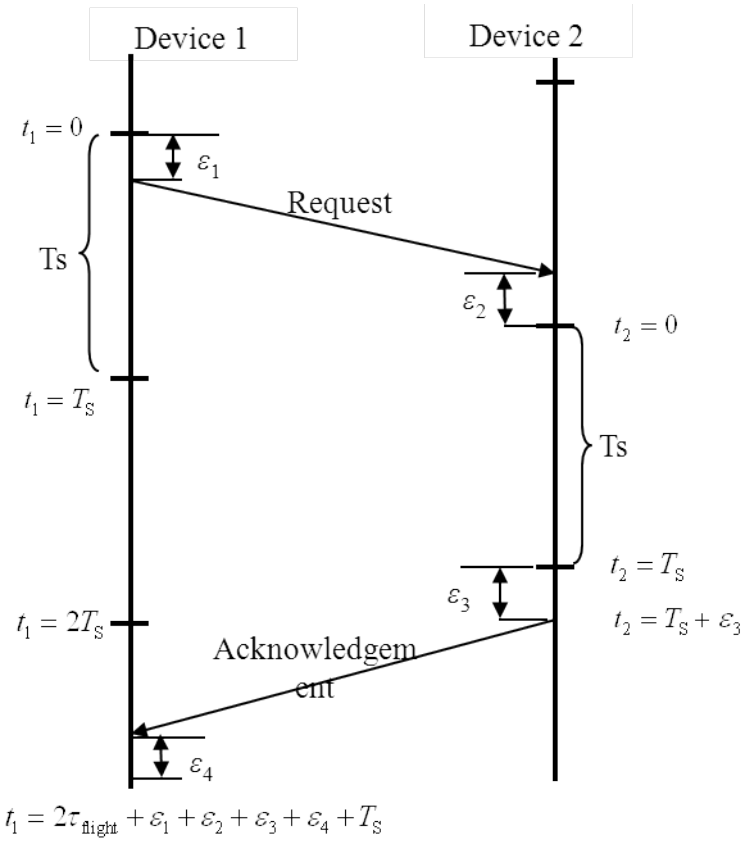

Figure 5.1 Illustration of ToF based method with RTT measurement protocol

- ToF based Method

ToF based ranging method relies on the measured travelling time of radio signal between transmitter and receiver. When transmitter and receiver have common time, one-way measurement is enough to get the propagation delay. Normally it is a difficulty to have well synchronized common time on separate devices. Alternatively the RTT measurement could be applied, since in the RTT protocol no common clock between ranging devices is required. The procedure of the RTT measurement is illustrated in Figure 5.1. Let us assume that Device 1 and Devices 2 in Figure 5.1 apply a Time Division Multiple Access (TDMA) scheme, each is considered to have the same duration T_s. Device 1 starts one ranging procedure by sending the ranging request packet to Device 2. After received the ranging request packet and doing some signal processing, Device 2 answers to Device 1

with the ranging acknowledgment packet. Device 1 receives the ranging acknowledgment, and then calculates the RTT. The RTT is formulated by

$$\tau_{\mathrm{RTT}} = 2\tau_{\mathrm{filgh}} + \varepsilon_1 + \varepsilon_2 + \varepsilon_3 + \varepsilon_4 + T_{\mathrm{s}} \tag{5.1}$$

ε_1, and ε_3 are time drift due to signal processing delay in transmitting chain, and ε_2, ε_4 is time drift due to signal processing delay in receiving chain. These values depend on the hardware of the devices, and their expectation could be measured a priori and stored by the devices. The flight time of the signal τ_{filgh} could be estimated from τ_{RTT} by excluding the time drifts, and the distance is calculated by $c \cdot \tau_{\mathrm{filgh}}$, where c is speed of light.

The RTT measurement protocol is the most commonly used in the professional ranging systems, and provides high accurate ranging performance. Of course, the complexity of ToF based ranging is higher than the RSS based, it requires complex hardware design and has more signal processing tasks.

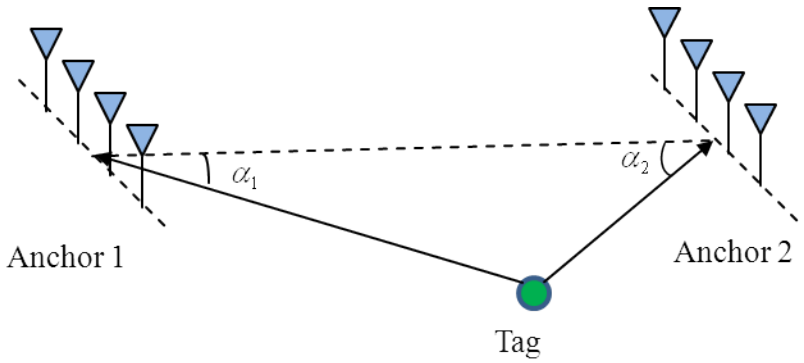

Figure 5.2 Illustration of AoA based Ranging Method

- AoA based Method

The AoA based positioning involves measuring angles of the target device seen by the anchor devices. In such systems, antenna array should be deployed on the anchor devices. Different from the RSS and ToF based methods, AoA based method does not estimate distance between devices. In order to determine the location of a tag device in a two-dimensional space, at least two anchor devices are needed. The principle of AoA based positioning method is illustrated in Figure 5.2. In Figure 5.2 Uniform Linear Array (ULA) is applied, other types of antenna array, such as Uniform Circular Array (UCA), could also be applied as

alternative. When the AoAs from the tag device to all anchor devices are known, the position of the target could be estimated through the trigonometry.

The AoA based positioning method is not practical for the UWB system. Since the bandwidth of an UWB signal is large, the UWB channel has considerable angle dispersion during the propagation. Besides, since the number of multipath components is very large in indoor environments, an implementation of maximum likelihood approach to estimate the AoA of each path requires a computationally expensive multidimensional search with the dimension determined by the number of signal path [Ars06]. Therefore, accurate positioning becomes very challenging with AoA based method in an UWB system.

The mentioned ranging methods are the most commonly used schemes. When design a ranging system, they could be applied separately or jointly. In [WiM09], ToF based RTT protocol is proposed for the MB-FODM UWB systems.

5.2.2 Timing Synchronization in the MB-OFDM System

To a ToF based ranging method, accurate ToA detection of the radio signal is one of the key issues to the ranging procedure. In an OFDM based UWB system, ToA detection could be directly derived from the OFDM timing synchronization. However the Symbol Timing Offset (STO) exiting in the synchronization is a problematic issue to the OFDM systems, especially to the ranging applications. STO is the time difference between the determined starting time of the sampled OFDM symbol and its real arrival time. To get a high precise ranging result based on ToA, it is necessary to understand the timing synchronization of OFDM signal.

In the discrete-time baseband signal processing, starting time of an OFDM symbol can be estimated in either time domain or frequency domain. In packet based OFDM systems, user data are organized into packets, and the maximum length of one packet is limited, so that channel impairments and synchronization parameters remain almost stationary within one packet [Chi07]. Each packet starts with preamble signals for time synchronization and channel estimation. In such systems, an ISI-free DFT window must be derived as soon as possible in order to process with tasks such as channel estimation and packet header detection [Chi07]. Synchronization must be promptly established. Therefore in the packet-based OFDM systems timing synchronization is normally carried out with time domain method.

MB-OFDM UWB systems are packet based, and the synchronization shall be also performed in time domain. Since the TFC hopping is applied to the MB-OFDM UWB systems, the preamble processing should not only solve the general synchronization problems, but also be responsible to identify the TFC pattern applied by the received packet. There are only a few studies on synchronization in MB-OFDM systems reported. In [YeZ08] and [LiY08] the timing synchronization for MB-OFDM UWB systems with time domain method could be found. There are usually two stages during the timing synchronization, namely, coarse timing detection and fine timing detection. For instance, in [LiY08] the MB-OFDM receiver deals the samples with following order: Sync detection (TFC pattern detection), coarse timing detection, fine time detection, oscillator frequency offset (OFO) estimation, channel estimation, equalization and data detection. The preamble structure for an MB-OFDM UWB used in [LiY08] is illustrated in Figure 5.3. The preamble has length of 30 OFDM symbols, and is divided into three parts. The first six OFDM symbols belong to Part a, and they are used for coarse timing detection and TFC pattern detection. The following 18 OFDM symbols are in Part b, and fine timing detection is carried out through these symbols. The last 6 OFDM symbols are in Part c, and they are applied to estimate channel.

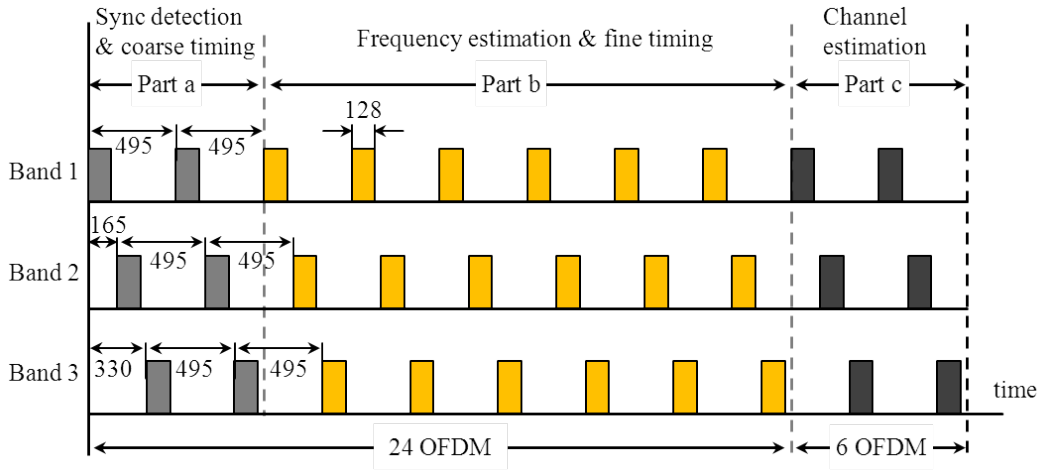

Figure 5.3 Structure of preamble pattern and synchronization method in [LiY08]

- Coarse timing detection

Let us denote the received baseband OFDM samples in time domain as $\underline{r}_i$, and i is the received sample index in the receiver. One complete OFDM symbol has length of $N_{\text{sys}} = N_{\text{FFT}} + N_{\text{ZP}}$ samples. Due to the repetition feature of the received

OFDM preamble, the receiver could detect the starting time of an OFDM symbol through the Auto-Correlation Function (ACF) based method given by

$$\begin{aligned} \mathrm{ACF}(i) &= \sum_{m=1}^{N_{\mathrm{FFT}}} \underline{r}_{m+i}^{*} \underline{r}_{m+i+N_{\mathrm{sys}}} \\ &= \mathrm{ACF}(i-1) + U(N_{\mathrm{FFT}}+i) - U(i), \end{aligned} \tag{5.2}$$

where

$$U(i) \triangleq \underline{r}_{i}^{*} \underline{r}_{i+N_{\mathrm{sys}}}^{*}. \tag{5.3}$$

ACF is carried out between the segments of the received signals with delay of N_{sys} samples. Output of ACF reflects the auto-correlation property of the received sample vector of length N_{FFT}. When assuming the received i-th sample is the start of an preamble OFDM symbol, ACF(i) gets peak value. The coarse timing detection is an optimization problem to search for the sample that can the maximize the output of ACF,

$$\hat{i} = \arg\max_{i} \left\{ \mathrm{ACF}(i) \right\} \tag{5.4}$$

The ACF method is with low computation complexity. As shown in (5.2), ACF could be calculated in an iterative manner, only one complex multiplication and two complex additions are required for every new received sample [YeZ08].

- Fine timing Synchronization

The coarse timing detection acquires only rough timing synchronization, and after that there may be still a large STO error. Fine time detection is required to get accurate timing synchronization. Normally fine timing detection in the MB-OFDM UWB system is carried out by cross-correlation method.

Instead of correlating received signal with its delayed version using ACF in (5.2), the receiver correlates the received samples with the known synchronization symbols $\underline{s}$. The Cross-correlation function (CCF) between the received samples and the pure signal $\underline{s}$ is given by,

$$\mathrm{CCF}(i) = \sum_{m=0}^{N_{\mathrm{FFT}}-1} \underline{r}_{m+i}^{*} \underline{s}_{m} \tag{5.5}$$

Output of CCF reflects the correlation between the received samples and the known synchronization sequence without noise. Similar to coarse timing detection, fine timing detection is also an optimization problem subject to

$$\hat{i} = \arg\max_{i} \{\mathrm{CCF}(i)\}. \tag{5.6}$$

In the case of MB-OFDM UWB, synchronization symbols {s[m]} with the length of $N_{\mathrm{FFT}} = 128$ samples, CCF calculation for each new received sample, 256 real multiplications (or 64 complex multiplications) and 127 complex additions for every received sample are needed. It is more expensive than the ACF-based coarse timing detection.

5.3 Fine ToA Detection for Ranging

In Section 5.2.2, the timing synchronization of an OFDM UWB system is reviewed. Fine timing synchronization is able to estimate the ToA of the received signal with sample level accuracy. This timing accuracy is enough for data detection, but not enough for the ranging applications.

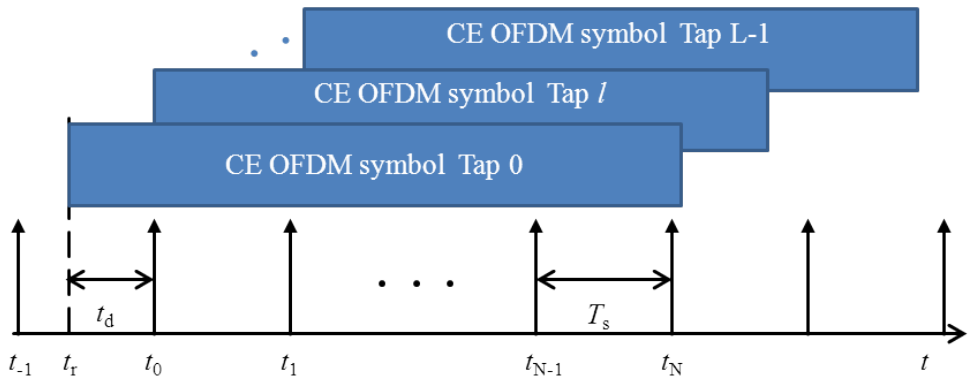

Figure 5.4 illustration arrival of OFDM symbol from multiple paths

Let us assume that after coarse timing and fine timing detection good synchronization is established, and the receiver can find the correct starting sample of the received OFDM symbol. Due to the sampling quantization error, there is still a fraction bias between the real ToA and the estimated starting sample through timing synchronization. As illustrated in Figure 5.4, let us assume that the first OFDM sample arrives at time t_r, and the estimated starting time is t_0, the fraction STO is the time difference between t_0 and t_r .Le us denote is as t_d, and let us assume that $t_d \in [-0.5T_s, 0.5T_s]$, and is uniformly distributed. This fraction

STO does not affect the performance of payload data detection, since it is included in the estimated channel. When applying t_0 to the ranging applications, there is an uncertainty of $t_d \cdot c$ meter in ranging result, and c is the speed of light in free space. To get fine ToA of the OFDM UWB signal and better ranging accuracy, this fraction STO should be estimated and compensated.

In this section, fine ToA detection method of MB-OFDM UWB for ranging application is studied. In Section 5.3.1, conventional phase shift method to estimate the fraction STO is introduced. It is analyzed that phased shift method does not work in multipath propagation channel. In Section 5.3.2 fine ToA detection method based on CIR energy of the estimated channel is designed. The simulation results show that the CIR energy based fine ToA detection method has good performance in multipath propagation channel.

5.3.1 Phase Shift based Method

To estimate the fraction STO as illustrated in Figure 5.4, frequency domain phase shift method in [Chi07] can be applied. The idea of phase shift based method is to estimate the fraction STO through the phase difference of the received symbols which are modulated to different subcarriers. This method could be better interpreted by using the estimated channel.

Let the received OFDM symbols affected by fraction STO and AWGN noised be

$$\begin{aligned} \underline{\boldsymbol{e}}_f &= \underline{\boldsymbol{E}}_f \underline{\boldsymbol{H}}_f \underline{\boldsymbol{d}}_{ce} + \underline{\boldsymbol{n}}_f \\ &= \underline{\hat{\boldsymbol{H}}}_f \underline{\boldsymbol{d}}_{ce}, \end{aligned} \tag{5.7}$$

where $\underline{\boldsymbol{e}}_f$, $\underline{\boldsymbol{d}}_{ce}$ and $\underline{\boldsymbol{n}}_f$ represents the received OFDM symbol, the transmitted OFDM channel estimation symbol and equivalent noise, respectively. $\underline{\boldsymbol{H}}_f$ is CTF matrix defined in (3.16). $\underline{\boldsymbol{E}}_f$ describes the estimated channel phase shift introduced by t_d . In this study, only STO error is discussed, other synchronization errors, such as Carrier Frequency Offset (CFO), etc. are not assumed to appear.

$$\underline{\boldsymbol{E}}_f = \begin{bmatrix} e^{j\varphi_0} & 0 & \cdots & 0 \\ 0 & e^{j\varphi_1} & \cdots & 0 \\ \vdots & \vdots & \ddots & \vdots \\ 0 & 0 & \cdots & e^{j\varphi_{N_{FFT}-1}} \end{bmatrix} \tag{5.8}$$

In frequency domain, t_{d} causes phase shift to the received symbols. The phase shift introduced to the symbols modulated to the *m*-th subcarrier is [Chi07],

$$\varphi_m = \frac{m \cdot t_{\mathrm{d}} \cdot 2\pi}{N_{\mathrm{FFT}} T_{\mathrm{s}}}, m = 0, \ldots, N_{\mathrm{FFT}} - 1 \tag{5.9}$$

After channel estimation, this phase shift will be included in the estimated channel $\hat{\underline{\boldsymbol{H}}}_{\mathrm{f}}$, as indicated in (5.10), where $\underline{\boldsymbol{n}}_{\mathrm{fe}}$ denotes the equivalent noise added to the estimated channel. Therefore one may estimate the phase shift φ_m from the estimated channel phase, and further estimate t_{d}. Without regarding the AWGN noise, the phase of $\hat{\underline{\boldsymbol{H}}}_{\mathrm{f}}$ is determined by both t_{d} and channel itself. The key problem is to distinguish the phase shift caused by t_{d} and the phase contains in $\underline{\boldsymbol{H}}_{\mathrm{f}}$ itself.

When the propagation channel is single path, the problem becomes much easier. Since the phase of each diagonal entry of CTF matrix (for short, we term it as 'sub-channel'), are identical. To extract STO from the estimated channel, one can compute the phase difference between sub-channels as proposed in [Chi07].

$$\begin{aligned} \hat{\underline{\boldsymbol{H}}}_{\mathrm{f}}^{(n)} &= \underline{\boldsymbol{E}}_{\mathrm{f}} \underline{\boldsymbol{H}}_{\mathrm{f}} + \mathrm{diag}\left(\underline{\boldsymbol{n}}_{\mathrm{fe}}\right) \\ &= \begin{bmatrix} \underline{H}_{\mathrm{f},0} e^{\mathrm{j}\varphi_0} & 0 & \cdots & 0 \\ 0 & \underline{H}_{\mathrm{f},1} e^{\mathrm{j}\varphi_1} & \cdots & 0 \\ \vdots & \vdots & \ddots & \vdots \\ 0 & 0 & \cdots & \underline{H}_{\mathrm{f},N_{\mathrm{FFT}}-1} e^{\mathrm{j}\varphi_{N_{\mathrm{FFT}}-1}} \end{bmatrix} + \mathrm{diag}\left(\underline{\boldsymbol{n}}_{\mathrm{fe}}\right) \end{aligned} \tag{5.10}$$

In (5.11) the estimation of the STO through phase difference between two adjacent estimated sub-channels is given [Chi07] . Where $\angle(\cdot)$ is operator to get phase of a complex argument, and $(\cdot)^*$ is operator to get conjugate value of a complex argument.

$$\begin{aligned} \hat{t}_{\mathrm{d}} &= \frac{N_{\mathrm{FFT}} T_{\mathrm{s}}}{2\pi} \angle \left(\sum_{m=1}^{N_{\mathrm{FFT}}-1} \hat{\underline{H}}_{\mathrm{f},m-1}^{*} \hat{\underline{H}}_{\mathrm{f},m} \right) \\ &= \frac{N_{\mathrm{FFT}} T_{\mathrm{s}}}{2\pi} \angle \left(\sum_{m=1}^{N_{\mathrm{FFT}}-1} \left(\underline{H}_{\mathrm{f},m-1}^{*} e^{-j\varphi_{m-1}} + \underline{n}_{\mathrm{fe},m-1}^{*} \right) \left(\underline{H}_{\mathrm{f},m} e^{j\varphi_m} + \underline{n}_{\mathrm{fe},m} \right) \right) \\ &= \frac{N_{\mathrm{FFT}} T_{\mathrm{s}}}{2\pi} \angle \left(\sum_{m=1}^{N_{\mathrm{FFT}}-1} \left(\begin{array}{l} \underline{H}_{\mathrm{f},m-1}^{*} \underline{H}_{\mathrm{f},m} e^{j\frac{t_{\mathrm{d}} \cdot 2\pi}{N_{\mathrm{FFT}} T_{\mathrm{s}}}} + \underline{H}_{\mathrm{f},m-1}^{*} e^{j\varphi_{m-1}} \underline{n}_{\mathrm{fe},m} \\ + \underline{H}_{\mathrm{f},m} e^{j\varphi_m} \underline{n}_{\mathrm{fe},m-1}^{*} + \underline{n}_{\mathrm{fe},m} \underline{n}_{\mathrm{fe},m-1}^{*} \end{array} \right) \right) \end{aligned} \tag{5.11}$$

From the (5.11) one can notice that the estimation $\hat{t}_{\mathrm{d}}$ is determined by the sub-channel $\underline{H}_{\mathrm{f},m}$, fraction STO t_{d}, and the noise. In (5.11) the element $\underline{H}^{*}_{\mathrm{f},m-1}\underline{H}_{\mathrm{f},m}$ is the significant factor to the estimation, the other three elements are noise. In the single path propagation channel, $\underline{H}_{\mathrm{f},m}$ and $\underline{H}_{\mathrm{f},m-1}$ have the same phase, therefore $\underline{H}^{*}_{\mathrm{f},m-1}\underline{H}_{\mathrm{f},m}$ is real value. The method in (5.11) has good performance.

However it is noticed that, the phase difference calculated in (5.11) is between two adjacent sub-channel, which is corresponding to $2\pi \cdot t_{\mathrm{d}} / \left(T_{\mathrm{s}} N_{\mathrm{FFT}}\right)$. Amplification by factor of N_{FFT} is made to the phase difference to estimate t_{d}. This amplification factor will also amplify the noise, therefore the method should have great variance. To overcome the variance problem, a modified phase shift method is presented in (5.12). The difference between (5.12) and (5.11) is, phase shift between m-th sub-channel and $m+ N_{\mathrm{FFT}}/2$ sub-channel, rather than two adjacent sub-channel, are calculated.

$$
\begin{aligned}
\tilde{t}_{\mathrm{d}} &= \frac{T_{\mathrm{s}}}{\pi} \angle \left(\sum_{m=0}^{N_{\mathrm{FFT}}/2-1} \hat{\underline{H}}^{*}_{\mathrm{f},m} \hat{\underline{H}}_{\mathrm{f},m+N_{\mathrm{FFT}}/2} \right) \\
&= \frac{T_{\mathrm{s}}}{\pi} \angle \left(\sum_{m=1}^{N_{\mathrm{FFT}}/2-1} \left(\underline{H}^{*}_{\mathrm{f},m} e^{j\varphi_m} + \underline{n}^{*}_{\mathrm{fe},m} \right) \left(\underline{H}_{\mathrm{f},m+N_{\mathrm{FFT}}/2} e^{-j\varphi_{m+N_{\mathrm{FFT}}/2}} + \underline{n}_{\mathrm{fe},m+N_{\mathrm{FFT}}/2} \right) \right) \\
&= \frac{T_{\mathrm{s}}}{\pi} \angle \left(\sum_{m=1}^{N_{\mathrm{FFT}}-1} \left(\begin{array}{l} \underline{H}^{*}_{\mathrm{f},m} \underline{H}_{\mathrm{f},m+N_{\mathrm{FFT}}/2} e^{j\frac{t_{\mathrm{d}} \cdot \pi}{T_{\mathrm{s}}}} + \underline{H}^{*}_{\mathrm{f},m} e^{j\varphi_m} \underline{n}_{\mathrm{fe},m+N_{\mathrm{FFT}}/2} \\ + \underline{H}_{\mathrm{f},m+N_{\mathrm{FFT}}/2} e^{j\varphi_{m-1}} \underline{n}^{*}_{\mathrm{fe},m} + \underline{n}_{\mathrm{f},m} \underline{n}^{*}_{\mathrm{fe},m+N_{\mathrm{FFT}}/2} \end{array} \right) \right)
\end{aligned}
\qquad (5.12)
$$

The modified method also assumes that the propagation channel is single tap. The phase difference caused by STO between m-th sub-channel and $m+ N_{\mathrm{FFT}}/2$ sub-channel is $\left(t_{\mathrm{d}}/T_{\mathrm{s}}\right)\pi$. With (5.12), estimation variance should be suppressed.

In Figure 5.5 phase shift based method in (5.11) and (5.12) are compared. In this simulation, the channel estimation sequence defined in [WiM09] is applied and single tap channel is used. We assume that well synchronization is obtained during the timing synchronization phase, only fraction STO smaller than T_{s} exists. The received channel estimation sequences are polluted by AWGN noise. The upper diagram in Figure 5.5 gives the mean value of the estimated t_{d}, and the lower diagram is the Mean Square Error (MSE) of the estimation. It is observed that both the methods work well in the single path channel scenarios. The advantage of proposed method is that it has less variance, and the MSE of the modified method in (5.12)is much smaller than the conventional method in (5.11).

However when there are multiple MPCs in the propagation channel, $\underline{H}_{\mathrm{f},m}$ and $\underline{H}_{\mathrm{f},m-1}$ do not have identical phase, and $\underline{H}^{*}_{\mathrm{f},m-1}\underline{H}_{\mathrm{f},m}$ is not real value. The method in (5.11) does not work anymore. The modified method in (5.12) is not expected to be good either. It has the same problem as the conventional method.

In Figure 5.6 the simulation results of the phase shift based method in IEEE 802.15.3a CM3 channel are presented. From the mean value curve, one can notice that both conventional method and the proposed method do not work. The mean value of estimation through the modified method is close to zero, since the *m*-th sub-channel and $m+N_{\mathrm{FFT}}/2$ sub-channel are almost independent in the multipath channel, the phase difference between them is random, estimation of (5.12)does not make any sense. The conventional method does not work either. In low E_{s}/N_0 cases, the noise dominants in the estimation channel, therefore the mean value of estimation is small. In high E_{s}/N_0 cases, due to the amplification factor N_{FFT} in (5.11), even there is only small phase shift between $\underline{H}_{\mathrm{f},m-1}$ and $\underline{H}_{\mathrm{f},m}$ in (5.11), however this difference will be amplified by the factor of N_{FFT} , and the mean value of the estimation is big.

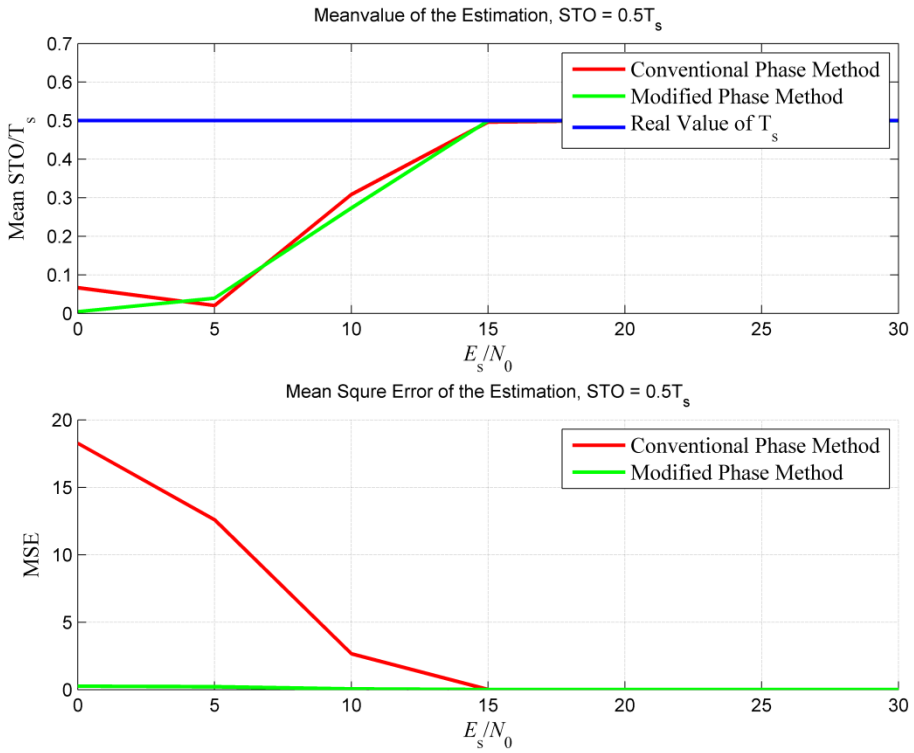

Figure 5.5 Performance of Phase shift method in single tap no fading channel

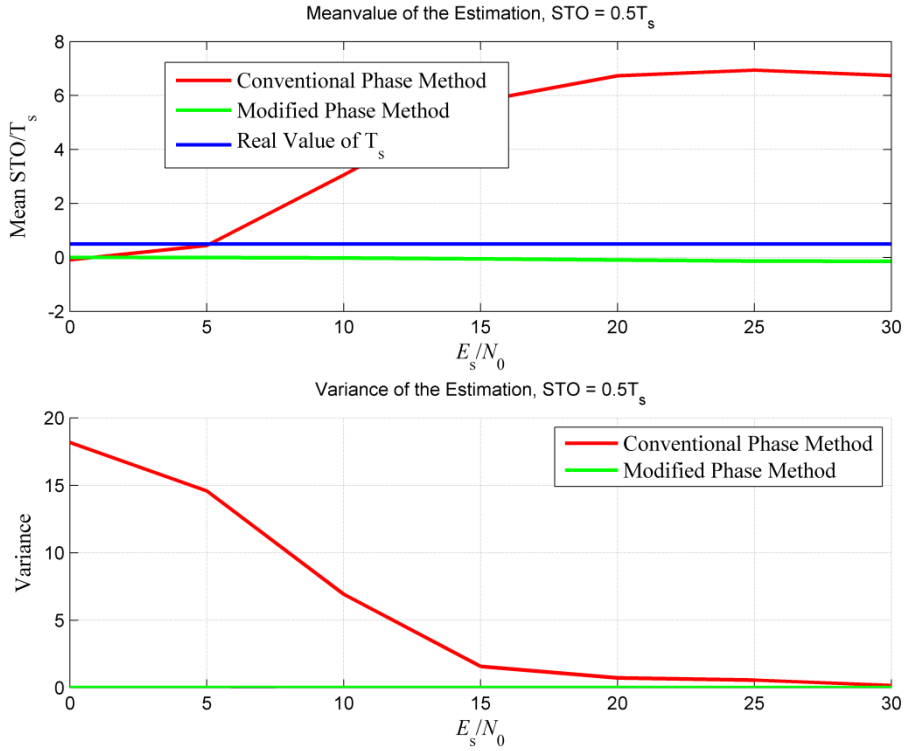

Figure 5.6 Performance of Phase shift method in IEEE 802.15.3a CM3 multipath channel

From the analysis and the simulation results, it is known that phase shift based methods are able to estimate the fraction STO in the singe path channel. The modified phase shift method could suppress the estimation variance in the singe path channel. However in the multipath channel, the phase shift methods do not work. Efficient methods should be investigated to estimate fine ToA in multipath propagation channel environments.

5.3.2 CIR energy based Method

In the last subsection, fine ToA detection based on phase shift has been proved not suitable in multipath propagation channel environments. In this subsection, the fine ToA detection based on CIR energy of the estimated channel is investigated. Let us also assume that, after coarse timing and fine timing detection good synchronization is established for the OFDM system. The receiver could find the correct starting sample, and only fraction STO exits, as shown in Figure 5.4. To

explain the CIR energy based fine ToA detection method in the multipath propagation environments, it is necessary to analyze firstly the CIR character of the estimated channel.

The CIR of the estimated channel could be obtained by IDFT to the diagonal entries vector of $\hat{\underline{\boldsymbol{H}}}_{\mathrm{f}}^{(n)}$ defined in (5.10).

$$\begin{aligned}\hat{\underline{\boldsymbol{h}}}^{(n)} &= \underline{\boldsymbol{D}}\mathrm{diag}\left(\hat{\underline{\boldsymbol{H}}}_{\mathrm{f}}^{(n)}\right) \\ &= \left[\hat{h}_0^{(n)}, \hat{h}_1^{(n)} \cdots, \hat{h}_{N_{\mathrm{FFT-1}}}^{(n)}\right]^{\mathrm{T}}\end{aligned} \tag{5.13}$$

By comparing (3.14) and (5.13), one can notice an interesting thing. Without regard to the effects by noise, when the sampling time perfectly matches the real ToA of an OFDM symbol, in other words, no fraction STO exists after synchronization and $t_{\mathrm{d}} = 0$. There is no energy on the last elements of the estimated CIR $\hat{\underline{\boldsymbol{h}}}^{(n)}$, namely,

$$\sum_{l=L}^{N_{\mathrm{FFT}}} \left|\hat{h}_l^{(n)}\right|^2 = 0, \tag{5.14}$$

where L is the number of MPCs as in (3.14). When there is fraction STO, considerable energy on the last taps of $\hat{\underline{\boldsymbol{h}}}^{(n)}$ appear. In Figure 5.7 one realization of CM3 channel is used to show this interesting finding. The upper diagram of Figure 5.7 shows the CIR of the channel $\underline{\boldsymbol{h}}^{(n)}$, and the lower diagram shows the CIR of estimated channel $\hat{\underline{\boldsymbol{h}}}^{(n)}$, which has been effected by a fraction STO of $t_{\mathrm{d}} = 0.5T_{\mathrm{s}}$. Considerable energy in the last taps of the estimated CIR is shown. This energy is caused by the fraction STO. Based on this finding, the fine ToA detection method is invented.

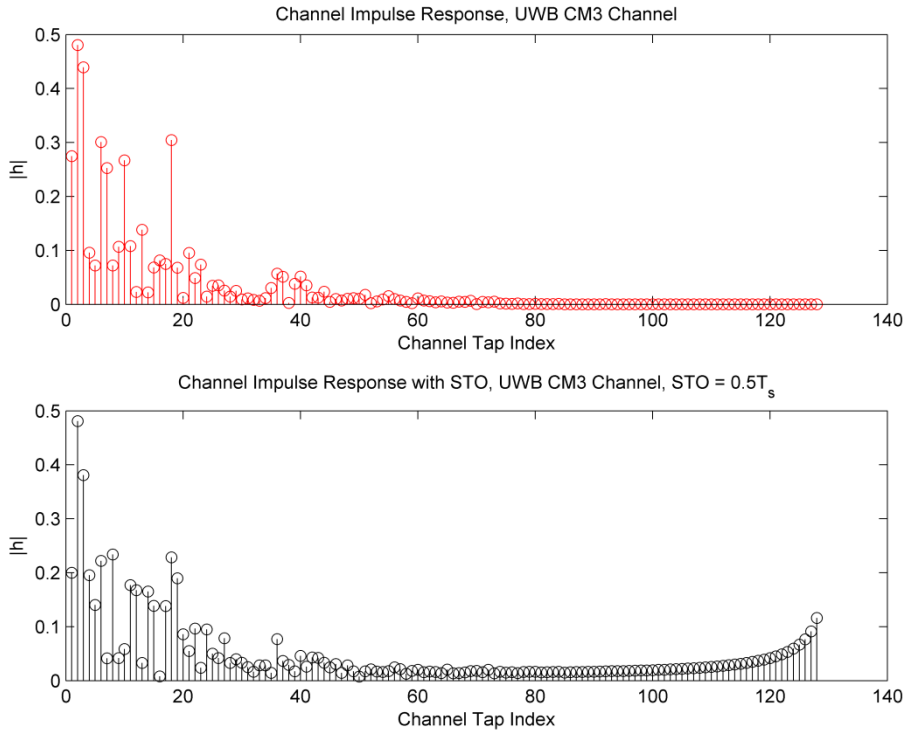

Figure 5.7 Amplitude comparison of CIR between IEEE 802.15.3a CM3 channel and estimated channel with fraction STO

The procedure of the fine ToA detection method is, firstly to make some fraction STO compensation to the estimated channel $\hat{\underline{\boldsymbol{H}}}_{\mathrm{f}}^{(n)}$ in frequency domain, and then calculate the energy of the tail taps of the CIR after compensation in time domain. An exhaustive searching algorithm over the whole possible space of the fraction STO, for instance, $t_{\mathrm{d}} \in [-0.5T_{\mathrm{s}}, 0.5T_{\mathrm{s}}]$ is carried out. Once the energy of the tail taps of the compensated CIR is suppressed, the compensated value could be selected as estimated fraction STO. And the fine ToA could be obtained by revising the synchronization sample time t_0 with the estimated fraction STO. In principle, the fine ToA detection method is an optimization searching problem. There are mainly three steps in the detection.

Firstly let us divide the possible space of the fraction STO into N small intervals.

$$t_{\mathrm{d},n} \in \left[-\frac{N}{2}, \ldots, \frac{N}{2}\right]\frac{T_{\mathrm{s}}}{N} \tag{5.15}$$

Secondly, executing the exhaustive searching throughout the set $\{t_{\mathrm{d},n}\}$. Let us define a cutting matrix as

$$\boldsymbol{C}_{\mathrm{CIR},N}=\begin{bmatrix}0 & 0 & \cdots & 0\\ 0 & 1 & \cdots & 0\\ \vdots & \vdots & \ddots & \vdots\\ 0 & 0 & \cdots & 1\end{bmatrix}, \tag{5.16}$$

where $\boldsymbol{C}_{\mathrm{CIR},N}$ is an $N_{\mathrm{FFT}}\times N_{\mathrm{FFT}}$ diagonal matrix, whose diagonal entries from N-th column are one, and the other elements are zero. This cutting matrix is used to select the last part of one column vector. And define a STO compensation vector in frequency domain as

$$\underline{\boldsymbol{\varphi}}\left(t_{\mathrm{d},n}\right)=\left(1,\exp\left(\frac{-\mathrm{j}2\pi t_{\mathrm{d},n}}{N_{\mathrm{FFT}}T_{\mathrm{s}}}\right),\ldots,\exp\left(\frac{-\mathrm{j}2\pi\left(N_{\mathrm{FFT}}-1\right)t_{\mathrm{d},n}}{N_{\mathrm{FFT}}T_{\mathrm{s}}}\right)\right)^{\mathrm{T}} \tag{5.17}$$

The STO estimation becomes an the optimization searching problem given by

$$\hat{t}_{\mathrm{d}}=\arg\min_{t_{\mathrm{d},n}}\left\|\boldsymbol{C}_{\mathrm{CIR},N}\underline{\boldsymbol{D}}\underline{\hat{\boldsymbol{H}}}_{\mathrm{f}}\underline{\boldsymbol{\varphi}}\left(t_{\mathrm{d},n}\right)\right\| \tag{5.18}$$

where $\|\cdot\|$ is the operator of inner product for a vector. Since the UWB channel has large number of MPCs, in (5.18) the cutting matrix is set to $N_{\mathrm{FFT}}/2$ for the severe multipath UWB channel. In this case, the last half part of taps of $\underline{\hat{\boldsymbol{h}}}^{(n)}$ are selected to do the energy accumulation. This number could be adjusted according to statistical features of the propagation channel. For instance, when less MPCs appear in the propagation channel, more paths from the tail could be chosen to accumulate the energy. The designing principle is, the number of selected tail taps should be smaller than $N_{\mathrm{FFT}}-L$, where L is the maximum number of MPCs in the multipath channel.

Finnaly, $t_{\mathrm{d},n}$ that minimizes the accumulated energy of the paths from tail is selected as estimated STO. The fine ToA is consequently estimated by compensating the estimated STO to the timing synchronization sample t_0.

From the above three steps the fine ToA is obtained. The more intervals T_{s} is divided, the smaller searching step is, and the better precision STO estimation could be achieved. However this also means more computational resources are required.

Even the real channel information is unknown, the statically features of the MPCs is known. In other words, the tail taps of the CIR is zero, namely $\boldsymbol{C}_{\mathrm{CIR},N}\underline{\boldsymbol{D}}\underline{\boldsymbol{H}}_{\mathrm{f}}$ is an all zero vector, is an a prior partial information in this estimation problem. Therefore the optimization problem in (5.18) is actually to minimize the distance between the estimated and the real CIR, which can be written as

$$\begin{aligned}\hat{t}_{\mathrm{d}} &= \arg\min_{t_{\mathrm{d},n}} \left\| \boldsymbol{C}_{\mathrm{CIR},N}\underline{\boldsymbol{D}}\hat{\underline{\boldsymbol{H}}}_{\mathrm{f}}\underline{\boldsymbol{\varphi}}\left(t_{\mathrm{d},n}\right) - \boldsymbol{C}_{\mathrm{CIR},N}\underline{\boldsymbol{D}}\underline{\boldsymbol{H}}_{\mathrm{f}} \right\| \\ &= \arg\min_{t_{\mathrm{d},n}} \left\| \boldsymbol{C}_{\mathrm{CIR},N}\underline{\boldsymbol{D}}\underline{\boldsymbol{H}}_{\mathrm{f}}\underline{\boldsymbol{E}}_{\mathrm{f}}\underline{\boldsymbol{\varphi}}\left(t_{\mathrm{d},n}\right) - \boldsymbol{C}_{\mathrm{CIR},N}\underline{\boldsymbol{D}}\underline{\boldsymbol{H}}_{\mathrm{f}} + \underbrace{\boldsymbol{C}_{\mathrm{CIR},N}\mathrm{diag}\left(\underline{\boldsymbol{n}}_{\mathrm{fe}}\right)\underline{\boldsymbol{\varphi}}\left(t_{\mathrm{d},n}\right)}_{\mathrm{AWGN}} \right\|,\end{aligned} \tag{5.19}$$

where $\mathrm{diag}\left(\underline{\boldsymbol{n}}_{\mathrm{fe}}\right)\underline{\boldsymbol{\varphi}}\left(t_{\mathrm{d},n}\right)$ is AWGN. It is noticed from (5.19) that the proposed fine ToA method is actually a Maximum Likelihood Estimator (MLE), the exhaustive searching algorithm searches the whole possible space of the t_{d} to find a minimized distance between two vectors, $\boldsymbol{C}_{\mathrm{CIR},N}\underline{\boldsymbol{D}}\underline{\boldsymbol{H}}_{\mathrm{f}}\underline{\boldsymbol{E}}_{\mathrm{f}}\underline{\boldsymbol{\varphi}}\left(t_{\mathrm{d},n}\right)$ and $\boldsymbol{C}_{\mathrm{CIR},N}\underline{\boldsymbol{D}}\underline{\boldsymbol{H}}_{\mathrm{f}}$. Since $\boldsymbol{C}_{\mathrm{CIR},N}\underline{\boldsymbol{D}}\underline{\boldsymbol{H}}_{\mathrm{f}}$ is zero vector, the problem can be simplified as in (5.18). Therefore the proposed fine ToA detection method is optimal.

In Figure 5.8 the performance of the CIR energy based the ToA detection method is evaluated through simulation in IEEE 802.15.3a CM3 channel. Mean value and MSE of estimation are presented. In the simulation, OFDM packet is organized as defined in [WiM09], the fraction STO is set to be $t_{\mathrm{d}} = 0.2T_{\mathrm{s}}$. Six OFDM symbols are used for channel estimation. The exhaustive space is divided into 8 subintervals. It is observed from the upper diagram in Figure 5.8 that, at low E_{s}/N_0 value around -8 dB, the estimated STO is converging to the real STO value. The lower diagram provides the MSE performance of the estimation through CIR energy algorithm.

From the simulation results, one can observe that proposed CIR energy based fine ToA detection method shows good performance in the multipath propagation channel. In a standard MB-OFDM UWB system, the channel estimation and synchronization are prerequisite. In carrying out the proposed method, no extra hardware support is required. The only cost is plenty of computational tasks introduced by exhaustive searching algorithm and extra IDFT operations.

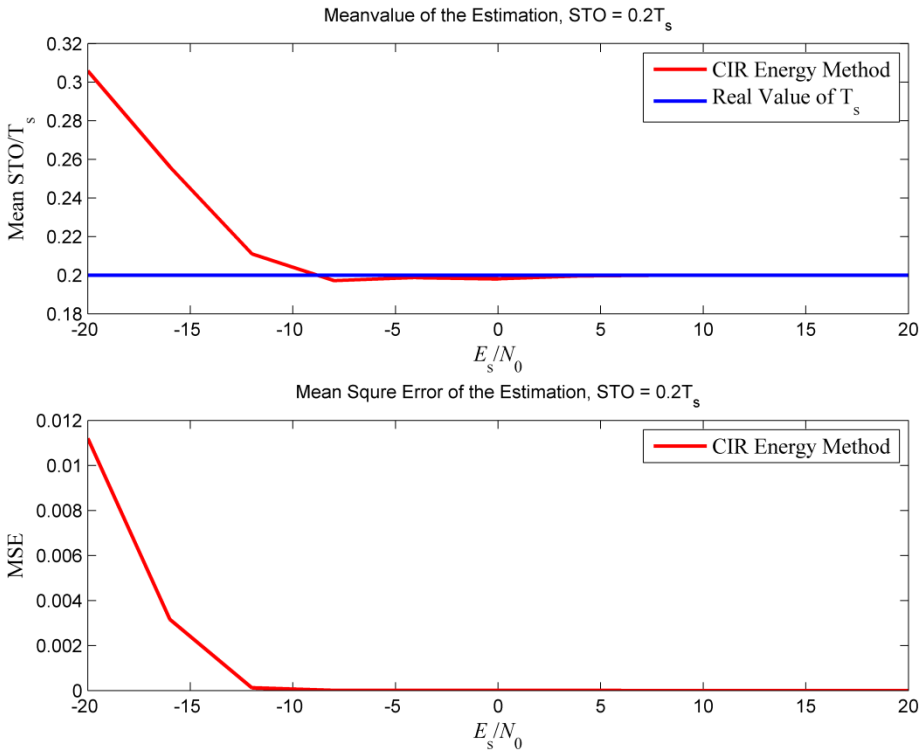

Figure 5.8 Performance of CIR Energy based method in IEEE 802.15.3a CM3 channel.

5.4 Modified RTT Protocol

In this section, the proposed CIR energy based fine ToA detection method is introduced to the RTT protocol [WiM09]. The principle of RTT is illustrated in Figure 5.9. As already announced in Section 5.3.2, the CIR energy based method brings extra computational tasks to the UWB devices. These operations are great burdens to the low cost UWB devices. In this section, the RTT protocol is modified in the sense of delivering all the computational tasks to one side device that is more powerful in the ranging device pair. With this modification, all the computational tasks in the fine ToA detection are burden to the powerful device, and leave the other devices free in complicated signal processing. We term this modified RTT as MRTT ranging protocol.

With the MRTT, it is feasible and simple to implement the proposed CIR energy based ToA detection method in the UWB ranging system with powerful anchor UWB device and low cost UWB tags. In Section 5.4.1 the MRTT measurement

protocol is shown, and in Section 5.4.2, the performance of the MRTT is evaluated.

5.4.1 Protocol Description

As illustrated in Figure 5.9, two MB-OFDM UWB devices, termed as Device 1 and Device 2, are associated as a ranging device pair during one RTT measurement. Without loss of generality, let us assume that Device 1 is the UWB anchor, and Device 2 is a UWB tag. The UWB anchor is more powerful than the UWB tag. In what follows, the MRTT measurement protocol applying the CIR energy based fine ToA detection method is presented. The protocol is carried out in five steps.

Step 1: Device 1 starts a ranging process by sending the ranging request packet, $\underline{\boldsymbol{d}}_{\text{req}}^{(n)}, n = 1, \cdots N$, where N is the packet length in OFDM symbols. According to [WiM09], the $n = 25, \cdots 30$-th OFDM symbols are used for channel estimation. The channel estimation sequence $\underline{\boldsymbol{d}}_{\text{ce}}$ could be found in [WiM09]. The arrival time of the first sample of $\underline{\boldsymbol{d}}_{\text{req}}^{(25)}$, namely the first channel estimation OFDM symbol, is defined as the reference arrival time for ranging [WiM09]. Device 1 should record the time on its own clock once $\underline{\boldsymbol{d}}_{\text{req}}^{(25)}$ is transmitted. Let us term this time as T_{1c}.

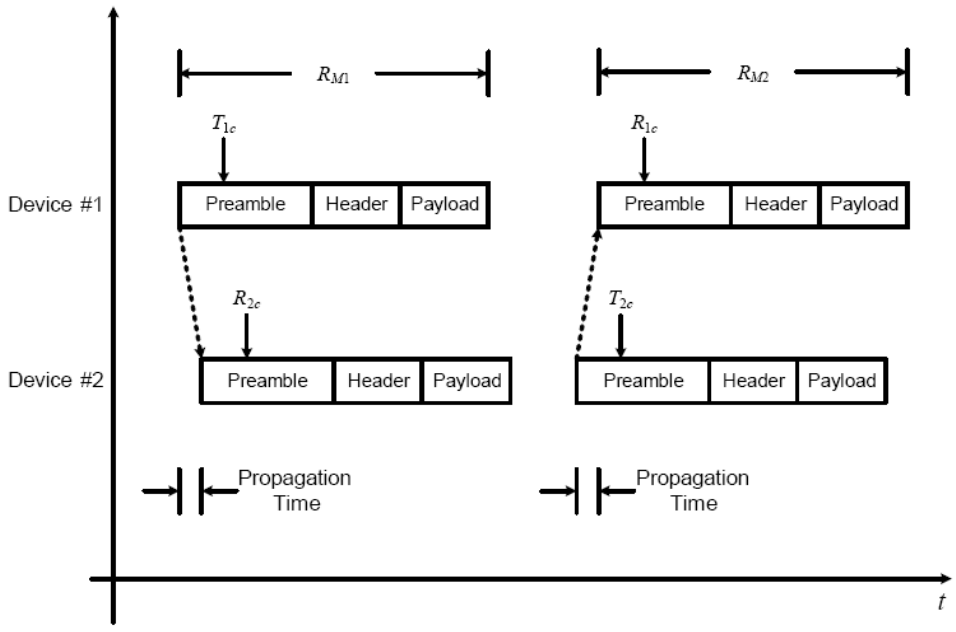

Figure 5.9 RTT measurement Protocol in WiMedia Specification [WiM09].

Step 2: Once Device 2 detects the ranging request packet from Device 1, the arrival time of first sample of $\underline{\boldsymbol{d}}_{\text{req}}^{(25)}$ should be recorded as R_{1c} referenced to the clock of Device 2. After that, Device 2 does the standard signal processing such as, timing synchronization, channel estimation, etc.

The n-th OFDM symbol of the ranging request packet received by Device 2 is given by

$$\underline{\boldsymbol{r}}_{\text{req}}^{(n)} = \underline{\boldsymbol{E}}_{\text{f,req}} \underline{\boldsymbol{H}}_{\text{f}} \underline{\boldsymbol{d}}_{\text{req}}^{(n)} + \underline{\boldsymbol{n}}_{\text{f,req}}^{(n)}, n = 1, \cdots N. \tag{5.20}$$

where $\underline{\boldsymbol{d}}_{\text{req}}^{(n)} = \underline{\boldsymbol{d}}_{\text{ce}}$ is channel estimation sequence when $n = 25, \cdots 30$. $\underline{\boldsymbol{E}}_{\text{f,req}}$ is the phase shift matrix caused by STO on Device 2, $\underline{\boldsymbol{H}}_{\text{f,req}}$ is the CTF matrix of OFDM channel seen by Device 2. Let us denote the fraction STO as $t_{\text{d,req}}$, and let us further assume that $t_{\text{d,req}} \in \left[-0.5T_{\text{s}}, 0.5T_{\text{s}}\right]$. The estimated CTF matrix by Device 2 is given by

$$\hat{\underline{\boldsymbol{H}}}_{\text{f,req}} = \underline{\boldsymbol{E}}_{\text{f,req}} \underline{\boldsymbol{H}}_{\text{f,req}} + \text{diag}\left(\underline{\boldsymbol{n}}_{\text{f,req}}^{(n)}\right) \text{diag}\left(\underline{\boldsymbol{d}}_{\text{ce}}\right)^{-1}, \tag{5.21}$$

where $\text{diag}(\cdot)$ builds a diagonal matrix with the vector argument, $(\cdot)^{-1}$ is inverse operator to a matrix.

Step 3: at time T_{2c} referenced to clock of Device 2, the ranging acknowledge packet is sent to Device 1. Let us assume that the same frequency band is applied to the ranging request packet and ranging acknowledgement packet in the MRTT protocol. Since the acknowledgement to the ranging request is quit prompt, propagation channel is assumed to be static during the period of MRTT protocol, namely, $\underline{\boldsymbol{H}}_{\text{f,req}} = \underline{\boldsymbol{H}}_{\text{f,ack}}$.

Different from the conventional RTT ranging protocol, in MRTT Device 2 delivers the estimated channel to Device 1 via the ranging acknowledgement packet in this step. Channel estimation sequences of the ranging acknowledgement packet is organized as,

$$\underline{\boldsymbol{d}}_{\text{ack}}^{(n)} = \begin{cases} \underline{\boldsymbol{d}}_{\text{ce}}, n = 25, 26, 27 \\ \left(\hat{\underline{\boldsymbol{H}}}_{\text{f,req}}^{\text{H}} \hat{\underline{\boldsymbol{H}}}_{\text{f,req}}\right)^{-\frac{1}{2}} \hat{\underline{\boldsymbol{H}}}_{\text{f,req}} \underline{\boldsymbol{d}}_{\text{ce}}, n = 28, 29, 30 \end{cases} \tag{5.22}$$

The first three channel estimation symbols, $\underline{\boldsymbol{d}}_{\text{ack}}^{(n)}$, $n = 25, 26, 27$, are standard ones, and are used for regular channel estimation by Device 1. The last three channel

estimation symbols are used for transfer the estimated channel $\underline{\hat{\boldsymbol{H}}}_{\mathrm{f,req}}$ by Device 2 to Device 1. The energy of the transmitted estimated channel information is normalized.

On Device 2, only the organization of the ranging acknowledgement packet is a little different from the conventional RTT protocol. The CIR energy based ToA detection method will not be carried out on Device 2. There is no complicated signal processing task on Device 2.

Step 4: Once Device 1 receives the ranging acknowledgement packet, the arrival time of first sample of $\underline{\boldsymbol{d}}_{\mathrm{ack}}^{(25)}$ should be recorded as $R_{2\mathrm{c}}$. The regular signal processing, such as synchronization and channel estimation is carried out, and then fine ToA detection is executed. As already explained, the first three channel estimation symbols are used for the regular channel estimation. The estimated channel CTF matrix by Device 2 is given by

$$\underline{\hat{\boldsymbol{H}}}_{\mathrm{f,ack}} = \underline{\boldsymbol{E}}_{\mathrm{f,ack}} \underline{\boldsymbol{H}}_{\mathrm{f,ack}} + \mathrm{diag}\left(\underline{\boldsymbol{n}}_{\mathrm{f,ack}}^{(n)}\right) \mathrm{diag}\left(\underline{\boldsymbol{d}}_{\mathrm{ce}}\right)^{-1}. \tag{5.23}$$

The last three channel estimation symbols, namely $\underline{\boldsymbol{d}}_{\mathrm{ce}}^{(n)}, n = 28, 29, 30$, are used to carry out the fine ToA detection. The received OFDM symbols for fine ToA detection are given by

$$\begin{aligned} \underline{\boldsymbol{r}}_{\mathrm{ack}}^{(n)} &= \underline{\boldsymbol{E}}_{\mathrm{f,ack}} \underline{\boldsymbol{H}}_{\mathrm{f,ack}} \underline{\boldsymbol{d}}_{\mathrm{ack}}^{(n)} + \underline{\boldsymbol{n}}_{\mathrm{f,ack}}^{(n)}, n = 28, 29, 30 \\ &= \underline{\boldsymbol{E}}_{\mathrm{f,ack}} \underline{\boldsymbol{H}}_{\mathrm{f,ack}} \left(\left(\underline{\hat{\boldsymbol{H}}}_{\mathrm{f,req}}^{\mathrm{H}} \underline{\hat{\boldsymbol{H}}}_{\mathrm{f,req}} \right)^{-1/2} \underline{\hat{\boldsymbol{H}}}_{\mathrm{f,req}} \right) \underline{\boldsymbol{d}}_{\mathrm{ce}} + \underline{\boldsymbol{n}}_{\mathrm{f,ack}}^{(n)} \\ &= \underline{\boldsymbol{E}}_{\mathrm{f,ack}} \underline{\boldsymbol{E}}_{\mathrm{f,req}} \underline{\boldsymbol{H}}_{\mathrm{f,ack}} \underline{\boldsymbol{H}}_{\mathrm{f,req}} \left(\underline{\hat{\boldsymbol{H}}}_{\mathrm{f,req}}^{\mathrm{H}} \underline{\hat{\boldsymbol{H}}}_{\mathrm{f,req}} \right)^{-1/2} \underline{\boldsymbol{d}}_{\mathrm{ce}} \\ &\quad + \underline{\boldsymbol{E}}_{\mathrm{f,ack}} \underline{\boldsymbol{H}}_{\mathrm{f,ack}} \left(\underline{\hat{\boldsymbol{H}}}_{\mathrm{f,req}}^{\mathrm{H}} \underline{\hat{\boldsymbol{H}}}_{\mathrm{f,req}} \right)^{-1/2} \underline{\boldsymbol{n}}_{\mathrm{f,req}}^{(n)} + \underline{\boldsymbol{n}}_{\mathrm{f,ack}}^{(n)} \end{aligned} \tag{5.24}$$

In (5.24) The $\left(\underline{\hat{\boldsymbol{H}}}_{\mathrm{f,req}}^{\mathrm{H}} \underline{\hat{\boldsymbol{H}}}_{\mathrm{f,req}} \right)^{-1}$ is real value diagonal matrix, which reflects the estimated channel energy of $\underline{\boldsymbol{H}}_{\mathrm{f,req}}$.

Let us define $\underline{\boldsymbol{E}}_{\mathrm{f,rtt}} = \underline{\boldsymbol{E}}_{\mathrm{f,ack}} \underline{\boldsymbol{E}}_{\mathrm{f,req}}$, which contains the overall phase shift caused by STO on Device 1 and Device 2. The $\underline{\boldsymbol{E}}_{\mathrm{f,rtt}}$ is also diagonal matrix, and has the same structure with (5.8). The diagonal entry of $\underline{\boldsymbol{E}}_{\mathrm{f,rtt}}$ is $\varphi_{\mathrm{rtt},m}$, and is determined by $t_{\mathrm{d,ack}} + t_{\mathrm{d,req}}$.

$$\varphi_{\mathrm{rtt},m} = \frac{m \cdot \left(t_{\mathrm{d,ack}} + t_{\mathrm{d,req}}\right) \cdot 2\pi}{N_{\mathrm{FFT}} T_{\mathrm{s}}}, m = 0, \ldots, N_{\mathrm{FFT}} - 1. \tag{5.25}$$

It is assumed that during period of RTT measurement, the channel is static and reciprocal. Let $\underline{\boldsymbol{H}}_{\mathrm{f}} = \underline{\boldsymbol{H}}_{\mathrm{f,req}} = \underline{\boldsymbol{H}}_{\mathrm{f,ack}}$ .To compensate the impact by $\left(\hat{\underline{\boldsymbol{H}}}_{\mathrm{f,req}}^{\mathrm{H}} \hat{\underline{\boldsymbol{H}}}_{\mathrm{f,req}}\right)^{-1/2}$, the received signal in (5.24) shall be firstly equalized by left multiplying the real value diagonal matrix $\left(\hat{\underline{\boldsymbol{H}}}_{\mathrm{f,ack}}^{\mathrm{H}} \hat{\underline{\boldsymbol{H}}}_{\mathrm{f,ack}}\right)^{1/2}$. The equalized signal is given by

$$\begin{aligned} &\left(\hat{\underline{\boldsymbol{H}}}_{\mathrm{f,ack}}^{\mathrm{H}} \hat{\underline{\boldsymbol{H}}}_{\mathrm{f,ack}}\right)^{1/2} \underline{\boldsymbol{r}}_{\mathrm{ack}}^{(n)} \\ &= \underbrace{\underline{\boldsymbol{E}}_{\mathrm{f,ack}} \underline{\boldsymbol{E}}_{\mathrm{f,req}}}_{\underline{\boldsymbol{E}}_{\mathrm{f,rtt}}} \underbrace{\underline{\boldsymbol{H}}_{\mathrm{f,ack}} \underline{\boldsymbol{H}}_{\mathrm{f,req}} \left(\hat{\underline{\boldsymbol{H}}}_{\mathrm{f,req}}^{\mathrm{H}} \hat{\underline{\boldsymbol{H}}}_{\mathrm{f,req}}\right)^{-1/2} \left(\hat{\underline{\boldsymbol{H}}}_{\mathrm{f,ack}}^{\mathrm{H}} \hat{\underline{\boldsymbol{H}}}_{\mathrm{f,ack}}\right)^{1/2}}_{\underline{\boldsymbol{H}}_{\mathrm{f,rtt}}, \mathrm{channel}} \underline{\boldsymbol{d}}_{\mathrm{ce}} \\ &+ \underbrace{\underline{\boldsymbol{E}}_{\mathrm{f,ack}} \underline{\boldsymbol{H}}_{\mathrm{f,ack}} \left(\hat{\underline{\boldsymbol{H}}}_{\mathrm{f,req}}^{\mathrm{H}} \hat{\underline{\boldsymbol{H}}}_{\mathrm{f,req}}\right)^{-1/2} \left(\hat{\underline{\boldsymbol{H}}}_{\mathrm{f,ack}}^{\mathrm{H}} \hat{\underline{\boldsymbol{H}}}_{\mathrm{f,ack}}\right)^{1/2} \underline{\boldsymbol{n}}_{\mathrm{f,req}}^{(n)} + \left(\hat{\underline{\boldsymbol{H}}}_{\mathrm{f,ack}}^{\mathrm{H}} \hat{\underline{\boldsymbol{H}}}_{\mathrm{f,ack}}\right)^{1/2} \underline{\boldsymbol{n}}_{\mathrm{f,ack}}^{(n)}}_{\mathrm{noise}} \end{aligned} \tag{5.26}$$

Let us define $\underline{\boldsymbol{H}}_{\mathrm{f,rtt}}$ as the equivalent overall MRTT channel, and the estimated MRTT channel is denoted as

$$\hat{\underline{\boldsymbol{H}}}_{\mathrm{f,rtt}} = \underline{\boldsymbol{E}}_{\mathrm{f,rtt}} \underline{\boldsymbol{H}}_{\mathrm{f,rtt}} + \underline{\boldsymbol{n}}_{\mathrm{eq}}. \tag{5.27}$$

where $\underline{\boldsymbol{H}}_{\mathrm{f,rtt}}$ is defined as

$$\underline{\boldsymbol{H}}_{\mathrm{f,rtt}} = \underline{\boldsymbol{H}}_{\mathrm{f,ack}} \underline{\boldsymbol{H}}_{\mathrm{f,req}} \left(\hat{\underline{\boldsymbol{H}}}_{\mathrm{f,req}}^{\mathrm{H}} \hat{\underline{\boldsymbol{H}}}_{\mathrm{f,req}}\right)^{-1/2} \left(\hat{\underline{\boldsymbol{H}}}_{\mathrm{f,ack}}^{\mathrm{H}} \hat{\underline{\boldsymbol{H}}}_{\mathrm{f,ack}}\right)^{1/2}, \tag{5.28}$$

and $\underline{\boldsymbol{n}}_{\mathrm{eq}}$ is equivalent noise denoted as

$$\underline{\boldsymbol{n}}_{\mathrm{eq}} = \underline{\boldsymbol{E}}_{\mathrm{f,ack}} \underline{\boldsymbol{H}}_{\mathrm{f,ack}} \left(\hat{\underline{\boldsymbol{H}}}_{\mathrm{f,req}}^{\mathrm{H}} \hat{\underline{\boldsymbol{H}}}_{\mathrm{f,req}}\right)^{-1/2} \left(\hat{\underline{\boldsymbol{H}}}_{\mathrm{f,ack}}^{\mathrm{H}} \hat{\underline{\boldsymbol{H}}}_{\mathrm{f,ack}}\right)^{1/2} \underline{\boldsymbol{n}}_{\mathrm{f,req}}^{(n)} + \left(\hat{\underline{\boldsymbol{H}}}_{\mathrm{f,ack}}^{\mathrm{H}} \hat{\underline{\boldsymbol{H}}}_{\mathrm{f,ack}}\right)^{1/2} \underline{\boldsymbol{n}}_{\mathrm{f,ack}}^{(n)} \tag{5.29}$$

Since $\underline{\boldsymbol{E}}_{\mathrm{f,ack}}$, $\underline{\boldsymbol{H}}_{\mathrm{f,ack}}$, $\hat{\underline{\boldsymbol{H}}}_{\mathrm{f,req}}^{\mathrm{H}}$, and $\hat{\underline{\boldsymbol{H}}}_{\mathrm{f,ack}}$ are diagonal matrix, the equivalent noise is still Gaussian.

Step 5: The CIR based fine ToA detection is carried out to (5.27). The overall STO $t_{\mathrm{d,ack}} + t_{\mathrm{d,req}}$ is estimated. It should be pointed out that, $t_{\mathrm{d,req}} \in \left[-0.5T_{\mathrm{S}}, 0.5T_{\mathrm{S}}\right]$ and $t_{\mathrm{d,ack}} \in \left[-0.5T_{\mathrm{S}}, 0.5T_{\mathrm{S}}\right]$, the exhaustive searching space in (5.15) should be extended to

$$t_{\mathrm{d},n} \in \left[-N,\ldots,N\right]\frac{T_{\mathrm{s}}}{N} \tag{5.30}$$

With (5.18), (5.27), and (5.30), the overall STO could be estimated by the CIR energy algorithm. The fine RTT obtained by revising the estimated round time with the overall STO $\hat{t}_{\mathrm{d,rtt}}$ is given by

$$\tau_{\mathrm{RTT}} = R_{2\mathrm{c}} - T_{1\mathrm{c}} + R_{1\mathrm{c}} - T_{2\mathrm{c}} - \hat{t}_{\mathrm{d,rtt}} \tag{5.31}$$

5.4.2 Performance Evaluation

In this subsection, the performance of the MRTT is evaluated through simulation. As a benchmark, performance of the conventional RTT measurement protocol with the CIR energy based fine ToA detection method carried out on both Device 1 and Device 2 is presented. IEEE 802.15.3a CM3 channel is used. The STO on Device 2 is set to be $t_{\mathrm{d,req}} = 0.23T_{\mathrm{s}}$, and the STO Device 1 is set to be $t_{\mathrm{d,ack}} = 0.46T_{\mathrm{s}}$. The transmitted symbols have E_{s}/N_0 of 0 dB.

In Figure 5.10 the quasi PDF of the estimated STO is shown. The exhaustive searching space is divided into 50 small intervals. The red stems show the PDF of $\hat{t}_{\mathrm{d,req}}$ estimated on Device 2. The green stems show the PDF of $\hat{t}_{\mathrm{d,ack}}$ estimated on Device 1. The blue curve stems show the PDF of the sum value of $\hat{t}_{\mathrm{d,req}}$ and $\hat{t}_{\mathrm{d,ack}}$, which indicates the estimated overall STO when the CIR energy based fine ToA detection on both Device 1 and Device 2 are carried out. The black stems show PDF of $\hat{t}_{\mathrm{d,rtt}}$, namely, the overall STO estimation through the MRTT measurement protocol. When comparing the blue curve and the black curve, one can notice that, the mean value has only very tiny shift, and the variance has perceptible difference. The variance of the estimation through MRTT ranging protocol is larger than variance of the $\hat{t}_{\mathrm{d,req}} + \hat{t}_{\mathrm{d,ack}}$. However the performance loss is not much, this implies that the performance of MRTT still impressive. In view of the feasibility of implementation for low cost UWB devices, the MRTT and the CIR energy based fine ToA method is already competitive and attractive.

One thing is noticed that, the PDP of the $\hat{t}_{\mathrm{d,rtt}}$ is not symmetric, while the PDP of $\hat{t}_{\mathrm{d,ack}}$, $\hat{t}_{\mathrm{d,req}}$ are symmetric. This is because, in the MRTT protocol, the estimated channel $\underline{\hat{\boldsymbol{H}}}_{\mathrm{f,req}}$ on Device 2 is carried out by using six channel estimation OFDM symbols, and the estimated channel $\underline{\hat{\boldsymbol{H}}}_{\mathrm{f,ack}}$ on Device 1 is carried out only with three channel estimation OFDM symbols. Due to the different quality of $\underline{\hat{\boldsymbol{H}}}_{\mathrm{f,req}}$ and $\underline{\hat{\boldsymbol{H}}}_{\mathrm{f,ack}}$, the PDP of the $\hat{t}_{\mathrm{d,rtt}}$ does not look symmetric.

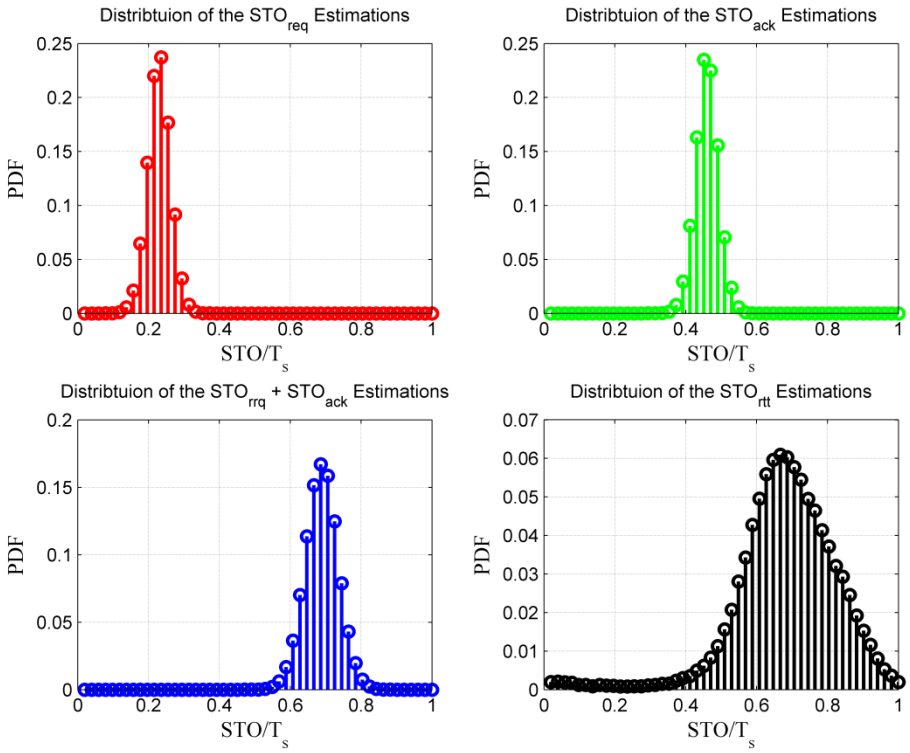

Figure 5.10 PDF of the estimated overall STO (E_s/N_0 = 0 dB, 50 exhaustive searching steps)

In Figure 5.11 the distribution of the estimated STO is illustrated when the exhaustive searching space is divided into 8 intervals. Compared with the results shown in Figure 5.10, the estimation has bigger quantization errors since the exhaustive searching step is larger, and therefore there is some performance degradation is noticed.

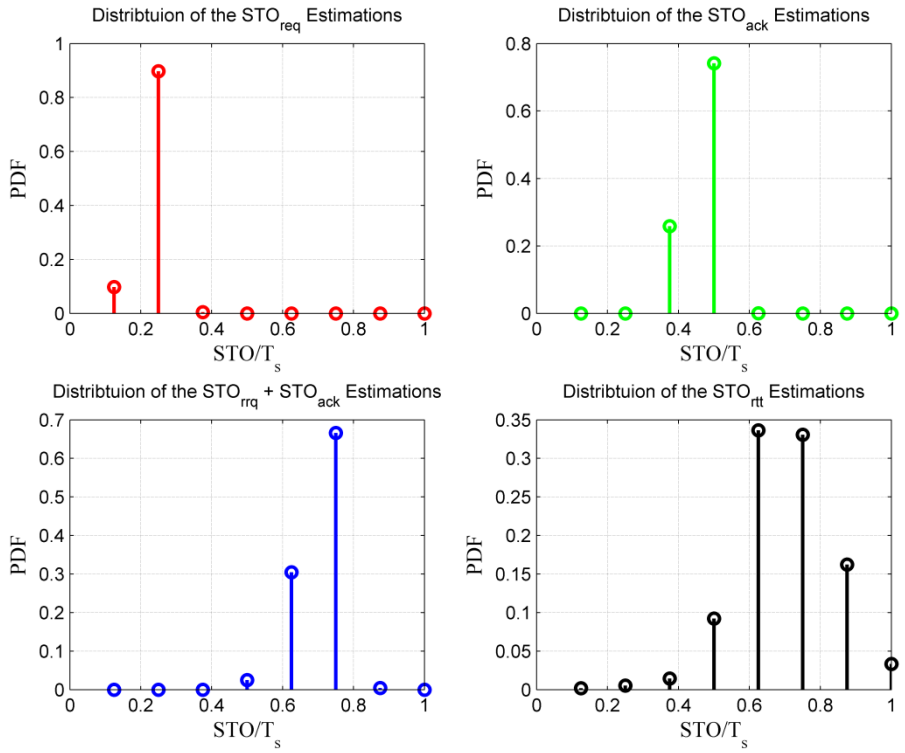

Figure 5.11 PDF of the estimated overall STO (E_s/N_0 = 0 dB, 8 exhaustive searching steps)

In Figure 5.12 the ranging performance based on the MRTT protocol and the fine ToA detection carried on both devices are presented. The simulation parameters are same as above simulations. When considering the assumed STO, $t_{\mathrm{d,req}} = 0.23T_s$ and $t_{\mathrm{d,ack}} = 0.46T_s$, the ranging error with the conventional RTT ranging protocol without any ToA refinement is, $\Delta d = \left(t_{\mathrm{d,req}} + t_{\mathrm{d,ack}}\right)T_s \cdot c$. This is about 36 cm, in the case of $T_s = 1.92$ Nano second.

The upper diagram in Figure 5.12 represents the ranging error PDF of the estimated distance with the conventional RTT protocol when fine ToA detection is applied on both Device 1 and Device 2. The lower diagram in Figure 5.12 represents the ranging error PDF of the estimated distance with the MRTT protocol. The exhaustive searching space is divided into 50 intervals. It is shown in Figure 5.12 that, by applying the fine ToA method, ranging error with the ± 10 cm is with high probability. Compared to the 36 cm error, the ranging performance is greatly improved. In Figure 5.13 the simulation results with 8 exhaustive searching steps are shown. Compared with the ranging performance in Figure 5.12, although some performance degradation is found due to the quantization error, the performance is still promoted greatly.

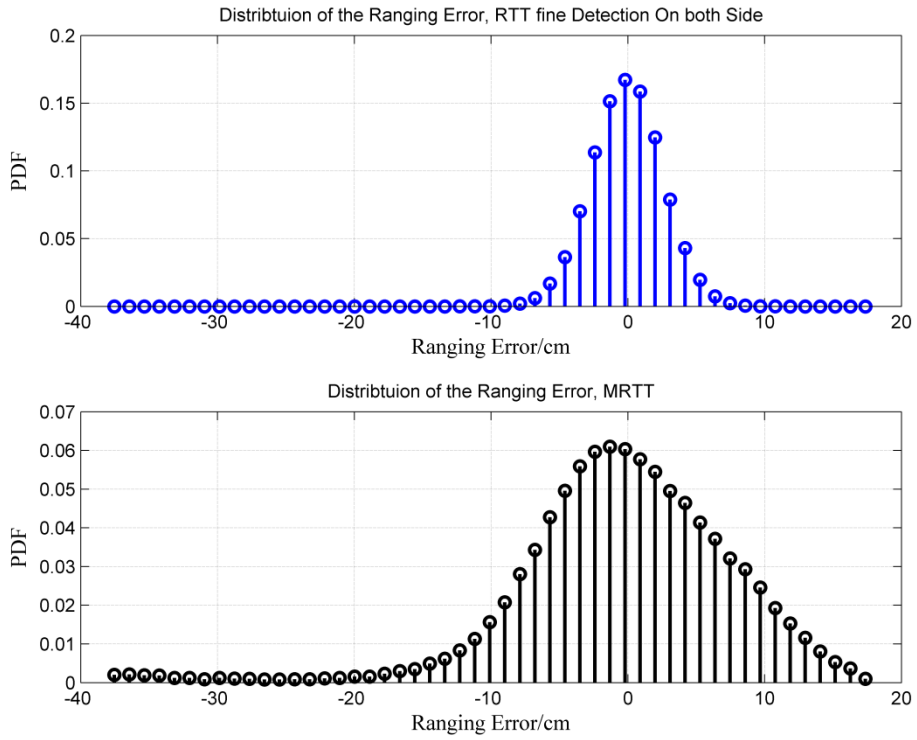

Figure 5.12 Ranging Error Distribution with the proposed schemes (E_s/N_0 = 0 dB, 50 exhaustive searching steps).

From the simulation, one can easily find that, the proposed fine ToA detection method and the MRTT measurement protocol introduce great improvement in ranging accuracy to the MB-OFDM UWB system. With the proposed schemes, accurate ranging applications in the MB-OFDM UWB systems are supported and the feasibility in implementation is also provided.

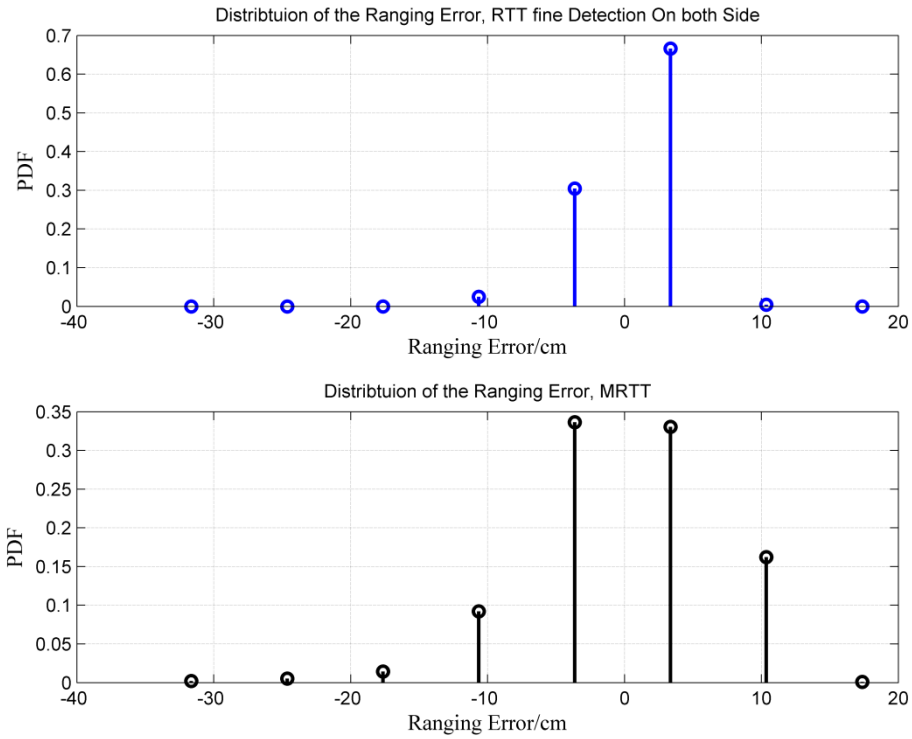

Figure 5.13 Ranging error distribution with the proposed schemes (E_s/N_0 = 0 dB, 8 exhaustive searching steps)

5.5 Chapter Summary

Studies in this chapter are focusing on the second objective of this work, namely, improving the accuracy of ranging in an OFDM based UWB system. A fine ToA detection method based on CIR energy as well as a MRTT ranging protocol is designed to achieve this objective. The third of the thesis presented in Section 1.3.2 is finished.

From analyzing the CIR property of the estimated OFDM channel, the raise of tail energy of the CIR is caused by the fraction STO is observed. Base on this finding, the CIR energy based fine ToA detection method is invented. The idea is to compensated some phase shift value to the CTF of the estimated channel, and suppress the energy accumulated in the tail taps of CIR. In estimating the fraction STO, an optimization problem is formed, and an exhaustive searching algorithm is applied to solve the problem. By estimating the fraction STO, the fine ToA is subsequently obtained. The proposed ToA detection method has good performance even in the severe multipath propagation environment, such as in the

IEEE 802.15.3a CM3 channel. It is also noticed that, the accuracy of the ToA estimation depends on the searching step. The higher resolution the exhaustive searching step is, the better accuracy the ToA can be achieved. Of course more computational tasks are required.

To facilitate the implementation of the fine ToA detection method in low cost UWB system, the MRTT measurement protocol is designed. With MRTT protocol, the complicated computational tasks on the UWB tag are delivered to the relative powerful UWB anchor device. Simulation results show that the MRTT is only has a little performance degradation when comparing to the fine ToA method carried out on both devices in a ranging pair.

The proposed accurate ToA detection method and the MRTT protocol have introduced great ranging performance promotion to the MB-OFDM UWB systems. The ranging uncertainly could be reduced from ± 56cm to about ± 10cm when the searching space is divided into 8 intervals. Except for MB-OFDM UWB systems that is discussed in this thesis, the proposed schemes be also adapted to other OFDM based wireless communication.

Chapter 6

Conclusion and Outlook

6.1 Conclusion of This Thesis

Through the studies, all tasks presented in Section 1.3.2 have been solved, and the objective of the thesis, namely extending the communication range and improving accuracy of ranging of an OFDM based UWB system, is achieved.

In the studies of extending the communication range of the MB-OFDM UWB systems, the SFCB/FFH-OFDM scheme and an AF-based distributed SFBC-TFC cooperative protocol have been investigated. In the proposed SFBC/FFH scheme, the frequency domain diversity and spatial domain diversity are exploited by a joint design of the FFH/OFDM technique and Alamouti SFBC method. It is shown that, the proposed scheme can introduce considerable improvement of the transmission quality, and enlarge the point-to-point communication range in a multiple antenna MB-OFDM UWB system. The AF-based distributed SFBC-TFC cooperative protocol is designed to extend the network coverage through cooperation between multiple UWB devices. The advantages of the distributed SFBC-TFC scheme include high order degree of diversity exploitation, feasible in implementation, and good real time features.

In the studies of improving the ranging accuracy in the MB-OFDM UWB systems, fine ToA detection method and the MRTT measurement protocol are designed. The fine ToA detection method is based on the OFDM channel estimation. By minimizing the energy at the tail taps of the estimated CIR, fine

ToA is obtained. In solving the ToA detection problem, an exhaustive searching method is applied. To make the fine ToA detection method feasible implemented into low cost UWB devices, the MRTT protocol is designed. The idea behind the MRTT protocol is to deliver the complicated computational tasks form UWB tag to the powerful UWB anchor by transferring the estimated channel. With the proposed fine ToA detection method and MRTT protocol, ranging accuracy of MB-OFDM UWB could be greatly improved without introducing implementation and computational complexity to the UWB tag.

Throughout the studies, the low cost designing concepts are always taken care. For instance, in implementing the SFCB-FFH scheme, weighting operations to the IFFT output in time domain, instead of matrix multiplication in frequency domain, are carried out. In proposed the distributed SFBC-TFC cooperative protocol, only a few adaptions to a standard WiMedia UWB device are required. In the accurate ranging schemes, the MRTT protocol is able to burden all the complicated computations to UWB anchor and leave the low cost UWB tag free.

Through the studies, the weakness of limited communication range of MB-OFDM UWB is compensated, and high accurate ranging capability is supported. These improvements will bring more valuable UWB applications for customers and ensures a bright future for the OFDM UWB technique.

6.2 Outlook and Open issues

In fine ToA detection method, exhaustive searching algorithm is applied to find the solution of an optimization problem. Although the MRTT protocol can deliver the complicated computational tasks from UWB tag to UWB anchor, and leave the UWB tag free from complicated signal processing. However the computational tasks on UWB anchor are doubled. Efficient solution to the optimization problem is one of open issues for the future work.

Another interesting direction is the utilization of location information of devices in the location-aware MB-OFDM UWB systems. Currently the location information is used for relay selection, routing, etc. Physical layer signal processing with the aid of location information could be an interesting topic. For instant, in the adaptive array signal processing, AoA of the signal could be derived from the relative location of the devices.

References

[Abr10] Abreau, G. : Localization in Cooperative Wireless Networks: Theory,Algorithms and Applications, in *IEEE International Symposium on Personal, Indoor and Mobile Radio Communications*, 2010.

[Ala98] Alamouti, S : A Simple Transmit Diversity Technique for Wireless Communications, *IEEE Journal on Selected Areas in Communications*, vol. 16, no. 8, pp. 1451 - 1458 , Oct 1998.

[Ali07] Alinejad, A.H. : *Strategien zur Strahlformung bei Zeitduplex-Mobilfunksystemen*. Duisburg: Shaker Verlag, 2007.

[Ars06] Arslan, H. ; Cheng, Z. ; Benedetto, M.D. : *Ultra Wideband Wireless Communication*. Hoboken, new Jersey: John Wiley & Sons, Inc, 2006.

[Ben06] Benedetto, M.D. et al.: *UWB Communication Systems, A comprehensive Overview*. New York, USA: Hindawi Pubulishing Corporation, 2006.

[Ber93] Berrou, C. ; Glavieux, A. ; Thitimajshima, P. : Near Shannon Limit error-correcting coding and decoding: Turbo-codes, in *Proceedings of IEEE International Communications Conference*, 1993.

[Ber071] Berens, F. ; Rüegg, A. ; TScholand, T. ; Hessamian-Alinejad, A. ; and Jung, P. : Fast frequency hopping diversity scheme for OFDM-based UWB systems, *Electronic Letters*, vol. 43, no. 1, Jan. 2007.

[Bla98] Blanz, J.J. ; Jung, P. , "A flexibly Configurable Statial Model for Mobile Radio Channels," *IEEE transaction on Communications*, vol. 46, no. 3, pp. 367-374, 1998.

[Bov08] Bovelli, S. ; Leipold, F. : EUWB Deliverable D8.a1: Scenario description for public transport applications, 2008.

[Bra06] Brankovic, V. ; Zeisberg, S. : Intergrated Project PLLSERS Phase II, Deliverable 1.3, Public project presentation, Deliverable 2006.

[Bra07] Brack, T. ; Alles, M. ; Lehnigk-Emden, T. ; F., Berens ; A., Rüegg : A survey on LDPC Codes and Decoders for OFDM-based UWB

systems, , 2007.

[Bru04] Bruck, G.H. ; Faber, T. ; Scholand, T. ; Jung, P. : PHY Aspects of UTRA Evolution, Final Report (Confidential), IKT, Duisburg, Germany, Project Report 2004.

[Bur09] Burnic, A. et al.: UWB coverage in public transport scenarios , in *2nd International Symposium on Applied Sciences in Biomedical and Communication Technologies 2009*, Bratislava , 2009, pp. 1-4.

[Che09] Chen, Y. ; Teo, J. ; Lai, J.C.Y. ; Low, K.S. ; Soh, C.B.Rapajic, P.B. : Cooperative Communications in Ultra-Wideband Wireless body Area Networks: Channel Modeling and System Diversity Analysis, *IEEE Journal on Selected Areas in Communications*, vol. 27, no. 1, pp. 5-16, Jan. 2009.

[Chi07] Chiueh, T. ; Tsai, P. : *OFDM Baseband Receiver Design for Wireless Communications*. Singapore, Asia: John Wiley & Sons (Aisa), 2007.

[Doe57] Doelz, M.L. ; Heald, E.T. ; Martin, D.L. : Binary data transmission techniques for linear systems, *Proceedings of the IRE*, vol. 45, 1957.

[Dun11] Dunger, H. : EUWB Deliverable , D9.2c: Regulation and standardisation plan, 2011. [Online]. www.euwb.eu

[ECM05] ECMA-368, : *High rate ultra wideband PHY and MAC standard*.: ECMA, 2005.

[ETS09] ETSI EN 302 567: Broadband Radio Access Networks (BRAN); 60 GHz Multiple- Gigabit WAS/RLAN Systems; Harmonized EN covering the essential requirements of article 3.2 of the R&TTE Directive, 2009.

[EUW08] EUWB. (2008) www.euwb.eu.

[EUW111] EUWB Project: Ultra-Wideband: Past, Present and Future, EUWB Project, 2011.

[FCC02] FCC, : *Revision of Part 15 of the commission's rules regards ultra-wideband transmission systems, first report and order*. Washington, 2002.

[Fed95] Federal Communications Commission: CFR 47 Part 15 Radio Frequency Devices §15.255, Operation within the band 57–64 GHz, FCC, FCC 15.255, 1995.

[Fit06] Fitzek, F.H.P. ; Katz, M.D. : *Cooperative in wireless networks:principles and applications*.: Springer, 2006.

[Foe03] Foerster, J.: Channel Modeling Sub-committee Report Final, IEEE802.15-02/490, 2003.

[Gai09] Gaier, S. ; Kuhnert, C. ; Waadt, A. ; Viessmann, A. ; Bruck, G. : Channel model for complex automotive scenarios (in-car), EUWB Deliverable-D8b.4 2009.

[Gal62] Gallagher, R. : Low-density parity-check codes. IRE Transactions on Information Theory, vol. 8, pp. 21-28, 1962.

[Gha02] Ghassemzadeh, S.S. ; Tarokh, V. : The Ultra-wideband Indoor Path Loss Model, IEEE, IEEE P802.15 Working Group for Wireless Personal Area Networks IEEE P802.15-02/277r0-SG3a, 2002.

[Gio11] Giorgetti, A. et al.: Multiple Antennas and Beamforming Algorithms, Integrated Project - EUWB Contract No 215669, Project Deliverable D2.4.4, 2011.

[Has08] Hasch, J. : EUWB Deliverable D8b.1:Scenario description for automotive environment applications, 2008.

[Hei08] Heidari, G. : *WiMedia UWB: Technology of choice for wireless USB and Bluetooth*, 1st ed., CPI Antony Rowe, Ed.: John Wiley & Sons, Ltd., 2008.

[Ibr08] Ibrahim, A.S. ; Sadek, A.K. ; Su, W. ; Liu, K.J.R : Cooperative Communications with Relay-Selection: When to Cooperate and Whom to Cooperate With?, *IEEE TRANSACTIONS ON WIRELESS COMMUNICATIONS*, vol. 7, no. 7, pp. 2814-2827, JULY 2008.

[IEE03] IEEE: IEEE P802.15-02/490r1-SG3a02: Channel Modeling Sub-committee Report Final, IEEE, IEEE Proposal 2003.

[IEE07] IEEE: IEEE 802.15.4a Standard, Standard 2007.

[Jun96] Jung, P. ; Kammerlander, K. ; Berens, F. ; Plechinger, J. : On multicarrier CDMA mobile radio systems with joint detection and coherent receiver antenna diversity, in *Proceedings of the Fifth IEEE International Conference on Universal Personal Communications*, Boston, USA, 1996, pp. 61–65.

[Jun10] Jung, P. ; Bruck, : Robust OFDMA System Concept for the 3GPP LTE Downlink, IKT, Duisburg, Gernamy, Project Report, Confidential 2010.

[Kai09] Kaiser, T. ; Zheng, F. ; Dimitrov, E. : An Overview of Ultra-Wide-Band Systems With MIMO , *Proceedings of the IEEE* , vol. 97, no. 2, pp. 285-312 , Februar 2009.

[Kim07] Kim, J.H. ; Song, H.K. : Performance Improvement of Cooperative MB-OFDM System Based Coming Home Network , *IEEE Transactions on Consumer Electronics*, vol. 52, no. 2, pp. 442-447, 2007.

[Kra10] Krause, A. ; Kupeshmidt, H. ; Goldenberg, S. ; Shor, G. ; Weir, A. : Deliverable IR 7.1.2 - addition Ranging Feature, EUWB Report 2010.

[Lan02] Laneman, J. N. : *Cooperative diversity in wireless networks: Algorithms and Architectures.PhD thesis.* Cambridge, MA: Massachusetts Institute of Technology, 2002.

[LeG94] LeGoff, S. ; Glavieux, A. ; Berrou, C. : Turbo Codes and High Spectral Efficiency Modulation, in *Proceedings of IEEE International Conference of Communication*, New Orleans, LA, 1994, pp. 1-5.

[Lin04] Lin, Shu ; Costello, D.J. : *Error Control Coding*.: Prentice Hall, 2004.

[Lin07] Lin, F. ; Li, Q. ; Luo, T. ; Yue, G. : Impact of Relay Location

According to SER for Amplify-and-Forward Cooperative Communications , in *2007 IEEE International Workshop on Anti-counterfeiting, Security, Identification*, 2007, pp. 324-327.

[LiY08] Li, Y. ; Minn, H. ; Rajatheva, R.M.A.P. : Synchronization, Channel Estimation, and Equalization in MB-OFDM Systems, *IEEE Transactions on Wireless Communication*, vol. 7, no. 11, pp. 1-12, Nov 2008.

[LiY09] Li, Y. : Distributed Coding for Cooperative Wireless Networks: An Overview and Recent Advances, *IEEE Communications Magazine*, vol. 47, no. 8, pp. 71-77 , Auguest 2009.

[Luo04] Luo, J. ; Blum, R. S. ; Greenstein, L. J. ; Cimini, L. J. ; Haimovich, A. M. : New approaches for cooperative use of multiple antennas in ad hoc wireless networks, in *Proc. IEEE 60th Vehicular Technology Conference*, Los Angeles, CA , 2004, pp. 2769-2773.

[MII11] MII: TC-485: Technical specification and test method of detect-And-Avoid (DAA) mitigation techniques for Ultra WideBand (UWB), 2011.

[Muq02] Muquet, B. ; Wang, Z. ; Giannakis, G.B. ; Courville, M. ; Duhamel, P. : Cyclic Prefixing or Zero Padding for Wireless Multicarrier Transmissions?, *IEEE transactions on Communications*, vol. 50, no. 12, pp. 2136-2148, Dec 2002.

[Nik09] Nikookar, H. ; Prasad, R. : *Introduction to Ultra Wideband for Wireless Communications*, 1st ed., Lightning Source UK Ltd., Ed.: Springer, 2009.

[Niu08] Niu, W. ; Li, J. ; Talty, T. : Intra-Vehicle UWB Channel Measurements and Statistical Analysis and Statistical Analysis, in *Proceeding of Global Telecommunications Conference, 2008.*, 2008, pp. 1-5.

[Nyi06] Nyirongo, N. ; Malik, W.Q. ; Edwards, D.J : Concatenated RS-Convolutional Codes for Ultrawideband Multiband-OFDM, in *The 2006 IEEE 2006 International Conference on Ultra-Wideband, ,* 2006, pp. 137-142.

[Par00] Parsons, J. D. : *The Mobile Radio Propagation Channel*, 2nd ed. West Sussex, England: Hohn Wiley & Sons Ltd, 2000.

[Ped00] Pedersen, K. I. ; Mogensen, P. E. ; Fleury, B. H. : A Stochastic Model of the Temporal and Azimuthal Dispersion Seen at the Base Station in Outdoor Propagation Enviroments, *IEEE Transactions on Vehicular Technology*, vol. 49, no. 2, pp. 437-447, March 2000.

[Rob98] Robertson, P ; Woerz, T. : Bandwidth-efficient Turbo Trellis-coded Modulation Using Punctured Component Codes, *IEEE Journal on Selected Areas in Communication*, vol. 16, no. 2, pp. 206-218, Feb 1998.

[Sal87] Saleh, A.A.M. ; Valenzuela, R.A. : A statistical model for indoor

multipath propagation, *IEEE Journal on Selected Areas in Communications*, vol. 5, no. 2, pp. 128-137, 1987.

[Sch98] Schnell, M. ; De Broeck, I. : Application of IFDMA to mobile radio transmission., in *Proceedings of the IEEE 1998 International Conference on Universal Personal Communications*, 1998, pp. 1267–1272.

[Sch05] Scholand, T. et al.: Fast frequency hopping OFDM concept, *ELECTRONICS LETTERS*, vol. 41, no. 13, July 2005.

[Ser05] Sergio, B. : *Multiantenna wireless communcation systems*.: Artech House , 2005.

[She06] Shen, X. ; Guizanni, M. ; Qiu, R.C., Le-Ngoc, T. : *Ultra-Wideband wireless communications and networks*, 1st ed.: John Wiley & Sons Ltd., 2006.

[Shi07] Shin, O. ; Chan, A.M. ; Kung, H. T. ; Tarokh, V. : Design of an OFDM Cooperative Space-Time Diversity System, *IEEE TRANSACTIONS ON VEHICULAR TECHNOLOGY*, vol. 56, no. 4, pp. 2203-2215, July 2007.

[Sir06] Siriwongpairat, W.P. ; Su, W. ; Olfat, M. ; Liu, K.J.R. : Multiband-OFDM MIMO coding frame work for UWB communication systems, *IEEE Transaction on Signal Process*, vol. 54, pp. 214-224, 2006.

[Sir061] Siriwongpairat, W.P. ; Su, W. ; Han, Z. ; Liu, K.J.R. : Employing Cooperative Diversity for Performance Enhancement in UWB Communication Systems, in *IEEE Wireless Communications and Networking Conference, 2006*, 2006, pp. 1854-1859.

[Sni09] Sniffin, R. W. ; Pham, T. T. : DSN Telecommunications Link, California Institute of Technology, 2009.

[Spe00] Spencer, Q.H. ; Jeffs, B.D. ; Jensen, M.A. ; Swindlehurst, A.L. : Modeling the statistical time and angle of arrival characteristics of an indoor multipath channel , *IEEE Journal on Selected Areas In Communications*, vol. 18, no. 3, pp. 347-360 , March 2000.

[Tel99] Telatar, I.E. : Capacity of multi-antenna guassian channel, *European Trans. om Telecommun.*, vol. 10, no. 6, pp. 586-595, 1999.

[Tra08] Tran, L.C. ; Mertins, A. ; Wysocki, T.A. : Cooperative Communication in Space-Time_frequency Coded MB-OFDM UWB, in *IEEE 68th Vehicular Technology Conference*, 2008, pp. 1-5.

[Tra09] Tran, L.C. ; Mertins, A. : Space-time frequency code implementation in MB-OFDM UWB communications: design criteria and performance, *IEEE transaction on Wireless Communication*, vol. 8, no. 2, pp. 701-713, Feb. 2009.

[Tra091] Tran, L.C. ; Mertins, A. : Differential Space-Time-Frequency Codes for MB-OFDM UWB with Dual Carrier Modulation, in *IEEE International Conference on Communication*, Dresden , 2009, pp. 1-5.

[Tse05] Tse, D. ; Viswanath, P. : *Fundmentals of Wireless Communication*.:

Cambriage University Press, 2005.

[Van93] Vandendorpe, L. : Multitone direct sequence CDMA system in an indoor wireless environment, in *Proceedings of the IEEE First Symposium of Communications and Vehicular Technology*, 1993.

[Waa10] Waadt, A. ; Kocks, C. ; Wang, S. ; Bruck, G.H. ; Jung, P. : Maximum Likelihood Localization Estimation based on Received Signal Strength, in *3rd International Symposium on Applied Sciences in Biomedical and Communication Technologies*, Rome, 2010.

[Waa101] Waadt, A. ; Burnic, A. ; Xu, D. ; Kocks, C. ; Wang, S. and Jung, P. : Analysis of RSSI based positioning with multiband OFDM UWB, in *Future Network and Mobile Summit 2010*, Florence, 2010, pp. 1-8.

[Wan05] Wang, Y. ; Yang, L. ; Wei, L. : High Speed Turbo TCM Coded OFDM System for UWB channels, in *IEEE*, Adelaide, SA , 2005, p. Proceedings of International Symposium on Information Theory.

[Wan10] Wang, A. et al.: System implementation study on RSSI based positioning in UWB Networks, in *7th International Symposium on Wireless Communication Systems*, York, 2010, pp. 36-40.

[Wei71] Weinstein, S. ; Ebert, P.M. : Data transmission by frequency division multiplexing using the discrete Fourier transform, *IEEE Transactions on Communications*, vol. 19, pp. 628-364, 1971.

[WiM09] WiMedia Alliance: Multiband OFDM Physical Layer Specification, WiMedia Alliance, 2009.

[WiM11] WiMidea Alliance. (2011) http://www.wimedia.org/en/index.asp.

[Win87] Winters, J.,H., : On the Capacity of Radio Communication Systems with Diversity in a Rayleigh Fading Environment, *IEEE Journal on Selected Areas in Communications*, vol. 5, no. 5, pp. 871 - 878 , June 1987.

[XUD11] XU, D. ; Waadt, A. : EUWB Deliverable D7.5: Combined LDR/HDR platform study results, EUWB Project, 2011.

[YeZ08] Ye, Z. ; Duan, C. ; Orlik, P. ; Zhang, J. : A Low-Complexity Synchronization Design for MB-OFDM Ultra-wideband Systems, in *IEEE ICC 2008*, 2008, pp. 1-7.

[Zha05] Zhao, B. ; Valenti, M.C. : Practical relay networks: A generalization of hybrid-ARQ, *IEEE J. Select. Areas Commun*, vol. 23, no. 1, pp. 7-18, Jan. 2005.

[Zha08] Zhang, Y. ; Brown, A.K. ; Malik, W.Q. ; Edwards, D.J. : High Resolution 3-D Angle of Arrival Determination for Indoor UWB Multipath Propagation, *IEEE TRANSACTIONS ON WIRELESS COMMUNICATIONS*, vol. 7, no. 8, pp. 3047-3055, Auguest 2008.

[Zor03] Zorzi, M. ; Rao, R. R. : Geographic random forwarding (GeRaF) for ad hoc and sensor networks: multihop performance, *IEEE Trans. Mobile Comput.*, vol. 2, no. 4, pp. 337-348, Dec 2003.

[Zor031] Zorzi, M. ; Rao, R. R. : Geographic random forwarding (GeRaF) for

ad hoc and sensor networks: energy and latency performance, *IEEE Trans. Mobile Comput.*, vol. 2, no. 4, pp. 349-365, Dec 2003.

List of Figures

List of Tables

List of Symbols

$\alpha_{k,l}$	Path gain coefficient
$\underline{b}_l^{(n)}$	Discrete time OFDM sample
$\underline{\boldsymbol{b}}^{(n)}$	Discrete time OFDM symbol
$\underline{\tilde{\boldsymbol{b}}}^{(n)}$	Discrete time OFDM symbol with ZPS
$\underline{\boldsymbol{b}}_{\mathrm{H}}^{(n)}$	Discrete time FFH/OFDM symbol
d_{LOS}	Radio propagation distance of LOS path
d_{R}	Radio propagation distance of reflected path
$\underline{\boldsymbol{d}}^{(n)}$	Complex symbols vector in frequency domain
$\underline{\boldsymbol{D}}^{\mathrm{H}}$	DFT Matrix
$\underline{\boldsymbol{D}}_{\mathrm{H}}$	FFH Matrix
$\delta(\cdot)$	Dirac delta function
$\underline{\boldsymbol{e}}_{\mathrm{f}}^{(n)}$	Discrete time received OFDM signal in frequency-domain
E_{s}	Mean energy per OFDM symbol

f_{l}	Lower and frequency of radio signal
f_{s}	Sampling frequency
f_{u}	Upper frequency of radio signal
Δf	Subcarrier frequency spacing
$\boldsymbol{\Phi}$	FFH phase patterns matrix
G_{R}	Receive antenna gain
G_{T}	Transmit antenna gain
$\underline{\boldsymbol{H}}_{\mathrm{t}}^{(n)}$	Circular convolutional matrix of channel
$\underline{\boldsymbol{H}}_{\mathrm{f}}^{(n)}$	CTF matrix of channel
$\underline{\boldsymbol{h}}_{\mathrm{t}}^{(n)}$	Discrete time CIR vector
K_{C}	Number of cluster
K_{R}	Number of RX antennas
K_{T}	Number of TX antennas
Λ	Cluster arrival rate
λ	Ray arrival rate
$\underline{\boldsymbol{n}}_{\mathrm{f}}^{(n)}$	AWGN noise in frequency domain
N_0	Double-sided spectral noise density
N_{FFT}	Total number of subcarriers(FFT size)
N_{ZPS}	Number of samples in ZPS
P_{b}	Bit Error Ratio or Bit Error Probability

P_{R}	Received Signal Power
P_{T}	Transmitted Signal Power
R	Code Rate
$\underline{\boldsymbol{s}}^{(n)}$	OFDM symbol with ZPS
t	Time
T_{FFT}	IFFT and FFT period
T_{s}	Sampling time period
T_l	Cluster arrival time
T_{ZPS}	Zero-padded suffix duration in time
$\tau_{k,l}$	Ray arrival time
$\boldsymbol{u}$	Uncoded information bits vector
$\underline{\boldsymbol{U}}$	FFH pre-coding matrix
W	Signal bandwidth
X	Log-normal shadowing fading
$\underline{X}_k$	Complex constellation symbol

Abbreviations

AWGN	Additive White Gaussian Noise
AoA	Angle of Arrival
BER	Bit Error Ratio
BLAST	Bell Laboratories layered Space-Time System
CC	Convolutional Code
CIR	Channel Impulse Response
CMS	Cabin Management System
CEPT	European Conference of Postal and Telecommunications Administrations
CP	Cyclic Prefix
CR	Cognitive Radio
CTF	Channel Transfer Function
CSI	Channel State Information
DAA	Detection and Avoidance

DCM	Dual Carrier Modulation
DFT/IDFT	Discrete Fourier Transform/Inverse Discrete Fourier Transform
DS-CDMA	Direct Sequence Code Division Multiple Access
DVB-T	Digital Video Broadcasting-Terrestrial
DVB-S2	Digital Video Broadcasting-Satellite Second Generation
EC	European Commission
ECMA	European Computer Manufacturers Association
EGC	Equal Gain Combing
EIRP	Equivalent Isotropically Radiated Power
ETSI	European Telecommunications Standards Institute
EU	European Union
EUWB	Co-Existing Short Range Radio by Advanced Ultra-wideband Radio Technology
FCC	Federal Communications Commission
FDM	Frequency Division Multiplex
FDS	Frequency Domain Spreading
FFH	Fast Frequency Hopping
FFT/IFFT	Fast Fourier Transform/Inverse Fast Fourier Transform
GPS	Global Positioning System
GSM	Global System for Mobile Communications

GeRaF	Geographic Random Forwarding
Hi-Fi	High fidelity
HDR	High Data Rate
IEEE	Institute of Electrical and Electronics Engineers
IoT	Internet-of-Things
ISI	Inter-symbol Interference
ISM	Industrial, Scientific and Medical
ISO	International Organization for Standardization
FP6/FP7	Sixth/Seventh Framework Programme
LBS	Location-based Services
LDC	Low Duty Cycle
LDPC	Low Density Parity Check
LDR	Low Data Rate
LTE	Long Term Evolution (Project from 3GPP)
MBOA	MB-OFDM Alliance
MB-OFDM	Multiple Band Orthogonal Frequency Division Multiplexing
MIMO	Multiple Input Multiple Output
MLE	Maximum Likelihood Estimator
MMSE	Minimum Mean Square Error
MSE	Mean Square Error

MRRC	Maximal-Ratio Receive Combining
OFDM	Orthogonal Frequency Division Multiplexing
PAS	Power Azimuth Spectrum
PDP	Power Delay Profile
PHY	Physical
PLPC	Physical Layer Convergence Protocol
PULSERS	Pervasive Ultra-wideband Low Spectral Energy Radio Systems
PDF	Probability Density Function
QAM	Quadrature Amplitude Modulation
QPSK	Quadrature Phase Shift Keying
RX	Receiver
SDR	Software Defined Radio
SIG	Special Interest Group
SFBC	Space Frequency Block Codes
SNR	Signal to Noise Ratio
STBC	Space Time Block Codes
S-V	Saleh-Valenzuela
TDMA	Time Division Multiple Access
TDS	Time Domain Spreading
ToA	Time-of-Arrival

TTCM	Turbo Trellis-Coded Modulation
RTT	Round Trip Time
TX	Transmitter
US-LDPC	Ultra-Sparse LDPC
UWB	Ultra-wideband
WBAN	Wireless Body Area Networks
WiMaX	Worldwide Interoperability for Microwave Access
WPAN	Wireless Personal Area Networks
WLAN	Wireless Local Area Network
WLP	WiMedia Logic Link Control Protocol
WSNs	Wireless Sensor Networks
WUSB	Wireless Universal Serial Bus
ZF	Zero-Forcing
ZPS	Zero-Padding Suffix

Publications of the Author

[1] Xu, D. ; Bai, Z. ; Waadt, A. ; Bruck, G.H. ; Jung, P. : Combined MIMO and Network Coding for Wireless Relay Networks, *IET Communication*.(Accepted for publication)

[2] Xu, D. ; Bai, Z. ; Bruck, G.H. ; Jung, P. : Location-aided Transmit Strategy in Bidirectional Relay over MISO Rician Channels, in *2012 IEEE 75th Vehicular Technology Conference (VTC)*, Yokohama, Japan, 2012.

[3] Xu, D. ; Bai, Z. ; Waadt, A. ; Bruck, G. H. ; Jung, P. : Combining MIMO with Network Coding, A Viable Means to Provide Multiplexing and Diversity in Wireless Relay Networks, in *2010 IEEE International Conference on Communications (ICC)*, Cape Town, South Africa, 2010.

[4] Xu, D. ; Bai, Z. ; Bruck, G.H. ; Jung, P. : Location aided transmit strategy in two-way relay networks , in *IEEE 21st International Symposium on Personal, Indoor and Mobile Radio Communication (PIMRC)* , Instanbul, Turkey, 2010.

[5] Xu, D. ; Bai, Z. ; Rickers, S. ; Bruck, G.H. ; Jung, P. : A robust decoder for distributed turbo codes in relay channel, in *2010 3rd International Symposium on Applied Sciences in Biomedical and Communication Technologies (ISABEL)* , Rom, Italy, 2010.

[6] Xu, D. ; Bai, Z. ; Waadt, A. ; Bruck, G.H. ; Jung, P. : MIMO with network coding in relay networks: A combination of multiplexing and diversity, in *2009 2nd International Symposium on Applied Sciences in Biomedical and Communication Technologie (ISABEL)* , Bratislava, Slovakia, 2009.

[7] Jung, P. ; Xu, D. ; Waadt, A. ; Viessmann, A. : The EUWB open technology platforms for Ultra Wide band communications , in *2011 IEEE International Conference on Ultra-Wideband (ICUWB)*, Bologna, Italy, 2011.

[8] Burnic, A. ; Xu, Dong. et al.: UWB coverage in public transport scenarios , in *2nd International Symposium on Applied Sciences in Biomedical and Communication Technologies 2009*, Bratislava , Slovakia, 2009.

[9] Kocks, C. ; Scheiber, E.; Xu, D. et al.: A low-cost protocol and application for UWB localization, in *2009 IEEE International Conference on Ultra-Wideband (ICUWB)* , Vancouver, Canada, 2009.

[10] Waadt, A. ; Burnic, A. ; Xu, D. ; Kocks, C. ; Wang, S. and Jung, P. : Analysis of RSSI based positioning with multiband OFDM UWB, in *Future Network and Mobile Summit 2010,* Florence, Italy,2010.